Open access • Report • DOI:10.2172/4285215

Neon isotope separation by gaseous diffusion transport in the transition flow regime with regular geometries — Source link

D.E. Fain, W.K. Brown

Published on: 13 Sep 1974

Topics: Knudsen flow, Gaseous diffusion, Knudsen number, Real gas and Isotopes of neon

K-1863

NEON ISOTOPE SEPARATION BY GASEOUS DIFFUSION TRANSPORT IN THE TRANSITION FLOW REGIME WITH REGULAR GEOMETRIES

AUTHORS:

D. E. Fain
W. K. Brown

UNION CARBIDE

OAK RIDGE GASEOUS DIFFUSION PLANT
OAK RIDGE, TENNESSEE

prepared for the U.S. ATOMIC ENERGY COMMISSION
under U.S. GOVERNMENT *Contract* W-7405 eng 26

DISCLAIMER

Printed in the United States of America. Available from
National Technical Information Service
U.S. Department of Commerce
5285 Port Royal Road, Springfield, Virginia 22151
Price: Printed Copy $5.45; Microfiche $1.45

Date of Issue: September 13, 1974 Report Number: K-1863

Subject Category: UC-22, Isotope Separation

NEON ISOTOPE SEPARATION BY GASEOUS DIFFUSION TRANSPORT IN THE TRANSITION FLOW REGIME WITH REGULAR GEOMETRIES

D. E. Fain and W. K. Brown
Experimental Barrier Development Department
Gaseous Diffusion Development Division

UNION CARBIDE CORPORATION
NUCLEAR DIVISION
Oak Ridge Gaseous Diffusion Plant
Oak Ridge, Tennessee

THIS PAGE

WAS INTENTIONALLY

LEFT BLANK

ABSTRACT

A comprehensive study of the pressure dependence of the transport and transport ratio of neon isotopes by gaseous diffusion through regular geometries has been made. The pressure range was such that the Knudsen number or the ratio of capillary radius to gas mean free path varied from about 0.05 to 10. The measurements were made using parallel plates and capillaries with radii from 5 μ to 25 μ, length-to-radius ratios from 4 to 900, and materials of construction including glass, plastic, and gold. The results are compared with available theories and an interpolation formula for the data is given, which is an empirical modification of the Present and deBethune theory to include effects of flow anomalies and real gas flow pressure dependence. Both the flow and transport ratio measurements clearly show anomalies which are probably caused by deviations from cosine law wall scattering, but they are not completely consistent with each other.

THIS PAGE

WAS INTENTIONALLY

LEFT BLANK

TABLE OF CONTENTS

	Page
LIST OF TABLES	7
LIST OF FIGURES	9
INTRODUCTION	13
SUMMARY	14
REVIEW OF THE FLOW AND SEPARATION PHENOMENA	16
TRANSPORT PROCESSES	16
Poiseuille and Knudsen Flow	16
Slip Flow	16
Transition Flow	17
BINARY SEPARATION	24
Experimental Design	25
MATHEMATICAL MODELS	27
PRESENT AND deBETHUNE MODEL (PBM)	27
MODIFIED PRESENT AND deBETHUNE MODEL (PBFM)	31
GENERAL CAPILLARY MODEL (GCM)	32
EXPERIMENTAL TEST SAMPLES	34
SAMPLE SELECTION	34
SAMPLE PREPARATION	34
Capillary Samples	36
Short Capillary Sample	43
Parallel Plate Samples	43
FLOW MEASUREMENTS	43
SEPARATION MEASUREMENTS	48
SEPARATION EFFICIENCY CALCULATION METHOD	56
DISCUSSION OF RESULTS	60
CONCLUSIONS	97
ACKNOWLEDGMENTS	101
BIBLIOGRAPHY	102
APPENDIX A - NOMENCLATURE	104
APPENDIX B - COMPILATION OF DATA	106
APPENDIX C - ACCURACY AND PRECISION	131
MASS SPECTROMETER MEASUREMENTS	131
FLOW MEASUREMENTS	131

THIS PAGE

WAS INTENTIONALLY

LEFT BLANK

LIST OF TABLES

Table		Page
1	TEST SAMPLE CHARACTERISTICS	35
2	FLOW MEASUREMENT PARAMETERS	49
3	CONSTANTS FOR THE MODIFIED PRESENT AND deBETHUNE MODEL	69
4	MEASURES OF CAPILLARY RADIUS	73
5	DEVIATION FROM DIFFUSE WALL SCATTERING IMPLIED BY MEASUREMENTS	74
6	VARIATION IN FLOW PARAMETERS FOR SMALLEST GLASS CAPILLARIES.	75
7	COMPARISON OF GCM PARAMETERS OBTAINED FROM FLOW MEASUREMENTS WITH THOSE NEEDED TO FIT THE SEPARATION DATA.	78
8	SEPARATION EFFICIENCY INITIAL SLOPE RATIOS COMPARED WITH RADIUS RATIOS	79
9	COMPARISON OF THE STANDARD DEVIATION OF THE EXPERIMENTAL DATA OBTAINED WITH THE DIFFERENT MODELS	83
10	THE MODIFICATION CONSTANT K FOR THE PRESENT AND deBETHUNE MODEL FOR DIFFERENT GEOMETRIES AND CALCULATION METHODS	93
C-1	COMPARISON OF FLOW MEASUREMENTS FROM A VOLUMETRIC SYSTEM WITH THOSE FROM A GRAVIMETRIC SYSTEM	132
C-2	COMPARISON OF MEASURED AND THEORETICAL VALUES FOR DIFFERENT GASES	133

THIS PAGE

WAS INTENTIONALLY

LEFT BLANK

LIST OF FIGURES

Figure		Page
1	LOW PRESSURE NITROGEN FLOW DATA FOR A 25.97-MICRON-RADIUS ORIFICE SAMPLE.	18
2	HIGH PRESSURE NITROGEN FLOW DATA FOR A 25.97-MICRON-RADIUS ORIFICE SAMPLE.	19
3	LOW PRESSURE NITROGEN FLOW DATA FOR A 4.907-MICRON-RADIUS GLASS CAPILLARY	20
4	HIGH PRESSURE NITROGEN FLOW DATA FOR A 4.907-MICRON-RADIUS GLASS CAPILLARY	21
5	LOW PRESSURE NITROGEN FLOW DATA FOR A 10.29-MICRON PARALLEL PLATE SAMPLE	22
6	HIGH PRESSURE NITROGEN FLOW DATA FOR A 10.29-MICRON PARALLEL PLATE SAMPLE	23
7	A SECTION OF SAMPLE 64	37
8	GLASS CAPILLARY FROM SAMPLE 64	37
9	PROTOTYPE OF SAMPLE 1054	39
10	SAMPLE 1054.	40
11	GLASS CAPILLARY USED IN SAMPLE 1054.	41
12	STAINLESS STEEL WIRE ON METAL FRAME.	41
13	METAL FRAMES WITH STAINLESS STEEL WIRE CAST IN PLASTIC	42
14	CAPILLARIES IN PLASTIC SAMPLE.	42
15	CAPILLARY IN GOLD FOIL	44
16	PARALLEL PLATE SAMPLE 1.	45
17	INERT GAS SEPARATION SYSTEM	50
18	HIGH PRESSURE SIDE OF SAMPLE HOLDER.	52
19	LOW PRESSURE SIDE OF SAMPLE HOLDER	53
20	COMPLETE HOLDER ASSEMBLY	54
21	INERT GAS SEPARATION SYSTEM	57

LIST OF FIGURES (cont'd.)

Figure		Page
22	EXPERIMENTAL SEPARATION DATA FOR SAMPLE 212	61
23	EXPERIMENTAL SEPARATION DATA FOR SAMPLE 838	62
24	EXPERIMENTAL SEPARATION DATA FOR SAMPLE 924	63
25	EXPERIMENTAL SEPARATION DATA FOR SAMPLE 1054	64
26	EXPERIMENTAL SEPARATION DATA FOR SAMPLE 64	65
27	EXPERIMENTAL SEPARATION DATA FOR SAMPLE 2	66
28	EXPERIMENTAL SEPARATION DATA FOR SAMPLE 1	67
29	EXPERIMENTAL SEPARATION DATA FOR SAMPLE 5	68
30	EFFECTIVE PRESSURE PARAMETER FOR SEPARATION	71
31	SEPARATION EFFICIENCY OF 4.907-MICRON-RADIUS GLASS CAPILLARY SAMPLE	72
32	BEST AGREEMENT BETWEEN EXPERIMENTAL DATA AND THEORETICAL CURVES USING ADJUSTED PARAMETERS	76
33	SEPARATION EFFICIENCY OF 12.91-MICRON-RADIUS PLASTIC CAPILLARY SAMPLE	80
34	SEPARATION EFFICIENCY OF A 12.65-MICRON-RADIUS PLASTIC CAPILLARY SAMPLE	81
35	SEPARATION EFFICIENCY OF 22.01-MICRON-RADIUS GLASS CAPILLARY SAMPLE	82
36	CUT CURVE FOR A 12.65-MICRON-RADIUS CAPILLARY SAMPLE	85
37	CUT CURVE FOR A 4.907-MICRON-RADIUS CAPILLARY SAMPLE	86
38	LOW PRESSURE SEPARATION EFFICIENCY DATA FOR 4.907-MICRON-RADIUS GLASS CAPILLARY SAMPLE	88
39	LOW PRESSURE SEPARATION EFFICIENCY DATA FOR 12.65-MICRON-RADIUS PLASTIC CAPILLARY SAMPLE	89
40	COMPARISON OF GLASS LONG CAPILLARY, ORIFICE, AND PARALLEL PLATE DATA IN LOW PRESSURE REGION	90
41	COMPARISON OF SEPARATION EFFICIENCY OF LONG CAPILLARY, ORIFICE, AND PARALLEL PLATE	91

LIST OF FIGURES (cont'd.)

Figure		Page
42	SEPARATION EFFICIENCY OF 25.97-MICRON-RADIUS GOLD ORIFICE SAMPLE	92
43	SEPARATION EFFICIENCY OF STEEL PARALLEL PLATE SAMPLE WITH PLATE SPACING OF 25.58 MICRONS	94
44	SEPARATION EFFICIENCY OF STEEL PARALLEL PLATE SAMPLE WITH PLATE SPACING OF 10.29 MICRONS	95

THIS PAGE

WAS INTENTIONALLY

LEFT BLANK

NEON ISOTOPE SEPARATION BY GASEOUS DIFFUSION TRANSPORT IN THE TRANSITION FLOW REGIME WITH REGULAR GEOMETRIES

INTRODUCTION

It has been known for over one hundred years that the different gas species in a mixture can be partially separated by passing the gas mixture through a porous material if the dimensions of the openings in the material are small in comparison to the mean free path of the gas molecules. About 25 years ago, R. D. Present and A. J. deBethune [1] developed a theory for the separation of a binary gas mixture flowing through circular capillaries. Until now, there has been no definitive data which could be used to check the theory of Present and deBethune. The purpose of this study has been to obtain accurate data for the separation of a binary isotopic mixture flowing through well-defined regular geometries. These data are needed to define the effect of geometry on the pressure dependence of the separation phenomena and provide the information needed to check the theory of Present and deBethune or any other theory which may become available.

A comprehensive study of the pressure dependence of the separation of neon isotopes by gaseous diffusion through regular geometries has been made and the results are given in this report. Separation measurements have been made with capillaries with different length-to-radius ratios and with parallel plate geometries. The results are compared with available theories and an interpolation formula is also given.

The results of this study will be presented as follows. First, a summary of the report is given to indicate the general results which have been found. A discussion of the theories available is presented along with how they affect sample selections and define the experimental data which are needed. Some points of historical interest in the development of this subject are also given. The techniques of sample preparation are discussed next. A discussion of the flow measurement apparatus and the differences in details of the flow data obtained with different geometries are given. The separation apparatus, the measurement technique, and the data reduction are discussed. The results of the flow and the separation measurements are presented and their comparison with theory is discussed. In addition, an interpolation formula for the data and its possible physical significance is discussed. Finally, the conclusions reached as a result of this study and recommendations for further work are indicated.

Several appendices are included. Appendix A gives a listing of all symbols used and their definitions. Appendix B gives a listing of the separation data which were obtained. Appendix C gives information relative to the precision and accuracy of measurements.

SUMMARY

A listing of all the separation data which were obtained is given in Appendix B. Separation measurements were made with glass capillaries with radii of nominally 5 μ and 25 μ and length-to-radius ratios of nominally 900 and 450; with plastic capillaries with radii of nominally 12 μ and 25 μ and length-to-radius ratios of nominally 600 and 200; with gold capillaries with radii of nominally 25 μ and a length-to-radius ratio of about 4; and with metal parallel plates with spacing of nominally 10 μ and 25 μ and length-to-spacing ratios of nominally 900 and 350. An accurate determination of the capillary radii and the plate spacing was made by flow measurements.

When the experimental separation data are first examined on a broad scale, there appears to be no fundamental difference in the pressure dependence of the separation efficiency in these different geometries in contrast to the large differences in the pressure dependence of the flow in these same geometries. This result would appear to be consistent with the Present and deBethune theory using the hydraulic radius concept, and is probably due to the fact that most of the differences in the pressure dependence of the flows occur in the pressure region where the separation efficiency is above about 0.90. These differences in the pressure dependence of the flow do produce differences in the initial slope of the separation efficiency ratio curves, but these differences are not as dramatic as the differences in the flow curves. Apparently, below separation efficiencies of about 0.90, the separation curves are influenced more by slip flow than by free molecule flow. Since slip flow depends only on the hydraulic radius and not other details of geometry, the pressure dependence of separation appears to be essentially independent of geometry other than hydraulic radius below a separation efficiency of about 0.90.

Of the separation theories presently available, the Present and deBethune theory [1] generally predicts separation results somewhat lower than those which are measured. A calculation method by Malling [2], which is based on the flow equations of Lund and Berman [3] and is called the general capillary separation theory, generally predicts separation results higher than those of the Present and deBethune theory. Although closer to the measured values, they are still too low particularly in the region of separation efficiencies below about 0.60. An empirical modification of the Present and deBethune theory has been made to give a better approximation to the experimental data. This modification accounts for the change in flow velocity from the free molecule value to the slip value and includes a parameter to account for deviations from ideal free molecule flow. This empirical modification has resulted in calculations of separation efficiency ratios which agree most closely with the measured values and is considered the best interpolation formula for the data.

A closer inspection of the data reveals that deviations from diffuse scattering of molecules from the capillary walls were observed with these samples and that these deviations which affect the flow rates also affect

the slopes of the separation curves. The geometry of the flow channel also affects the relationship between the initial slopes of the separation curves and the channel dimension. In the modified Present and deBethune theory, the differences observed due to deviations in the wall scattering law and differences due to geometry appear in terms of the constants required to represent the experimental data. The constants indicating deviations in wall scattering are generally in about the same ratio as those obtained from the flow measurements. However, the constants relating to differences in geometry do not seem to be consistent with what would be predicted from the Clausing calculation of free molecule flow.

It is observed that in addition to this modification of the Present and deBethune theory, some apparently arbitrary changes in the Lund and Berman flow parameters can result in significantly better agreement with the experimental data obtained with the general capillary separation theory. This could imply that the Lund and Berman flow parameters were not appropriately determined. In fact, it is shown that the Lund and Berman flow equations result in significantly better agreement with the separation data when they are used as differential equations rather than an integrated equations as they were originally presented.

One change in the flow constants which results in better agreement with the separation data is a simple translation of the specific flow or transmission ratio with respect to the theoretical value as calculated by Clausing. However, the changes with respect to scattering law deviations are such as to indicate that the difficulties with the Malling calculation are of a more fundamental nature. The fact that both models indicate that the Clausing transmission probability may not be the best estimate of the flow velocity for predicting the pressure dependence of the separation efficiency ratios is probably sufficient reason to question the accuracy of the Clausing calculation. The accuracy is particularly questionable for the parallel plate geometries. It is relatively difficult to extrapolate the transmission ratio curves to zero pressure to determine accurately the free molecule transmission ratios for comparison with calculations. However, the differences between the measured and calculated separation efficiency ratio curves are clearly distinguishable and indicate a serious discrepancy between theory and measurement.

Further separation efficiency studies, particularly with parallel plate geometries, should be very helpful. These studies should include plates with different surfaces such as glass and a stable metal such as gold. The studies should also include parallel plates with an order of magnitude or greater difference in length-to-spacing ratio.

REVIEW OF THE FLOW AND SEPARATION PHENOMENA

The kinetic theory of gases is most important in any study of the detailed motion of a gas. The major developments in the kinetic theory of gases occurred between about 1857 and 1880 by Clausius [4], Maxwell [5], and Boltzmann [6]. But even before the development of kinetic theory, Graham [7] in 1829 showed that the effusion rate of a gas through a small orifice was proportional to the square root of the gas density and therefore could be used as a means of partially separating the components of a gas mixture. However, it was almost 100 years before Aston [8], in 1920, made practical use of this phenomenon to separate the isotopes of neon.

TRANSPORT PROCESSES

Before discussing the separation phenomena, some aspects of the transport process should be discussed. Kinetic theory accounts for the properties of a gas by treating the gas as an ensemble of molecules with random motions but with a definite distribution of velocities. The equilibrium velocity distribution, which was first determined by Maxwell, defines an average kinetic energy for the molecules which is proportional to the temperature of the gas. In its simplest form, the molecules are treated as billiard balls bouncing around at random colliding with each other. The average distance moved between a collision with another molecule is the mean free path and the number of collisions per unit time is the collision frequency.

Poiseuille and Knudsen Flow

When a gas flows through a channel under pressure and temperature conditions such that the mean free path is small compared to the smallest dimension of the flow channel, then there is a thorough exchange of momentum among the colliding molecules and the gas flows as a viscous continuum mass and is often called Poiseuille flow. When the mean free path is large compared to the characteristic channel dimension, then the molecules collide with the walls of the channel much more frequently than with each other, and therefore they tend to flow through the channel with their own characteristic thermal velocities. In the limit where there are no collisions between molecules, the flow is known as free molecule or Knudsen flow. The transport process results in a maximum separation of the components of a gas mixture when the flow is free molecule and no separation occurs when the flow is entirely viscous.

Slip Flow

In 1875, while studying the viscous damping of a vibrating disk by a surrounding gas, Kundt and Warburg [9] found that at low pressures the damping decreased. They attributed this effect to a slipping of the gas over the surface of the disk. In 1879 Maxwell developed an approximate theory to account for the slip effect. This effect is always observed when a gas flows past a stationary surface. In the early 1900's Knudsen [10] studied the flow of gases through capillaries at low pressures. He

showed that, as is indicated by Maxwell's slip theory, at high pressures slip flow is directly proportional to the pressure difference and independent of the pressure level, but at a sufficiently low pressure slip flow per unit pressure difference increases and extrapolates to a higher value at zero pressure. Knudsen explained the zero pressure limit in terms of a free molecule flow. This effect can best be observed by plotting the specific flow (mass or molar flow per unit pressure difference) as a function of the average pressure. At high pressures, the curve is linear with average pressure and extrapolates to a finite value at zero average pressure. The extrapolated value at zero pressure is due to the constant slip flow per unit pressure drop at the high pressures. At sufficiently low pressures, such that the gas mean free path is comparable to the capillary radius, a minimum is observed in the specific flow curve. At very low pressures the curve extrapolates to the higher free molecule value. Free molecule flow is similar to slip flow but larger in magnitude. These features in the specific flow curves can be seen in figures 1 through 6. Other experimental investigations of significance were performed during this period by Gaede [11] and Adzumi [12]. Gaede performed experiments with a parallel plate channel and showed that the minimum in the specific flow curve was much deeper than it was with a capillary.

Transition Flow

It has only been in recent years that a reasonable explanation for the minimum in the specific flow curve has been given. In 1948 Pollard and Present [13] developed a theory for the variation with pressure of the self-diffusion coefficient of a gas in a capillary. While this theory was applicable only to the diffusion of a gas with no net pressure difference across the capillary, it did give a qualitative explanation for the Knudsen minimum in terms of a decrease in the diffusion coefficient. They suggested that, at least at low pressures, the total flow might be described by the superposition of a diffusive flow as computed in their paper and a viscous drift component. In 1951 Visner [14], using xenon isotopes, showed that the Pollard and Present theory could accurately account for the variation with pressure of the self-diffusion coefficient. In 1952 Hiby and Pahl [15] used the same approach as Pollard and Present to describe the self-diffusion of a gas between infinite parallel plates. They showed that for the parallel plate, the decrease in the diffusion coefficient with pressure was more rapid than with a capillary and therefore qualitatively accounts for the difference in depth of the Knudsen minimum for these two geometries.

In 1954 Weber [16] applied the idea of the superposition of a diffusive and drift component to describe Knudsen's flow data quantitatively. He assumed that the total gas transport in a long capillary is given at all pressures by the addition of (1) *a diffusive component* as obtained from the Pollard and Present calculation, (2) *a slip component* which is zero at zero pressure and rises to a constant value at large pressure, and (3) *a viscous component* which rises linearly from zero at zero pressure. In 1965 Lund and Berman [3] extended the superposition idea to include

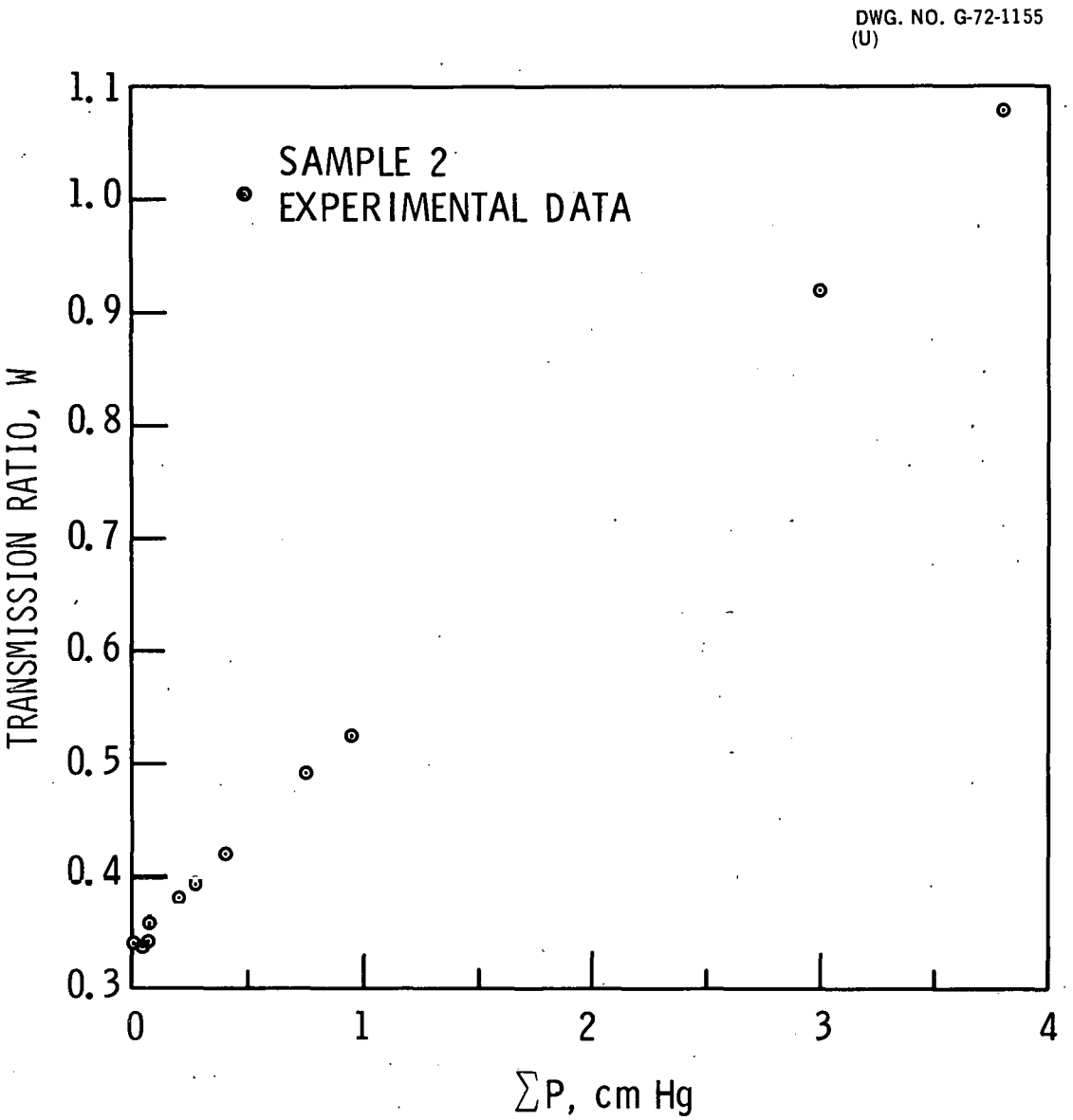

Figure 1

LOW PRESSURE NITROGEN FLOW DATA FOR
A 25.97-MICRON-RADIUS ORIFICE SAMPLE

DWG. NO. G-72-1154
(U)

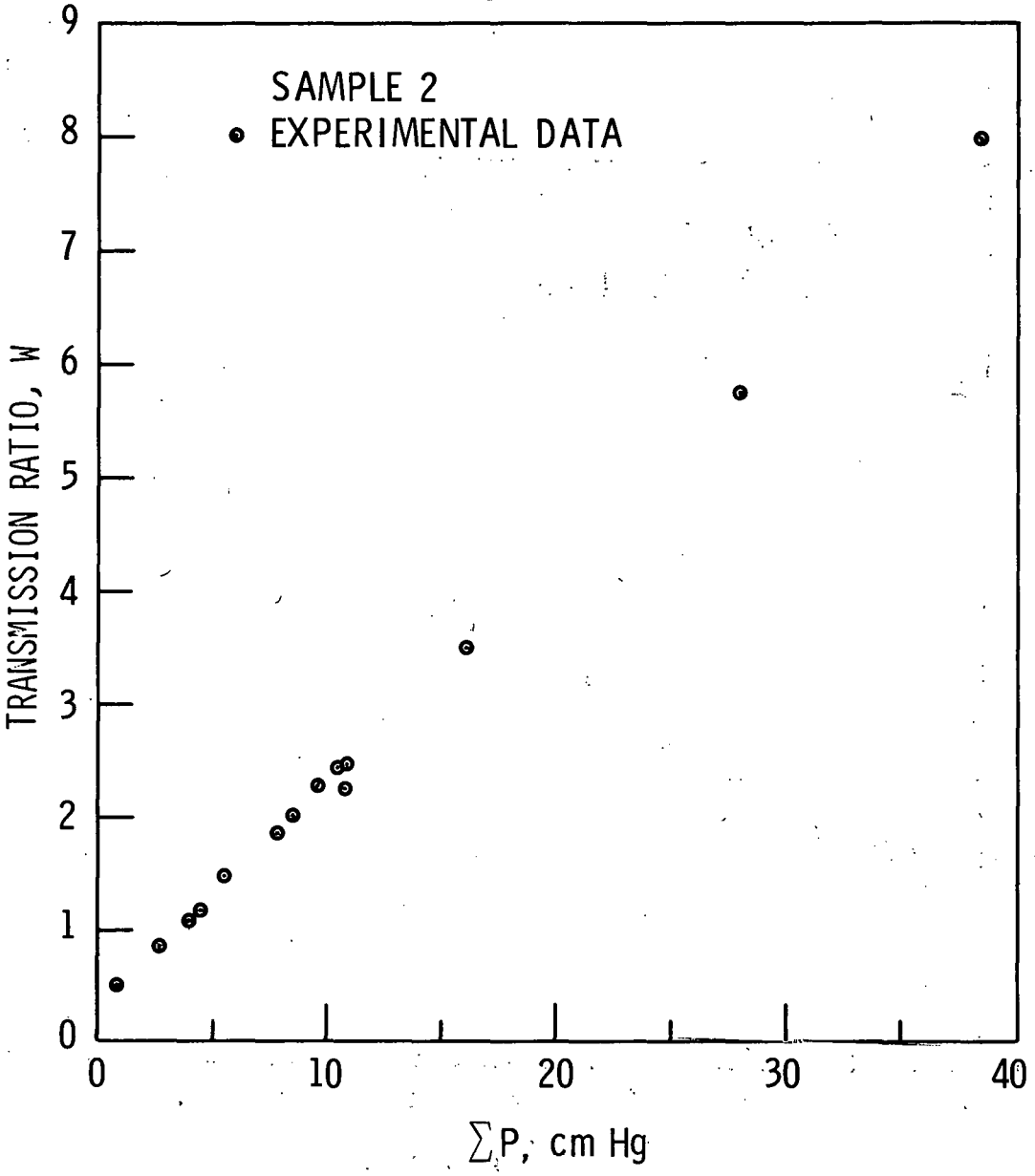

Figure 2

HIGH PRESSURE NITROGEN FLOW DATA FOR
A 25.97-MICRON-RADIUS ORIFICE SAMPLE

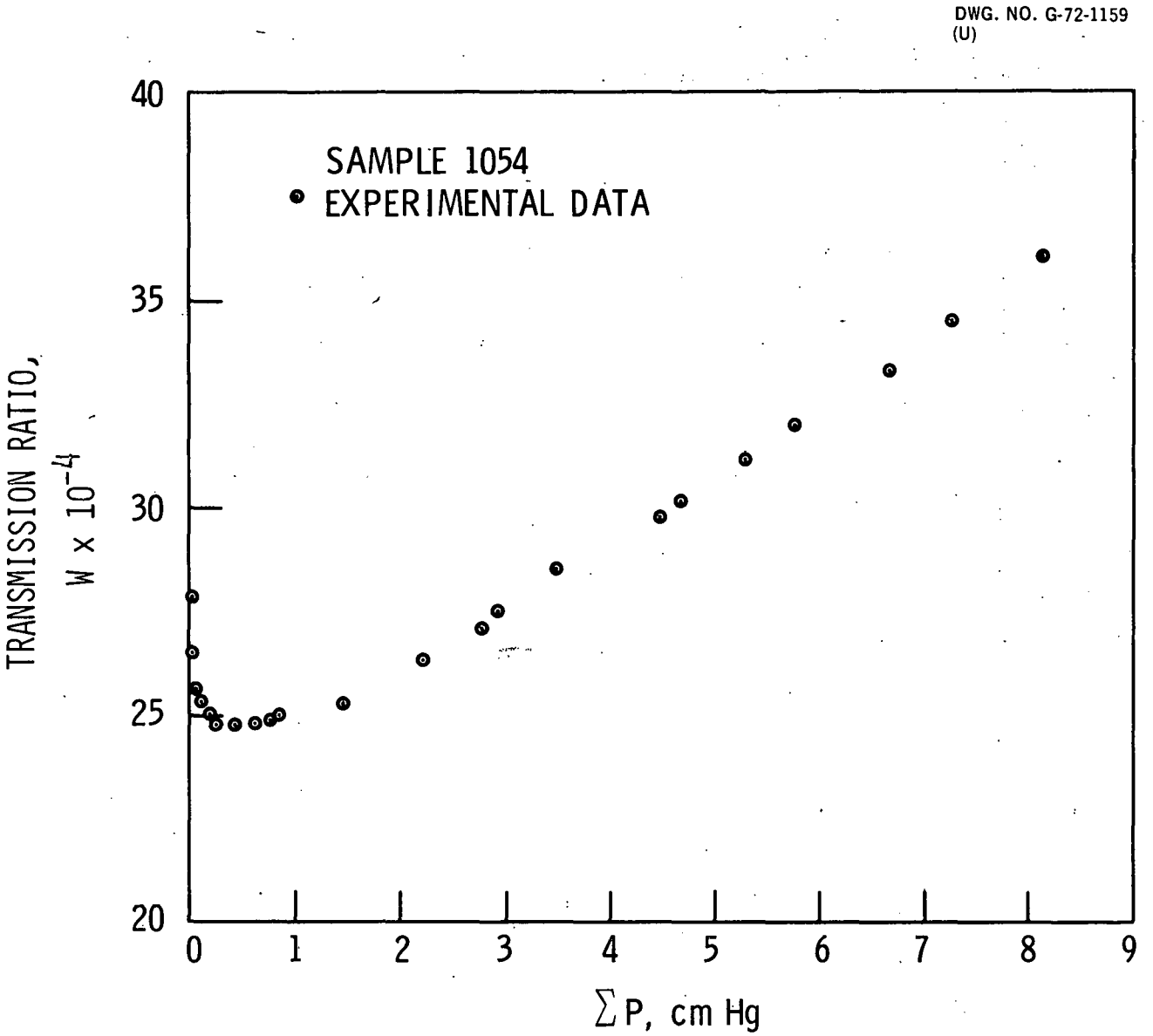

Figure 3

LOW PRESSURE NITROGEN FLOW DATA FOR
A 4.907-MICRON-RADIUS GLASS CAPILLARY

DWG. NO. G-72-1157
(U)

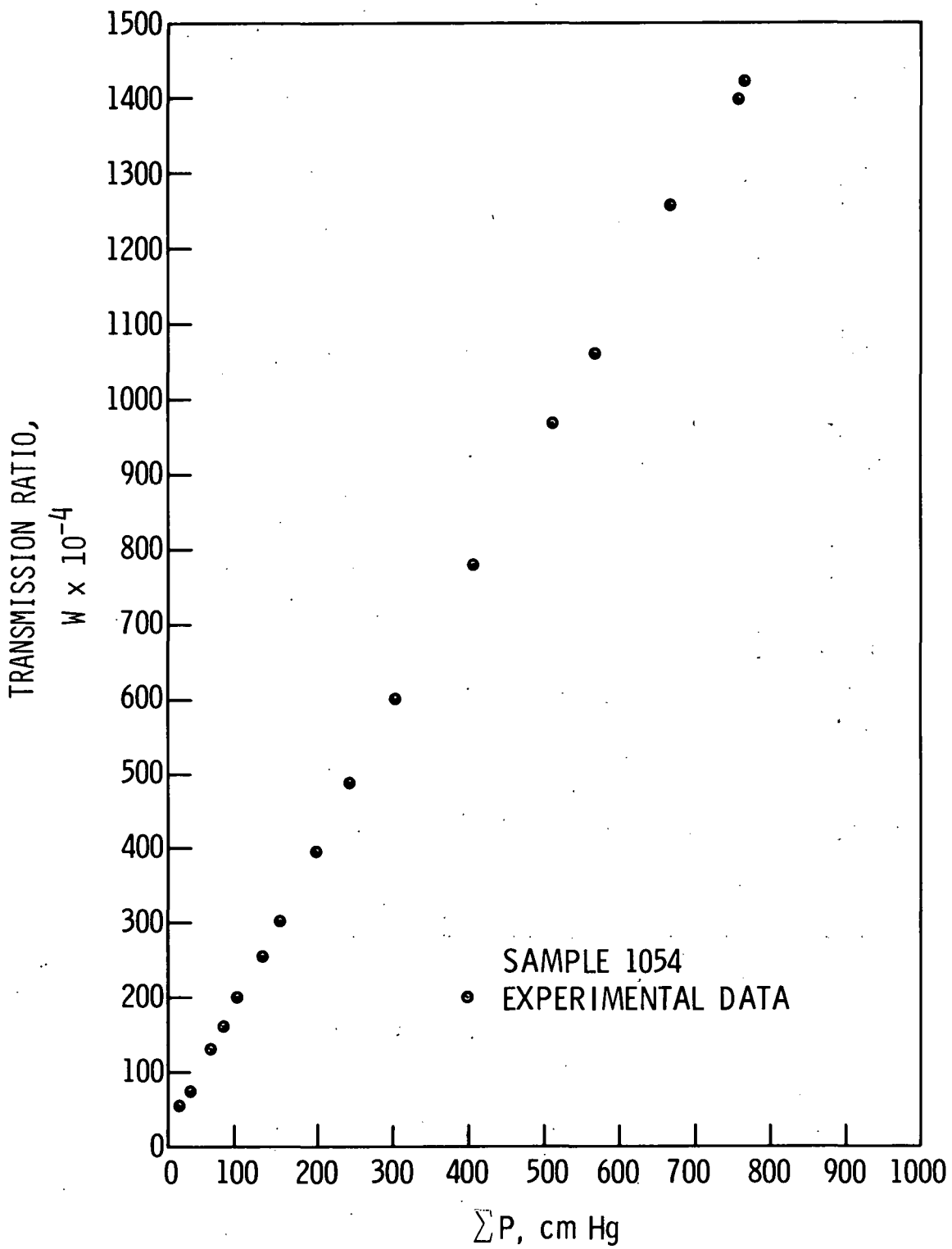

Figure 4

HIGH PRESSURE NITROGEN FLOW DATA FOR
A 4.907-MICRON-RADIUS GLASS CAPILLARY

DWG. NO. G-72-1158
(U)

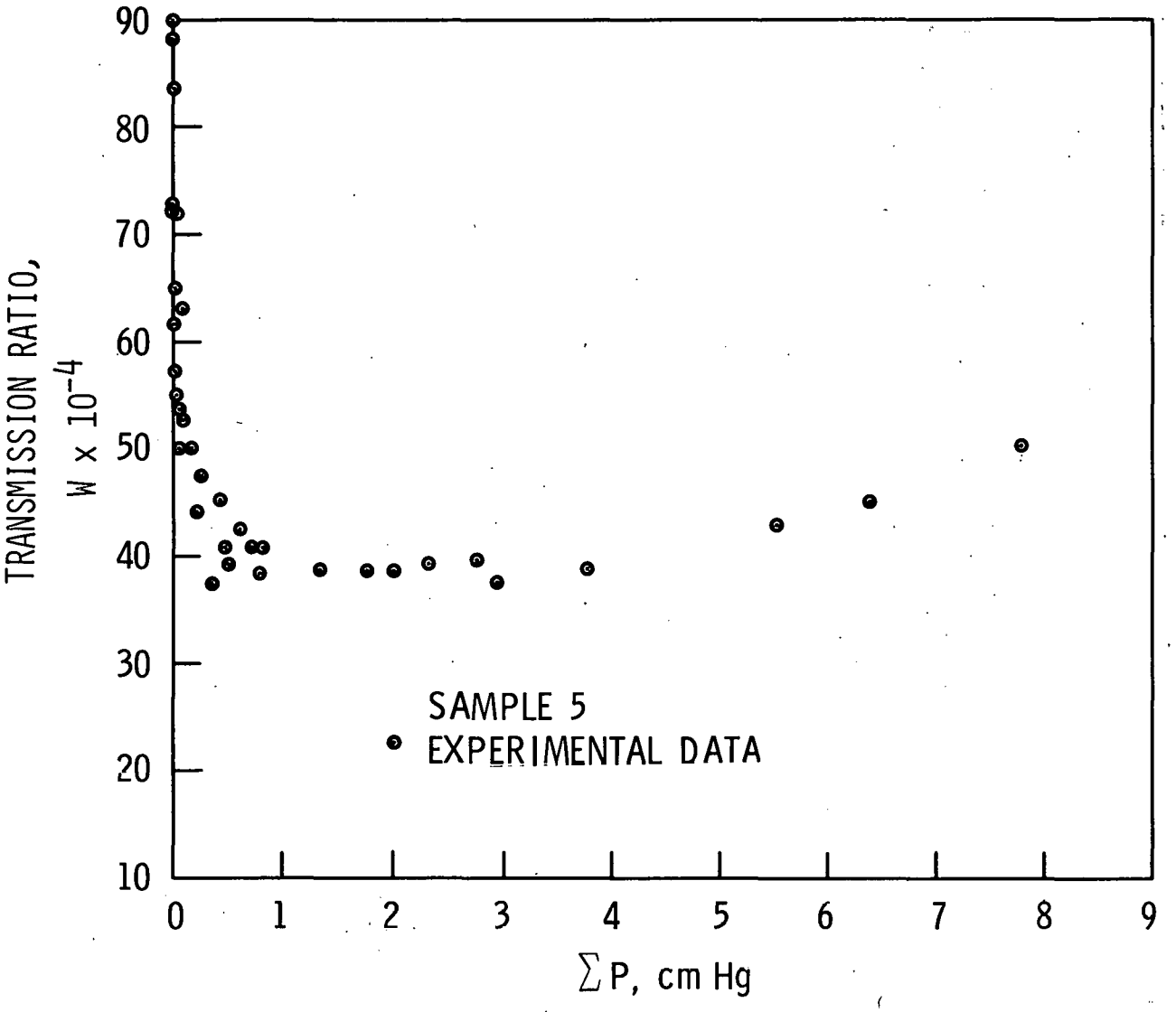

Figure 5

LOW PRESSURE NITROGEN FLOW DATA FOR
A 10.29-MICRON PARALLEL PLATE SAMPLE

DWG. NO. G-72-1156
(U)

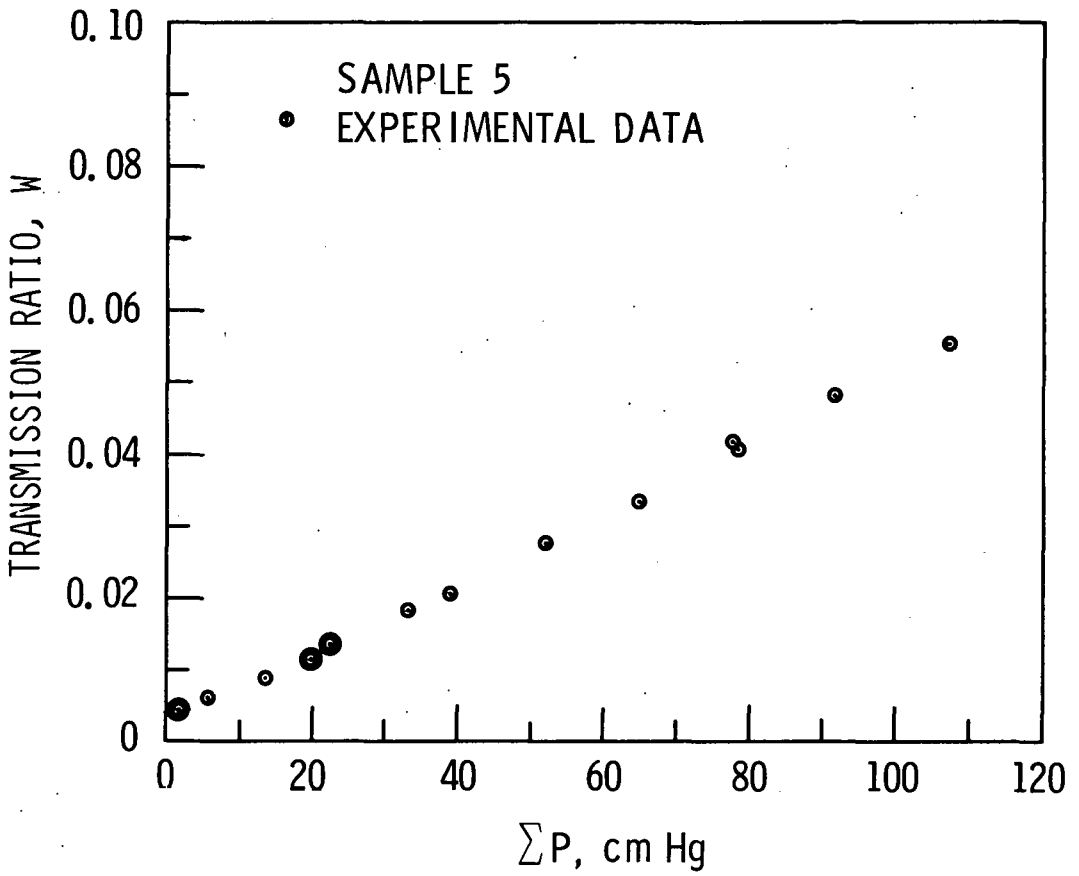

Figure 6

HIGH PRESSURE NITROGEN FLOW DATA FOR
A 10.29-MICRON PARALLEL PLATE SAMPLE

the transport through capillaries of any length-to-radius ratio. Other notable works include Scott and Dullien in 1962 [17], Fryer in 1966 [18], and Barrer and Nicholson in 1966 [19].

The superposition idea gives a good mechanistic picture of the transport phenomena, but it remains a model since there is no mathematical derivation of the slip term. However, analytical results are presently being obtained with the use of the linearized Boltzmann equations. This was first accomplished in 1963 by Albertoni, Cercignani, and Gatusso [20] for an infinite parallel plate. A more recent reference is the work of Maegley and Berman [21] with an annulus.

BINARY SEPARATION

After Aston's work in 1920, Hertz [22] in 1932 and Woolridge and Smythe [23] in 1936 set up cascades using porous tubes to separate neon isotopes. However, no experimental or theoretical work was done on the pressure dependence of the separation of a binary gas mixture. During World War II, when interest in separating uranium isotopes became of military significance, separation by gaseous diffusion was naturally considered. A great deal of both theoretical and experimental work ensued. Present and deBethune [1] and Bosanquet [24], working independently, developed a theory for the separation of gases flowing through uniform capillaries. Bosanquet used an approach based on generalized diffusion coefficients, and Present and deBethune used an approach based on momentum transfer. Using simple one-dimensional kinetic theory, Present and deBethune calculated the momentum transferred from one gas to the other by intermolecular collisions. These intermolecular collisions decrease the net drift velocity of the lighter gas and increase the net drift velocity of the heavier gas. The separation is therefore less than that which would be observed if the intermolecular collisions had not occurred. This momentum transfer between molecules does not change the total free molecule flow, but simply the ratio of the free molecule components of the two gases. In order to complete their theory, they added viscous flow as a nonseparative component. Thus, they assumed that the total flow was the sum of free molecule and viscous flows. This assumption is consistent with experimental data on porous materials where no Knudsen minimum is observed in the specific flow at low pressures. However, with long capillaries, long parallel plates, or any geometry which will result in a Knudsen minimum in the specific flow at low pressures, the total flow is not the sum of the free molecule and viscous flows. Therefore, the assumption of additivity of the two flows is expected to be, at best, only a good approximation for these geometries.

In order to investigate the accuracy of the Present and deBethune theory, separation data with well-defined capillaries are needed. The only data that have been available were obtained by Huggill [25] in 1952. He used capillaries with diameters of about 0.08 mm and observed changes in concentration of mixtures of nitrogen-carbon dioxide, argon-carbon dioxide, and nitrogen-ethylene. Partial pressures were measured to determine concentrations. Huggill's results indicated that the rate of decrease

of light gas enrichment with increasing pressure was less than predicted by the theory. However, his separation data also showed an anomaly at the zero pressure limit: the separation was greater than would be predicted for pure free molecule flow. This deviation indicates an anomaly in the free molecule flow of one or both of the two components. Free molecule flow anomalies have been observed and are treated in some detail by Lund and Berman [3]. Because of the lack of purity of his gases, Huggill also had some difficulty with his partial pressure measurements. Thus, Huggill's main conclusion was that there are significant anomalies in the free molecule flow of different gas species, presumably because of differences in the scattering law from the walls of the capillaries for the different species of molecules. Because of these anomalies and the lack of sufficient precision, his separation data could not be used to check the theory of Present and deBethune.

A much more critical analysis of the theory can be made by separating isotopes where there should be no difference in the free molecule flow anomaly for the two isotopic species and where the theory is generally expected to be more nearly correct for other reasons. It is also important to obtain precise data with isotopes in the region where the initial slope of the separation efficiency vs. pressure difference curve can be accurately estimated, because the slope of this curve can be accurately related to the dimensions of the flow channel.

Recently, Malling [2] has used the Lund and Berman flow equations to derive an expression for the separation of a binary isotopic gas mixture. In his derivation, Malling assumed that the diffusional flow is ideally separative, the slip and viscous flow are nonseparative, and there is no coupling between the separative and nonseparative flows. Although the derivation of Malling is different in principle from that of Present and deBethune, the differential equations for separation which are obtained by the two methods are quite similar. The advantage of Malling's formulation over that of Present and deBethune is that there are several parameters which account for the detailed differences in flow behavior data and therefore should produce a better correlation with separation data than the one-parameter equations of Present and deBethune.

Experimental Design

The primary purpose of the present work is to obtain data accurate enough to be used to test the accuracy of any model for the separation phenomenon. In order to obtain accurate experimental measurements, it is essential to use the least complicated test. There are two good reasons why so little experimental work has been performed on the separation of gases in regular capillaries. First, bundles of capillaries with sufficiently small diameters have not been generally available and are difficult to prepare. In order to measure a reasonable range in separation, the gas mean free path must be of the order of the diameter of the capillary. For large capillaries this means operating at low pressures. For example, measurements with neon at atmospheric pressure would require capillaries 1 μ in diameter or smaller; conversely, a 0.1-mm-diameter capillary would require

operating pressures below 0.01 atmospheres. However, if small capillaries were available, a large number of them would be required to provide the flow rate necessary to characterize the capillaries accurately and to obtain a gas sample large enough to analyze for mole fraction changes. A second reason for the lack of experimental data is the difficulty in accurately measuring the small changes in mole fraction produced by the phenomenon. In addition, the low pressures required make the separation measurements themselves rather difficult to perform.

Neon isotopes were chosen for use as the test gas because neon is a simple low molecular weight noble gas with only two natural isotopes which occur in significant amounts. The use of isotopes should eliminate anomalous separation data that would result from anomalies in the free molecule flow behavior of one of the isotopes relative to the other. The low molecular weight produces a high separation factor which can be accurately measured with a double-collector mass spectrometer. An additional advantage in using neon is that at a given pressure neon has a longer mean free path than that of most gases with an isotope pair. This allows higher separation with neon at a given pressure. For example, the pressure level needed to obtain a given separation efficiency can be twice as large for neon as that for argon.

MATHEMATICAL MODELS

PRESENT AND deBETHUNE MODEL (PBM)

In the theory developed by Present and deBethune [1] the flow rate is assumed to be the sum of two terms. One term represents the free molecule or Knudsen flow and the other represents the viscous or Poiseuille flow. When a single gas flows through a capillary, it is assumed that the Knudsen component is unaffected by molecular collisions. The molecules have the same mass and same average velocity so that the molecules cannot be distinguished before and after collision, and no net momentum is exchanged in a collision. However, when a binary mixture flows through a capillary, the two components have different average velocities and masses so that there can be a net momentum transfer between the unlike molecules due to collisions. The basis for the theory is the calculation of momentum transfer between the unlike molecules. The velocity of the faster, lighter molecule is reduced and that of the slower, heavier molecule is increased by the average momentum exchanged during collisions between unlike molecules. This decreases the relative amount of separation which occurs. In addition, the Poiseuille flow is the same for both molecules. This also reduces the amount of separation which occurs.

First, Present and deBethune considered the momentum transferred to the wall as a means of calculating the free molecule velocity:

$$m_1 u_1 \left(\frac{n_1 \bar{v}_1}{4}\right) 2\pi r dx = -\pi r^2 \left(\frac{dP_1}{dx}\right) dx \ . \tag{1}$$

The left-hand side of the equation is the momentum per second carried to a wall element of area $2\pi r dx$ by the molecules of component 1 with an average velocity of u_1 and a collision frequency of $(n_1\bar{v}_1)/4$. The right-hand side is the difference in the pressure at the entrance and exit to the element defined by the differential length dx.

$$\therefore \frac{dP_1}{dx} = \frac{m_1 \bar{v}_1 n_1 u_1}{2r} \ . \tag{2}$$

If Knudsen's expression for free molecule flow is put in this same form, then

$$\frac{dP_1}{dx} = \frac{3\pi m_1 \bar{v}_1 n_1 u_1}{16r} \tag{3}$$

which differs from equation (2) by a factor $3\pi/8$. Since equation (3) is generally considered to be the more accurate result, Present and deBethune used (3) in the further development of their theory. At this point a deviation from the original derivation of the theory will be made. A factor, K, will be introduced which will later be used to account for other geometries or any deviation in the relation between the mean velocity and the momentum transferred to the wall.

$$\frac{dP_1}{dx} = \frac{3\pi m_1 \bar{v}_1 n_1 u_1}{16Kr} \quad . \tag{4}$$

That is, K is the ratio of free molecule flow for any geometry to that for an infinitely long capillary with completely diffuse wall reflection as was calculated by Knudsen. If $u_1 > u_2$ and the scattering is isotropic in the center of mass coordinate system, then the average momentum of a molecule of component 1 after collision is

$$m_1 u_c = m_1 \left(\frac{m_1 u_1 + m_2 u_2}{m_1 + m_2}\right) \quad .$$

Since the average momentum before collision is $m_1 u_1$, the average momentum lost in one collision is

$$m_1(u_1 - u_c) = m^+(u_1 - u_2)$$

where m^+ is the reduced mass

$$m^+ = \frac{m_1 m_2}{m_1 + m_2} \quad .$$

Therefore, the average momentum loss per collision is proportional to the difference in the average velocity of the two molecules. This point is an important aspect of the problem and should be kept in mind when considering other geometries and flow anomalies.

The number of collisions per second per unit volume between unlike molecules is

$$n_1 n_2 \pi d_{12}^2 \left(\bar{v}_1^2 + \bar{v}_2^2\right)^{1/2}$$

and the momentum transferred per unit time per unit volume from component 1 to component 2 would appear to be

$$M_{12} = m^+(u_1 - u_2)\, n_1 n_2 \pi d_{12}^2 \left(\bar{v}_1^2 + \bar{v}_2^2\right)^{1/2} \tag{5}$$

on the average. This development of the theory is very instructive, but Present and deBethune pointed out that the average momentum transferred is not quite the same as the average momentum loss per collision times the number of collisions. Furthermore, the assumption of "hard elastic sphere" molecules is unnecessarily restrictive. It was then shown that the momentum transferred per unit time per unit volume can be put into the form

$$M_{12} = (u_1 - u_2) \frac{n_1 n_2 kT}{n D_{12}} \quad . \tag{6}$$

In this form the use of the experimental value for the diffusion coefficient, D_{12}, avoids the two above objections.

Now the momentum balance equations are

$$-\pi r^2 \frac{dP_1}{dx} = \frac{3\pi}{8K} m_1 u_1 \left(\frac{n_1 \bar{v}_1}{4}\right) 2\pi r + (u_1 - u_2) \frac{n_1 n_2 kT}{n D_{12}} \pi r^2 \tag{7}$$

$$-\pi r^2 \frac{dP_2}{dx} = \frac{3\pi}{8K} m_2 u_2 \left(\frac{n_2 \bar{v}_2}{4}\right) 2\pi r - (u_1 - u_2) \frac{n_1 n_2 kT}{n D_{12}} \pi r^2. \tag{8}$$

The abbreviation

$$b = \frac{8Kr}{3\pi} \left(\frac{kT}{2m}\right)^{1/2} \frac{\langle m^{1/2} \rangle_N}{(m_1 + m_2)^{1/2}} \frac{1}{pD_{12}} \tag{9}$$

is introduced, with

$$\langle m^{1/2} \rangle_N = N m_1^{1/2} + (1 - N) m_2^{1/2}.$$

N denotes the mole fraction of component 1.

Poiseuille flow is also introduced as being additive. Then

$$G_1 = \frac{2}{3} \frac{\bar{v}_1}{kT} Kr \left\{ \frac{1}{(1 + bP)} \frac{d(NP)}{dx} + \frac{m_1^{1/2}}{\langle m^{1/2} \rangle_N} \frac{NbP}{(1 + bP)} \frac{dP}{dx} + NaP \frac{dP}{dx} \right\}. \tag{10}$$

The first term is inversely proportional to $m_1^{1/2}$ and is ideally separative. The second and third terms are nonseparative. Equation (10) can now be rewritten for both components, and the differential equation for separation efficiency is obtained by setting the ratio of the molecular flows equal to the ratio of the mole fractions of components 1 and 2 in the outlet or product stream:

$$\frac{G_1}{G_2} = \frac{N_1}{1 - N_1}. \tag{11}$$

This differential equation can be converted into one for the separation efficiency by defining $Z = \delta/\delta^*$ where $\delta = N_1 - N$ and $\delta^* = N_1 - N^*$. N^* is the feed concentration necessary to give a product concentration of N_1 with a perfect Knudsen barrier operating at zero backpressure.

It is shown that for most cases (m_2/m_1 not too large) the differential equation can be integrated to give

$$Z = \frac{\int_{P_b}^{P_f} \exp\left[\left(\frac{\bar{f}b + a}{h}\right)P + \frac{ab}{2h} P^2\right] dP}{P_f \exp\left[\left(\frac{\bar{f}b + a}{h}\right)P_f + \frac{ab}{2h} P^2\right]} \tag{12}$$

where

$$\bar{f} = m_2^{1/2} \Big/ \langle m^{1/2} \rangle_N$$

$$h = 1 + (f^* - 1)(1 - N_1)$$

$$a = \frac{3K'r}{16\eta\bar{v}_2 K}$$

where K' is the ratio of Poiseuille flow for any geometry to that for a long capillary. As with the constant K, the constant K' does not appear in the original Present and deBethune theory. In this work equation (12) is referred to as the Present and deBethune equation.

As can be seen from this derivation, factors that affect the free molecule flow will affect the a and b values through the constant K. For example, deviations in the wall scattering law such as specular reflection or back-scattering will affect the a and b values through the constant K. Changes in geometry will affect a and b through both the constants K and K'.

There are three approximations which should be considered. The first is a perfect barrier. There are several ways to arrive at the same result. The easiest is to set a = b = 0. Then Z = (1 - w) is the separation efficiency of a perfect barrier, and Z/(1 - w) is the separation efficiency ratio, i.e., the ratio of the separation efficiency of a barrier to that for a perfect barrier operating with the same pressure ratio. The second is the effect of assuming no viscous flow. This can be done easily by setting the constant a = 0. Then the differential equation for the separation efficiency can be integrated to give

$$Z = \frac{\Delta P}{P_o} \frac{(1 - e^{-X})}{X}$$

where

$$X = \frac{\bar{f} b \Delta P}{h}$$

or

$$\frac{Z}{1 - w} = \frac{1 - e^{-X}}{X} .$$

An expansion of this equation gives

$$\frac{Z}{1 - w} = 1 - \frac{\bar{f} b \Delta P}{2h} + \frac{1}{3!} \left(\frac{\bar{f} b \Delta P}{h}\right)^2 + \ldots . \qquad (13)$$

This shows that when viscous flow is insignificant, i.e., at low average pressures, the separation efficiency ratio is linear with ΔP, the pressure difference across the separating element. This expression can be used to estimate the capillary radius when the initial slope of the separation efficiency ratio vs. pressure difference curve is known.

A third approximation can be obtained by expanding equation (12) to obtain

$$\frac{Z}{1-w} = 1 - \left(\frac{\bar{f}b + a}{h}\right)\frac{\Delta P}{2} + \left(\frac{\bar{f}b + a}{h}\right)^2 \frac{\Delta P^2}{3!} + \ldots . \qquad (14)$$

This gives the same results as (13) except the initial slope is increased by the additive factor a. This expression can also be used to estimate the capillary radius. It is particularly interesting to note that for a nearly perfect separation efficiency ratio the deviations from perfect behavior depend on the pressure difference and not on the average pressure.

MODIFIED PRESENT AND deBETHUNE MODEL (PBFM)

The Present and deBethune theory assumes the strict additivity of free molecule and viscous flows. It has been proven experimentally that this, in general, is not correct. Strict additivity appears to be correct only for porous materials. Therefore, the PBM theory can at best be considered a good approximate theory. An attempt has been made to modify the PBM theory to account for the known difficulties and also to produce better agreement with the experimental data obtained in this work.

In the PBM theory it is seen that the momentum transferred between unlike molecules is directly proportional to the difference in the velocity of the two molecules. Therefore, anything which increases or decreases the two velocities by the same ratio will increase or decrease the amount of momentum transferred between them. The minimum which is observed in the specific flow curves for long capillaries and parallel plate geometries is evidence of a decrease in the specific velocity of the gases. This minimum is observed for all gases. It therefore corresponds to approximately the same decrease in the specific flow velocity for both species of molecules in a binary mixture, and therefore the decrease in specific flow evidenced by a Knudsen minimum should correspond to a decrease in the momentum transferred between unlike molecules.

The b constant in the Present and deBethune equations can be affected by changes in the specific flow velocity through the constant K. Therefore, one way to reflect these changes in specific flow into the separation theory is to pressure-weight the b constant so that it varies from the free molecule value at zero pressure to the slip flow value at high pressure. It can be shown that for parallel plate geometry the contribution to the wall collision frequency from molecules leaving another wall is

$$\nu_w = \frac{n\bar{v}}{4}\left[\exp\left(-\frac{h}{\lambda}\right) - \frac{h}{\lambda}\exp\left(-\frac{h}{\lambda}\right) + \frac{h^2}{\lambda^2} E_1\left(\frac{h}{\lambda}\right)\right] \qquad (15)$$

where E_1 is the exponential integral, h is the plate separation, and λ is the mean free path. The contribution from molecules which had their last collision in the gas phase is

$$\nu_g = \frac{n\bar{v}}{4}\left[1 - \exp\left(-\frac{h}{\lambda}\right) + \frac{h}{\lambda}\exp\left(-\frac{h}{\lambda}\right) - \frac{h^2}{\lambda^2} E_1\left(\frac{h}{\lambda}\right)\right] . \qquad (16)$$

It may be assumed that a molecule striking a wall has a velocity equivalent to the free molecule value if it had its last collision with another wall and a velocity equivalent to the slip velocity if it had its last collision in the gas phase. Then a pressure-weighting function of this type should be appropriate to make the b constant in the Present and deBethune equation vary from the free molecule value at zero pressure to the slip flow value at high pressures. The third term in equation (15) is a small contribution, and so it was dropped for calculation convenience. The changes in the b constant caused by changes in the relation between the average velocity and the momentum transferred to the wall were introduced through the constant K.

Therefore the constant K is pressure-weighted according to

$$K_P = K \left\{ \left[\exp\left(-\frac{Br}{\lambda}\right) - \frac{Br}{\lambda} \exp\left(-\frac{Br}{\lambda}\right) \right] + \frac{W_m}{W_K} \left[1 - \exp\left(-\frac{Br}{\lambda}\right) + \frac{Br}{\lambda} \exp\left(-\frac{Br}{\lambda}\right) \right] \right\}, \tag{17}$$

where

B = a constant depending on geometry

r = capillary radius or plate spacing

λ = mean free path

W_m = Maxwell transmission ratio (transmission ratio from a linear extrapolation of Poiseuille flow)

W_K = free molecule transmission ratio.

The modification is accomplished by using K_P instead of K as given in the previous section. This change should roughly account for changes in both the a and b values due to variations in the velocity at the wall because of geometry, wall scattering law, or pressure dependence.

This type of approximation insures that it will also represent the flow data fairly well since it must agree at the high and low pressure limits and produce a pressure-weighted variation in between. A detailed inspection of this type of approximation to the flow equations has not yet been made. It should be obvious from this study that a much better approximation is needed to represent flow data than that required to represent the separation data.

GENERAL CAPILLARY MODEL (GCM)

G. F. Malling has used the Lund and Berman flow equation to form a general capillary model, GCM, for separation. Malling has used extensive arguments to justify the results and certain significant further variations can be introduced, but in its present simplest form the Lund and Berman flow equations were used for the component equations instead of equations (10) as used by Present and deBethune. The partial pressure gradient was used with the diffusion term, and the total pressure gradient was used with the slip and viscous terms.

The general equations are rather complex and, of course, machine calculations are required, but for comparison with the Present and deBethune equation they reduce to the following for long capillaries.

Lund and Berman's equation is

$$G = \frac{\bar{v}\Delta P}{4kT}\left\{\frac{(8/3)F}{L[c + (20/9\pi A^*)X]} + \frac{X}{4L}\left[1 + \frac{2.368\,\sigma A^*}{A^* + 0.592X}\right]\right\} \qquad (18)$$

where $X = (r\Sigma P/\eta\bar{v})$, also $X \propto (r/\lambda)$, c represents deviations from ideal free molecule flow, and σ represents the slip flow constant which is also affected by deviation in the wall scattering law. A* represents variations in the collision integrals for different molecules. F is a function which differs no more than 5% from unity and is equal to the ratio of the Pollard and Present to Bosanquet diffusion coefficients. It can easily be shown that

$$X = 1.414A^*bP$$

where b is the same as in the Present and deBethune equations.

The above equation (18), in the same form as equation (10), is

$$G = \frac{2\bar{v}_1 r}{3kT}\left\{\frac{F}{(c + bP)}\frac{\Delta P_1}{L} + \frac{0.6915\ (\sigma/\sigma_o)\ bP}{(1.094 + 0.9158bP)}N\frac{\Delta P}{L} + NaP\frac{\Delta P}{L}\right\}. \qquad (19)$$

If the Lund and Berman equations are considered as differential equations and $(\Delta P_1/L) \to (dP_1/dx)$ and $(\Delta P/L) \to (dP/dx)$, then there are only two significant differences between equations (10) and (19). The coefficient of the second term is smaller for the GCM than for PBM and is the primary source of the differences in the calculated separation efficiencies for the same long capillary. Nominal values of c and σ from flow data are $c = 1$ and $\sigma = \sigma_o = 1.84$. But, for example, if $c = 1$ and $\sigma = 1.446\sigma_o$, then nearly identical results will be obtained with either model. The other significant difference is in the manner in which deviations in the free molecule and slip flows due to wall scattering law deviations enter into the models. In the GCM, these deviations affect the equations through c and σ. In the PBM the effect is to change the a and b constants. This causes the PBM and therefore also the PBFM to have a stronger dependence on the deviations from ideal free molecule and slip flow than does the GCM. These will be emphasized further in the discussion of results.

The close correspondence between the forms of the GCM and PBM is probably sufficient to justify the assumption that the Lund and Berman equations should be differential equations instead of integrated equations as they were originally presented. Malling has made the calculations shown in figure 31 where bP in equation (19) was replaced by $b\bar{P}$. While this is not the same as using the differentiated Lund and Berman equations, it does show significantly different results and further indicates that the Lund and Berman equations should be differential equations.

EXPERIMENTAL TEST SAMPLES

SAMPLE SELECTION

In order to obtain data that can be used in evaluating a mathematical model, it is essential that the samples have very well-defined geometries. It would also be desirable to obtain data on samples that have different geometries. The geometries should exhibit the largest possible differences in their flow characteristics. The three geometries that have the greatest difference in their flow behavior in the transition region between free molecule flow and Poiseuille flow are the orifice, the long capillary, and the parallel plate channel. The orifice is a circular capillary with a length-to-radius ratio approaching zero, and a long capillary is a circular capillary with its length large compared to its radius.

If a curve is plotted of specific flow vs. average pressure, in the transition region between free molecule and Poiseuille flow the following will be noted:

1. For a *short capillary*, where the length of the capillary is approximately 2 to 5 times its radius, the specific flow curve is essentially linear over the entire pressure range.

2. For a *long capillary*, where the capillary length is greater than approximately 12 times its radius, the specific flow curve will show a shallow minimum of as much as 10%.

3. A *parallel plate channel* will show a very deep minimum of 50% or greater in the specific flow curve.

Because of these significant differences in the flow characteristics and the differences predicted by the theories, a short capillary, a long capillary, and a parallel plate were chosen as the samples to be used for separation measurements. Examples of the flow curves obtained on representative test samples are shown in figures 1 through 6. Where possible, similar samples were prepared with different materials so that the surface finish would be different. By choosing different materials, the effect of gas phase flow anomalies such as specular reflection and backscattering on the flow and diffusion phenomena can be investigated. For example, one set of glass capillaries was fire polished to smooth the surfaces. Table 1 shows a description of the samples which were prepared for separation measurements.

SAMPLE PREPARATION

Test sample preparation was a particularly important part of this work. Capillary test samples with the smallest possible diameters were desired to allow the highest operating pressures. However, small diameters made it necessary to have a large number of capillaries mounted in parallel in order to have large enough flow rates to characterize the sample and to collect sufficient gas for analysis by the mass spectrometer.

Table 1

TEST SAMPLE CHARACTERISTICS

Sample Number	Sample Material	Number of Capillaries	Capillary Radius,[a] microns			Length Centimeters	Length Radius
			Poiseuille Flow	Kentron Microscope	Quantimet Area		
212	Epoxy Resin	212	24.62 ± 0.17	24.81 ± 0.55[b]		0.498 ± 0.013	202
838	Epoxy Resin	838	12.91 ± 0.07			0.772 ± 0.016	598
924	Methyl Methacrylate	924	12.64 ± 0.04	12.46 ± 0.39[b]		0.579 ± 0.018	458
1054	Glass	1054	4.91 ± 0.01	4.75 ± 0.27[c]	4.980 ± 0.001[c]	0.437 ± 0.001	891
64	Glass	64	22.01 ± 0.05	24.33 ± 7.0[c]		0.995 ± 0.004	452
2	Gold Foil	10	25.97 ± 0.20	29.7 ± 2.1[c]	26.8 ± 0.8[c]	0.0111 ± 0.0003	4.3
1	Steel	2 x 0.9 cm[d]	25.58 ± 0.04[e]			0.907 ± 0.002	356
5	Steel	2 x 0.9 cm[d]	10.29 ± 0.03[e]			0.907 ± 0.002	884

[a]Comparison of capillary radius measured by three techniques.

[b]Samples prepared in the same manner, but polished by metallographic techniques before measuring.

[c]These samples were not polished; therefore, focus and definition of diameter were difficult.

[d]Width and length of plates.

[e]Height or spacing between plates.

Capillary Samples

The first test samples were made from two different sizes of glass capillaries. Each required a somewhat different fabrication method. The largest size capillary tubing which was used to prepare test samples had a nominal inside diameter of 2 mils or 50 μ and an outside diameter of 0.25 in. The first step in the preparation was to score and break the tubing into 1-cm lengths. The tubing was broken rather than cut to avoid getting dust into the capillaries. Because of the large outside diameter, some of the excess glass was removed by grinding the diameter so that more capillaries could be placed in a given sample area. Wet grinding was used and care was taken to avoid getting dust into the capillaries. After the grinding operation, the glass tubing had a triangular-shaped outside cross section. To be certain the capillaries were still open, a 1-mil wire was passed through each capillary. They were then cleaned with hot chromic acid and washed in distilled water. The capillaries were next heated to 550°C to clean them further and to give the wall a smooth, fire-polished surface finish. Small pieces of tape (Scotch transparent tape) were placed over each end of the capillary to avoid contamination during handling. The outside of the glass was coated with an epoxy resin wetting agent, and 64 capillaries were arranged on end on a piece of tape in order to hold them in position. This assembly was then placed in a silastic mold and the capillaries were cast in a block of epoxy resin. Care was taken not to cover the top of the capillaries with the epoxy resin. After the resin had hardened, the tape was removed and the sample was examined microscopically to assure that there was no adhesive obstructing the opening. The test sample was stored in a desiccator to avoid dust and possible moisture etching of the fire-polished surfaces. This sample was designated as sample 64. A photograph of the sample and one of the capillaries is shown in figures 7 and 8.

While test sample 64 provided an excellent sample, a test sample with a smaller radius was needed to provide separation data at higher separation efficiencies. Therefore, a search was made for smaller capillary tubing. A special order of capillary tubing with a tube diameter of 20 mils and a capillary diameter of approximately 10 μ was obtained from the Fredrich and Dimmock Glass Co. in Milleville, New Jersey.

Because of the small capillary diameter, a very large number of capillaries were required. The capillary tubing was first coated with a silane wetting agent; then the capillaries were scored and broken into approximately 3/16-in. lengths. In order to assemble this sample, a jig was made with two pieces of wire screen. The screens were separated by a spacer and positioned so that their grid structures were coincident. They were then fastened in position. The area available for the capillaries was confined to a rectangle 0.75 in. by 1.5 in. The 3/16-in.-long capillaries were placed in the first row of the wire screen grid structure. A silica-filled epoxy resin was carefully placed on the outside of each capillary and the top screen wire with a hypodermic needle. Enough epoxy resin was placed on each capillary to fill the void between them and the void in the screen. It was very important not to allow the epoxy resin to get into the next row of the grid. More capillaries had to be placed into

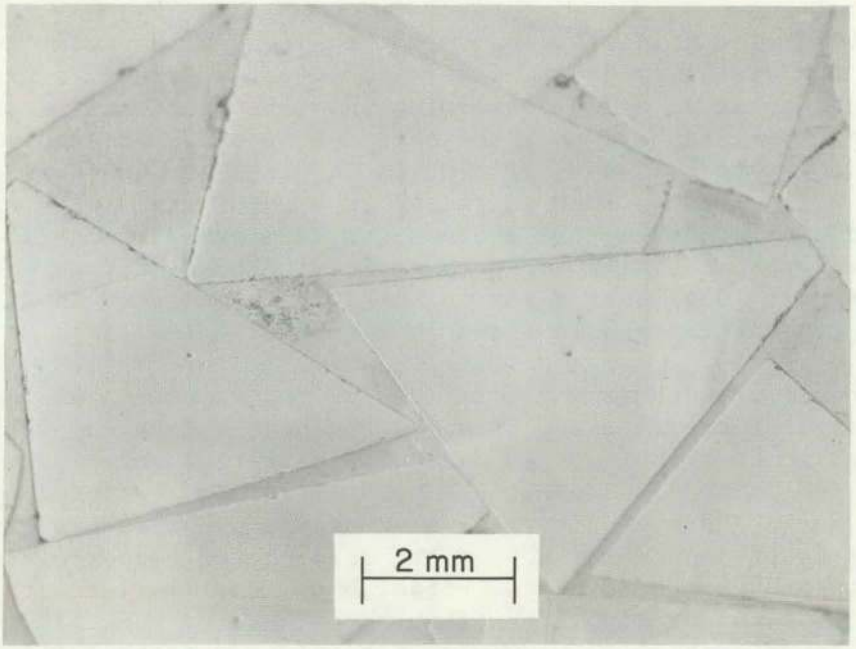

Figure 7
A SECTION OF SAMPLE 64

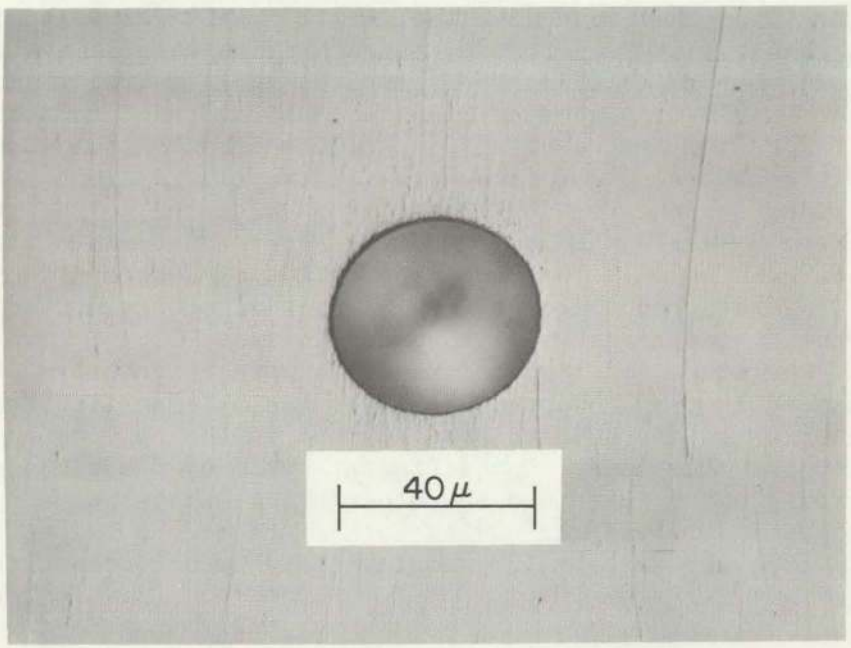

Figure 8
GLASS CAPILLARY FROM SAMPLE 64

the next row of the grid structure without allowing the epoxy to contact the end of the capillary during insertion into the screen. This process was continued until an array containing 1054 open capillaries was completed. After the epoxy resin hardened, the bottom screen was removed since its only purpose was to hold the capillaries in place during fabrication. The array of capillaries was then contained in a metal frame with epoxy resin. A prototype of the sample that shows a complete array of capillaries and wire screen grids, but with no epoxy resin, is shown in figure 9. The completed sample 1054 mounted in its metal frame is shown in figure 10, and one of its capillaries is shown in figure 11.

The glass capillaries were the first choice for preparing uniform, well-defined arrays of capillaries. But, as has been indicated previously, it is important to have capillaries made with different materials. An array of capillaries formed in a plastic block similar to that used by Huggill [22] seems to be the best alternative. Huggill prepared his arrays of capillaries by encapsulating copper and gold-plated copper wires in methyl methacrylate and then etching the copper out. Capillaries with length-to-radius ratios considerably larger than those used by Huggill were desired. Since very large etching times would be required using Huggill's method, other means of forming them were investigated. The following technique was developed.

First, stainless steel wire was wound around a rectangular frame as shown in figure 12. Then the frame with the wire in place was washed with trichloroethylene, sodium hydroxide, and distilled water. Next, it was dipped into an acetone solution of an experimental fluorocarbon surfactant, called FX-161, furnished by Minnesota Mining and Manufacturing Co. This deposited a monolayer coating of a fluorocarbon on the wires. Since hydrocarbons do not wet fluorocarbons well, the fluorocarbon coating would subsequently prevent the molding plastic from adhering to the wires. In order to make the sample the desired size, about 100 turns of the wire were wound on each frame. This gave approximately 200 capillaries from each frame. The desired number of capillaries were obtained by fastening several of the frames together with spacers between each frame. The frames with the wires in a vertical position were placed in a silastic mold. A plastic casting compound was deaerated by centrifuge and care was taken to see that no air bubbles were trapped in the casting compound as it was poured into the mold. Two different types of plastic samples were made: one using epoxy resin and the other using methyl methacrylate. Figure 13 shows a sample after having both sides of the frames cast in plastic. In this way two similar samples could be prepared with each set of frames.

After hardening, the sample was removed from the mold and the ends and bottom of the sample were ground off to remove the frame. The bottom was then metallurgically polished. At this point the wires were removed by pulling them out of the plastic one at a time using a microscope and a pair of tweezers. This was possible because the fluorocarbon prevented the plastic from adhering to the wires. Some of the wires did break when attempting to remove them; therefore all of the wires were not removed. Those that did remain in the sample were held very tightly and did not

PHOTO NO. PH-70-2302

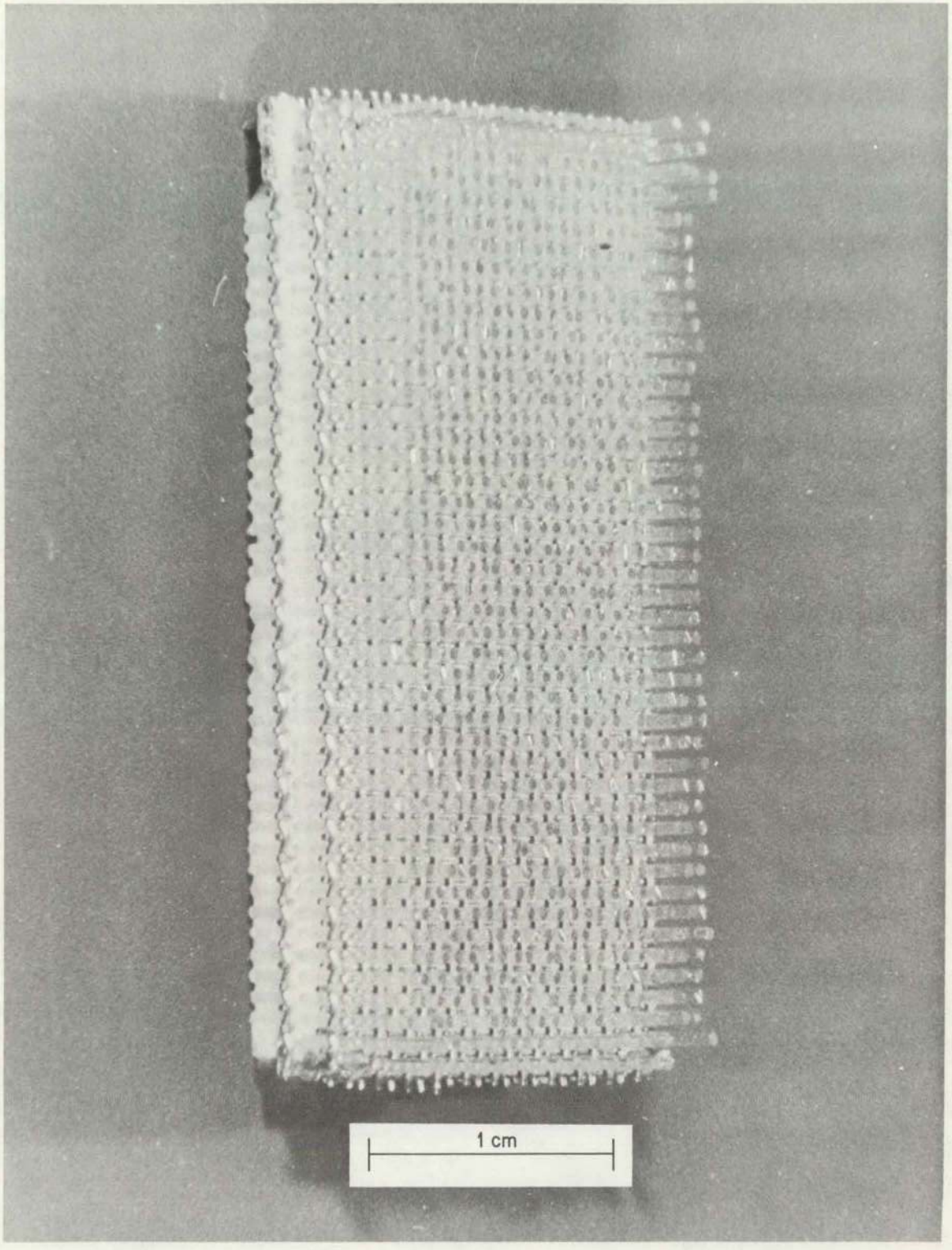

Figure 9
PROTOTYPE OF SAMPLE 1054

PHOTO NO. PH-70-2304

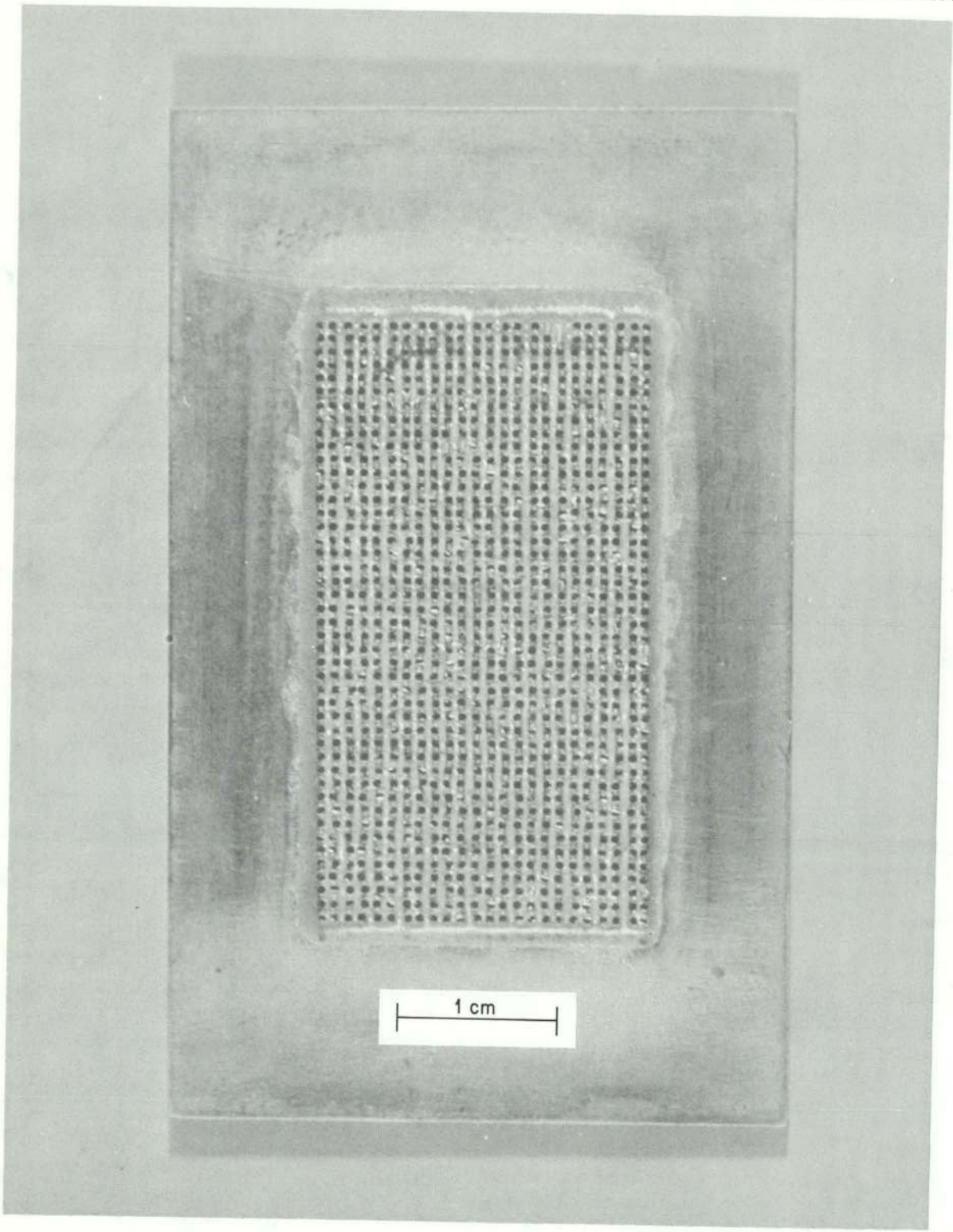

Figure 10
SAMPLE 1054

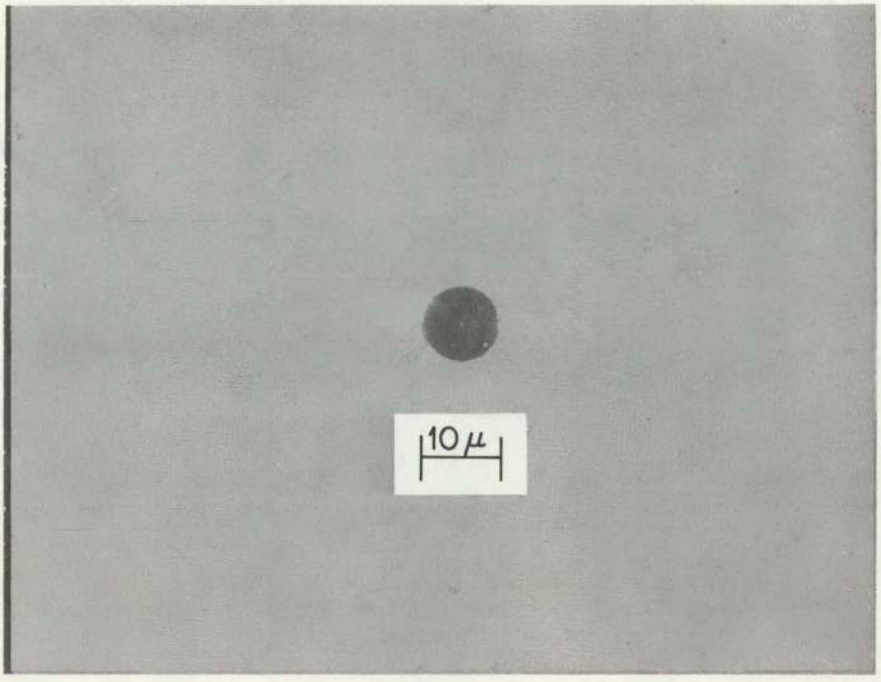

Figure 11
GLASS CAPILLARY USED IN SAMPLE 1054

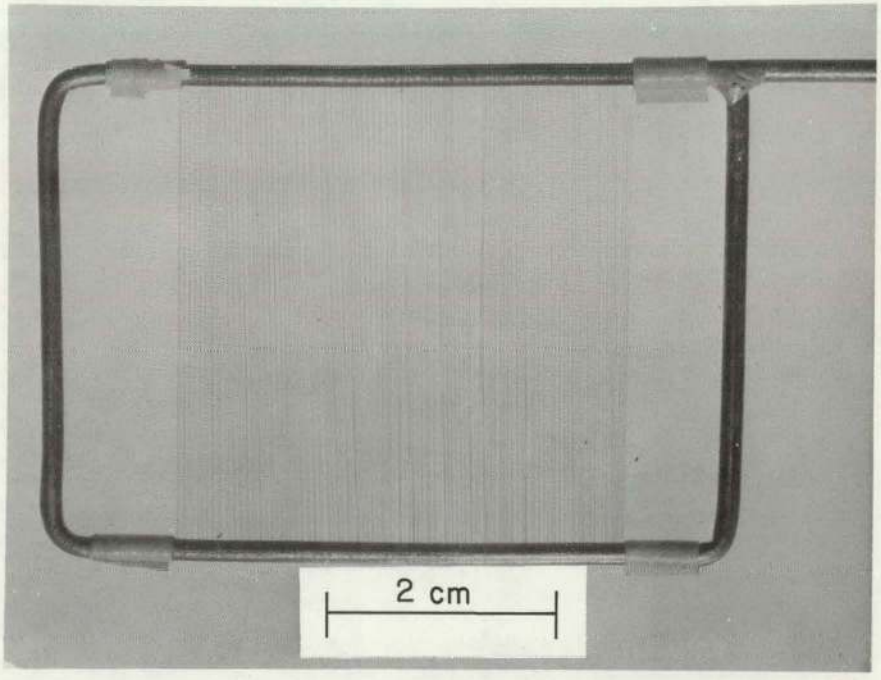

Figure 12
STAINLESS STEEL WIRE ON METAL FRAME

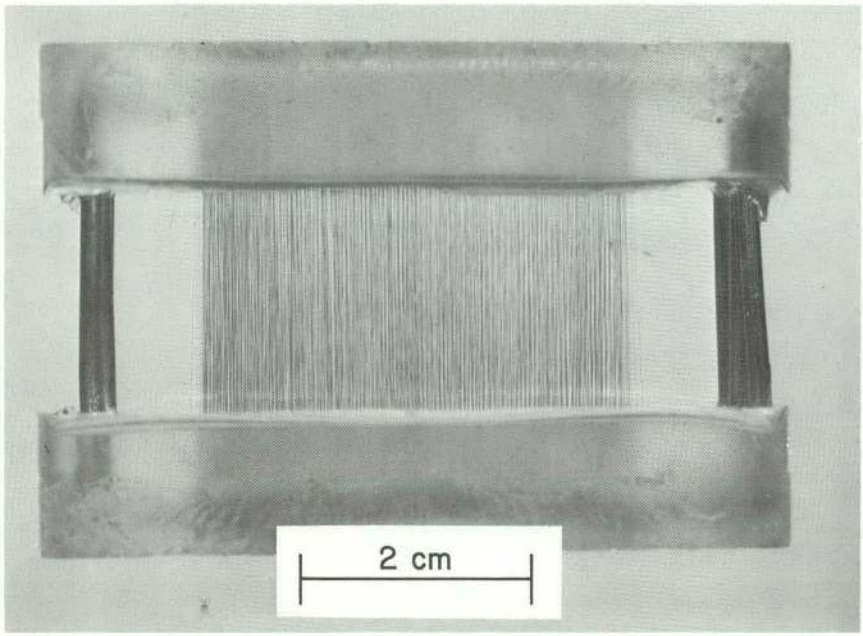

Figure 13
METAL FRAMES WITH STAINLESS STEEL WIRE CAST IN PLASTIC

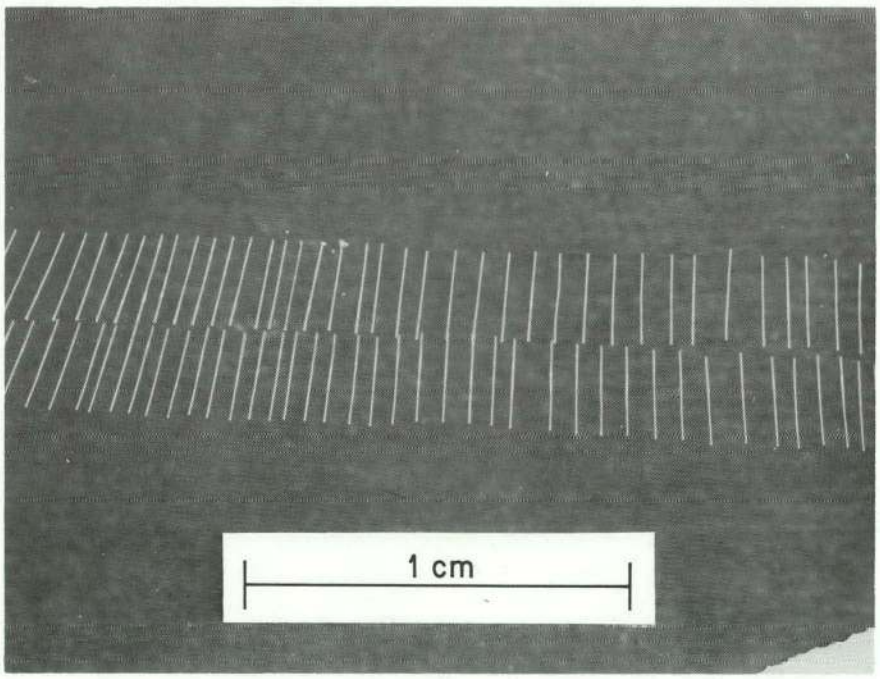

Figure 14
CAPILLARIES IN PLASTIC SAMPLE

represent a problem or adversely affect the sample. Again, because of the size of the sample holder, the area available for the capillaries was confined to a rectangle 0.75 in. by 1.5 in.

Samples were made with 1- and 2-mil-diameter stainless steel wire. The samples made with 1-mil wire contained approximately 1000 capillaries, and those with the 2-mil wire contained approximately 250 capillaries. Several samples of each size were made for flow measurements, and generally good reproducibility of 1% or better in the capillary radius inferred from the flow measurements was obtained. Figure 14 shows one of the preliminary samples made with methyl methacrylate and only two rows of capillaries.

Short Capillary Sample

Several methods were considered for preparing an orifice or short capillary sample. However, because of the many difficulties involved, a drilled metal foil was chosen. A 1-in. square of 5-mil-thick gold foil was rolled to a thickness of about 3 mils. Then ten 2-mil-diameter holes were drilled into the gold foil with a precision drilling instrument. The holes which were made were very slightly elliptical, but the biggest difficulty was in defining the length. The drilling process tended to push the soft gold through toward the back side, causing a mound which made the length of the capillaries larger than the foil thickness. However, the length was fairly well defined by optical measurements. Unfortunately, the capillaries were not perfectly clean. Several of the capillaries had significant burrs resulting from the drilling. These burrs were the primary source of the difference in capillary radius as observed by the area measured by an Imanco Quantimet Image Analyzer and the radius measured with a Kentron microscope. The length-to-radius ratio using the radius determined by the Quantimet was 4.3. Figure 15 shows one of the capillaries. This sample was designated sample 2.

Parallel Plate Samples

One of the requirements for the parallel plate samples was that the faces of the channel be very smooth, flat, and parallel. This was accomplished by using hardened steel grade A+ gage blocks, which have a flatness of 4 microinches and an RMS surface finish of 0.09 microinches. The gage blocks were thoroughly cleaned and degreased. The blocks were positioned with a metal foil spacer between them on each end to determine the approximate channel height. They were placed in a press and approximately 1000 psi. pressure was applied while epoxy resin was applied to the ends of the blocks to fasten them together. After the epoxy resin hardened, they were removed from the press and mounted in a plastic block. Figure 16 shows test sample 1.

FLOW MEASUREMENTS

While microscopic measurements were made to estimate the dimensions of the samples, the most accurate means of characterizing these small dimensions is with flow measurements. The Hagen-Poiseuille law for laminar flow of fluids is so well established that this law can be used to calculate the

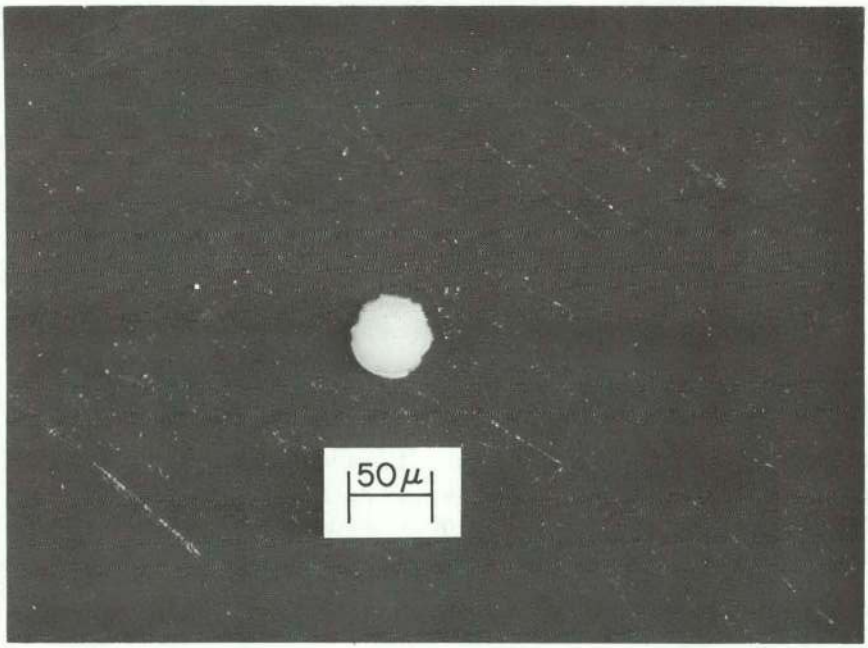

Figure 15
CAPILLARY IN GOLD FOIL

PHOTO NO. PH-72-2126

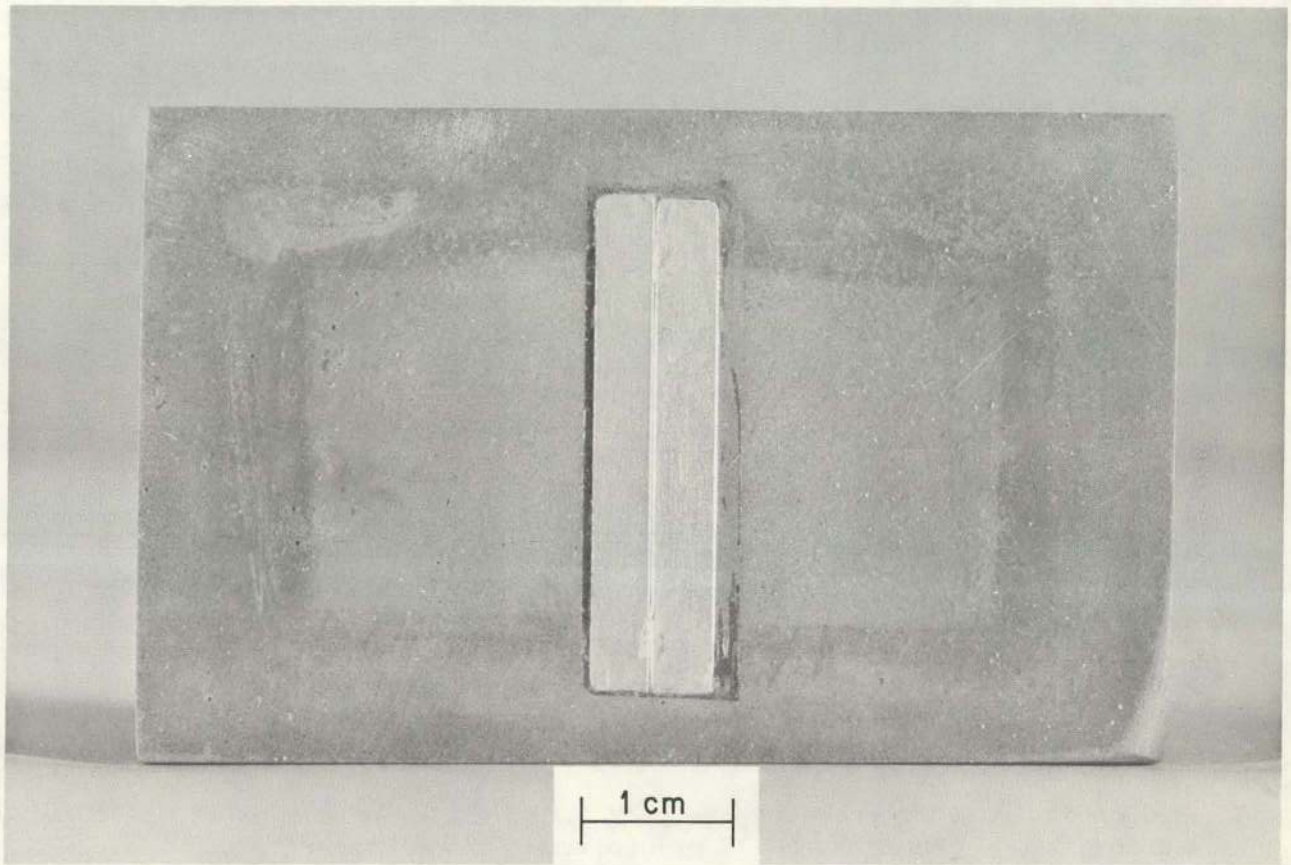

Figure 16
PARALLEL PLATE SAMPLE 1

appropriate characterizing dimension of a test sample. Very precise flow measurements were made on all of the test samples as part of a flow study which will be discussed in a later report. The measurements were made with a specially designed flow system which can be used to make either steady state flow measurements or pressure decay measurements at constant average pressure.

The steady state measurements were made by a volumetric technique in which the time required for a given pressure change in a calibrated volume was measured. The calibrated volume was evacuated at the beginning of a measurement so that the change in pressure was large compared to the starting pressure. This method reduces errors associated with temperature changes in the volume during the measurement time. However, the temperature of the volume was monitored and no significant changes were observed. The test sample was isolated from the calibrated volume with a needle valve which was operated with a critical pressure drop across it so that the pressure on the downstream side of the test sample was not affected by the pressure change in the calibrated volume. The pressure on the upstream side of the test sample was kept constant with a pressure regulator.

The pressure decay measurements were made with a specially designed test sample holder which made use of a small high vacuum butterfly valve. The sample was located on a flange very close to the butterfly. The holder was arranged so that when the butterfly was open, there was a volume of 100 cc on each side of the test sample. When the butterfly valve was closed, the volume on the valve side of the sample was divided into two segments. The segment between the sample and the valve was about 15 cc with the other segment about 85 cc. With the butterfly open, the holder was filled to some measured pressure. Then the butterfly was closed and the 85-cc volume was filled to a somewhat higher pressure. The butterfly was then opened and the time interval for a specific differential pressure decay was measured.

Reproducibility and regression analyses indicate the precision of the flow measurements was generally ±0.1% or better. Barocel capacitance manometers and the timing device which was triggered by the output from the Barocel were the principal reasons for the high degree of precision.

The pressure decay technique was used principally for the low pressure measurements where the specific flow deviates from linearity with pressure. The steady state measurements were made in the high pressure region where the specific flow was linear with pressure. The continuum expression for viscous flow through a capillary with slip at the wall as developed by Maxwell is given in Kennard [26]. Written in terms of the transport ratio, defined as the flow rate divided by the free molecule flow through an ideal orifice with the same cross-sectional area, this expression is

$$W\Lambda = S\Sigma P + W_m A \,, \tag{20}$$

where

$$S = \frac{\pi r^4}{2\eta\bar{v}\ell} \,.$$

The capillary radius can then be calculated from the slope, S, of the curve obtained by plotting the transport ratio times the area vs. the sum of the upstream and downstream pressures. The intercept at zero average pressure, W_mA, is also related to the capillary radius. Maxwell's slip theory given by Kennard shows that

$$W_mA = \frac{(2 - f)}{f} \frac{\pi^2}{2} \frac{r^3}{\ell} \tag{21}$$

where the gas interaction with the wall is divided simply into diffuse or random and specular or mirror reflections from the wall. The quantity f is the fraction of diffuse reflections. Hanks and Weissberg [27] calculate a value of the slip coefficient which gives

$$W_mA = \frac{(2 - f)}{f} \frac{2\pi^2}{3} \frac{r^3}{\ell} . \tag{22}$$

An exact solution using the modeled linearized Boltzmann equation gives W_mA equal to 1.1466 times Maxwell's value.

The corresponding expressions for the slope and intercept for a semi-infinite parallel plate channel are

$$S = \frac{wh^3}{6\eta\bar{v}\ell} \tag{23}$$

and

$$W_mA = \frac{(2 - f)}{f} \frac{\pi}{2} \frac{wh^2}{\ell} . \tag{24}$$

Berman [28] has shown that when backscattering is present instead of specular reflection, the term $(2 - f)/f$ is replaced by

$$\frac{2}{\pi} + \frac{\alpha}{2(2 - \alpha)}$$

where α is the fraction of diffusion reflections, and $1 - \alpha$ is the fraction of backscattered reflections.

The low pressure transmission ratios measured with the pressure decay method were also plotted against average pressure and extrapolated to zero pressure. According to Knudsen, the free molecule transport ratio for an infinitely long capillary should be

$$W_K = \frac{8}{3} \frac{r}{\ell} . \tag{25}$$

Smoluchowski [29] showed that specular reflections produce the same effect on free molecule flow as they do on slip flow:

$$W_K = \frac{(2 - f)}{f} \frac{8}{3} \frac{r}{\ell} . \tag{26}$$

For finite capillaries, Clausing [30] showed that an end correction was necessary, giving

$$W_K = \frac{(8/3)r}{\ell + \Delta \cdot r} . \tag{27}$$

The Clausing end correction, Δ, for capillaries is given by Lund and Berman [3]. DeMarcus [31] has made a more rigorous calculation confirming this result and also showed that the Maxwell correction for specular reflections apply but only for the infinite capillary. Similarily, for a semi-infinite parallel plate channel,

$$W_K = \frac{(2 - f)}{f} \frac{h}{\ell} \ln \frac{\ell}{h} . \tag{28}$$

An appropriate end correction for the finite parallel plate slit has also been calculated by Clausing and is given by Berman [32]. Berman [28] has also shown that for free molecule flow when backscattering is present, the term $(2 - f)/f$ should be replaced with $\alpha/(2 - \alpha)$.

A listing of the flow parameters measured on all of the test samples is given in table 2.

SEPARATION MEASUREMENTS

Figure 17 shows a schematic diagram of the neon separation system. The system provides a means of flowing neon gas past the test sample at a gas velocity of 100 to 1000 times higher than the gas velocity through the test sample. In one mode of operation the gas was recirculated in a closed loop with sealed piston-type pumps. This mode of operation was used at the higher flow rates to conserve gas. At the lower pressures and flow rates, operating conditions could be obtained better when the neon was simply exhausted to atmosphere through vacuum pumps. The feed throttle valve was interchangeable. The valve used was dependent upon the forepressure and the sample being tested. At the higher pressures and flow rates a hand-controlled needle valve or ball valve was adequate. At low flow rates a Granville-Phillips Automatic Pressure Controller was used to control a servo-driven variable leak valve. The reject throttle valve was a needle valve. A Meriam Laminar flowmeter was used to measure the feed flow. The pressure drop across the flowmeter was measured with a 0- to 1-in. water pressure Pace transducer. This permitted measurement of feed flow rates of less than one standard cc of gas per minute.

The pressures were measured with a Datametric Electronic manometer using a Barocel pressure sensor type 511, 0 to 10 cm Hg, for the forepressure and a type 538, 0 to 1 psi., for the backpressure. This provided a very accurate means of measuring the pressures. When the forepressure exceeded the limits of the Barocel, a mercury manometer referenced to vacuum was used to measure the forepressure.

Table 2

FLOW MEASUREMENT PARAMETERS

Sample Number	Nitrogen			Helium			Argon			Neon		
	$S \times 10^{-4}$ (cm^{-1} Hg)	$w_o \times 10^{-4}$	$w_m \times 10^{-4}$	$S \times 10^{-4}$ (cm^{-1} Hg)	$w_o \times 10^{-4}$	$w_m \times 10^{-4}$	$S \times 10^{-4}$ (cm^{-1} Hg)	$w_o \times 10^{-4}$	$w_m \times 10^{-4}$	$S \times 10^{-4}$ (cm^{-1} Hg)	$w_o \times 10^{-4}$	$w_m \times 10^{-4}$
212	47.23	-	97.3	16.0	107	80.3						
838	8.55	-	33.4	-	-	-						
924	10.71	53.5	44.1	-	-	-						
1054	1.91	28.0	21.9	0.632	26.0	21.0	1.81	28.0	21.4	0.904	29.6	21.7
64	19.2	60.8	44.2	6.60	60.5	44.0	17.7	-	46.7	9.12	-	44.4
2	1949	3500	3400	666	-	3600						
1	20.02	-	54.1	-	-	-						
5	4.95	66.0	17.3	1.59	75	36						

[a]Measured several months later after separation measurements.

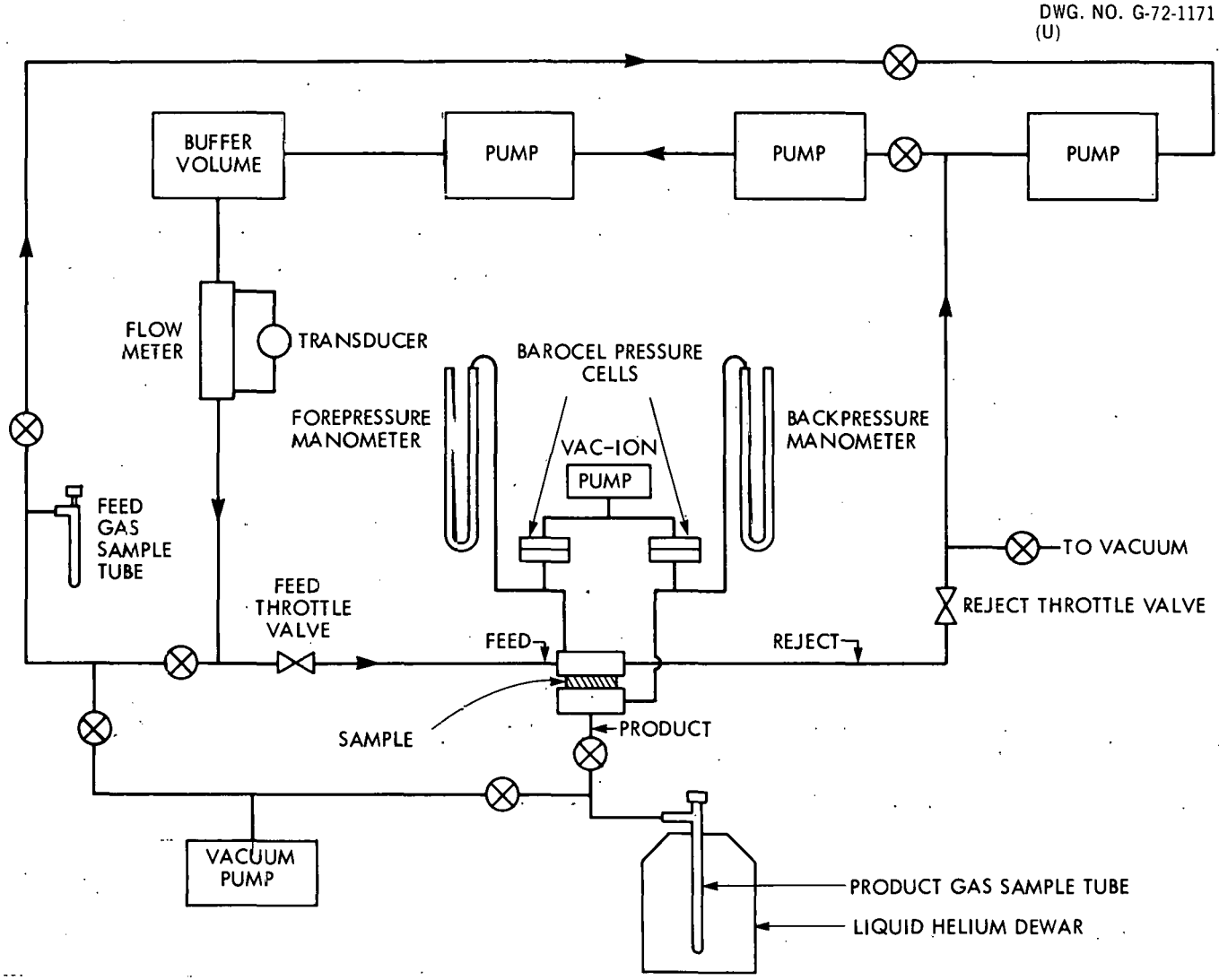

Figure 17

INERT GAS SEPARATION SYSTEM

The samples were mounted in a holder in which the feed gas flows horizontally across the face of the sample. Figure 18 shows the high pressure side of the holder. Three pressure taps are located in the holder to permit measurement of the forepressure, P_f, and the pressure drop across the face of the holder. The flow channel across the holder is 20 mils deep, 7/8 in. wide, and $1\frac{5}{8}$ in. long. The gas enters the holder perpendicular to the channel. Figure 19 shows the low pressure side of the holder. A pressure tap for measuring the backpressure, P_b, is located at point A. The product flow line is 0.5 in. in diameter to help reduce the pressure drop between the test sample and the sampling tube. Figure 20 shows the complete holder assembly bolted together, without a sample.

A very important and necessary part of the system was a 25-liter dewar of liquid helium which was used to freeze out the neon product sample. It proved to be a very efficient and inexpensive method of collecting the product gas. The product sample tubes were made of Inconel with a 6-mil wall thickness in order to reduce the amount of liquid helium boiled off each time a sample was taken.

The apparatus and sample holder were constructed with concern that no significant concentration gradients ever develop on the high pressure side of the sample. This is necessary in order that any observed isotopic concentration changes will accurately reflect only those changes which occur as a result of flow through the sample. Because of the wide variety of conditions under which measurements were to be made and since a large number of the small capillaries were required for the flow measurements, it was felt that more accurate and reproducible results could be obtained by analyzing collected gas samples of the feed and diffused or product streams under similar conditions in the mass spectrometer laboratory rather than having a mass spectrometer physically attached to the separation system.

The mass spectrometer laboratory prepared a special spectrometer with a double-collector system for use in analyzing the neon samples. The ion current produced by the neon-20 isotope and the small amount of neon-21 present is measured by the first collector. The first collector has an appropriately located slit to allow the neon-22 ions to pass through to the second collector. The ion current produced by the neon-22 isotope is measured by the second collector. The ratio of the ion currents gives the ratio of mole fractions in a given sample. The neon-21 isotope collected with the neon-20 isotope is such a small fraction of the neon-20 isotope that analytically it produces a negligible error and can be ignored. The ratio of mole fractions of neon-20 and neon-22 is measured for both the feed and product streams. The ratio of these ratios then gives the separation factor for a given measurement.

Separation measurements by the laboratory revealed that best results could be obtained with a gas sample at about 10 cm Hg absolute pressure. This requirement made sampling of the product stream difficult and could have greatly restricted the conditions under which separation measurements would be made. Initial attempts at collecting a product gas sample in an evacuated sample tube under varying backpressure conditions were totally

PHOTO NO. PH-69-895

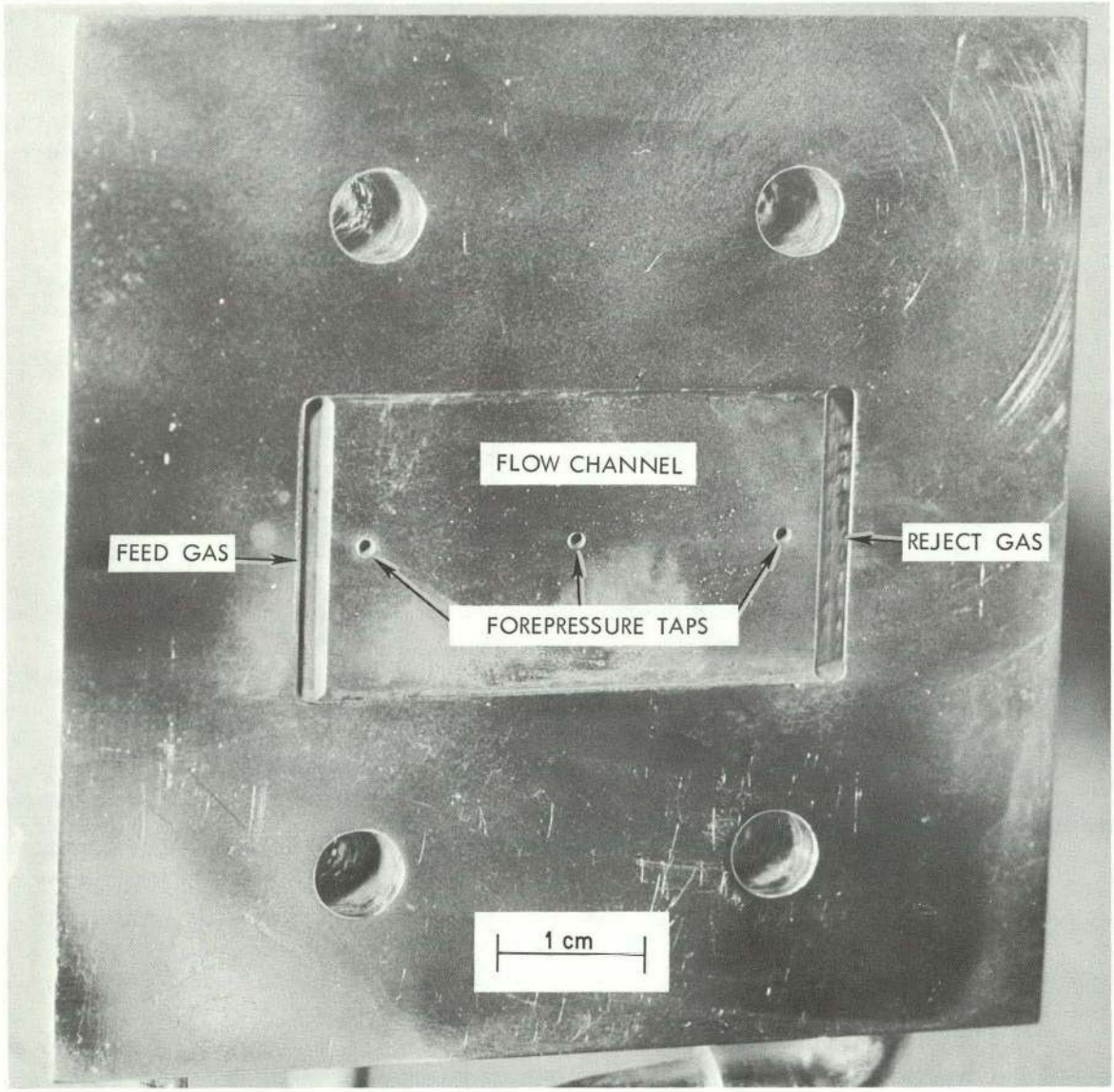

Figure 18
HIGH PRESSURE SIDE OF SAMPLE HOLDER

PHOTO NO. PH-69-897

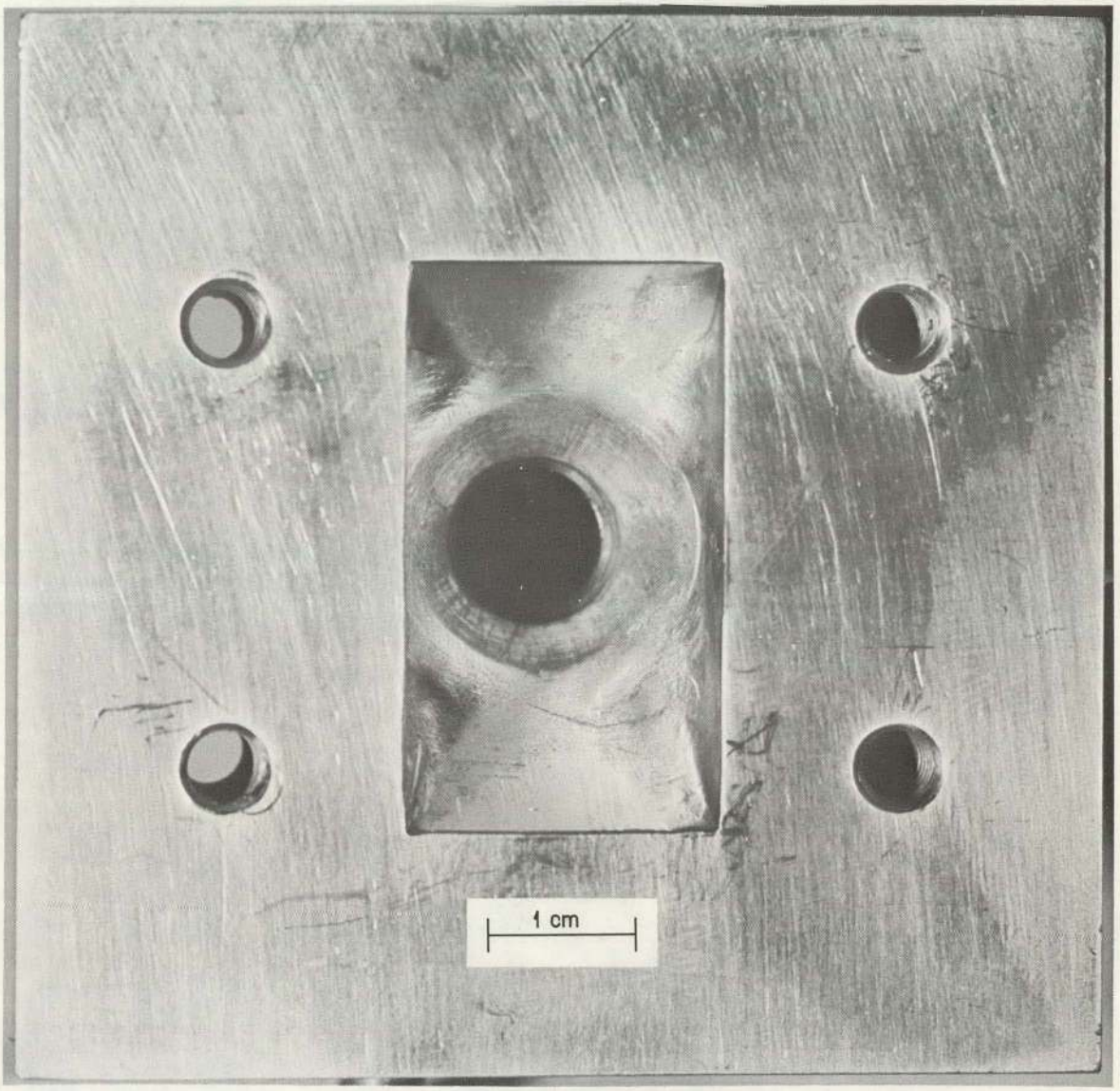

Figure 19
LOW PRESSURE SIDE OF SAMPLE HOLDER

PHOTO NO. PH-69-896

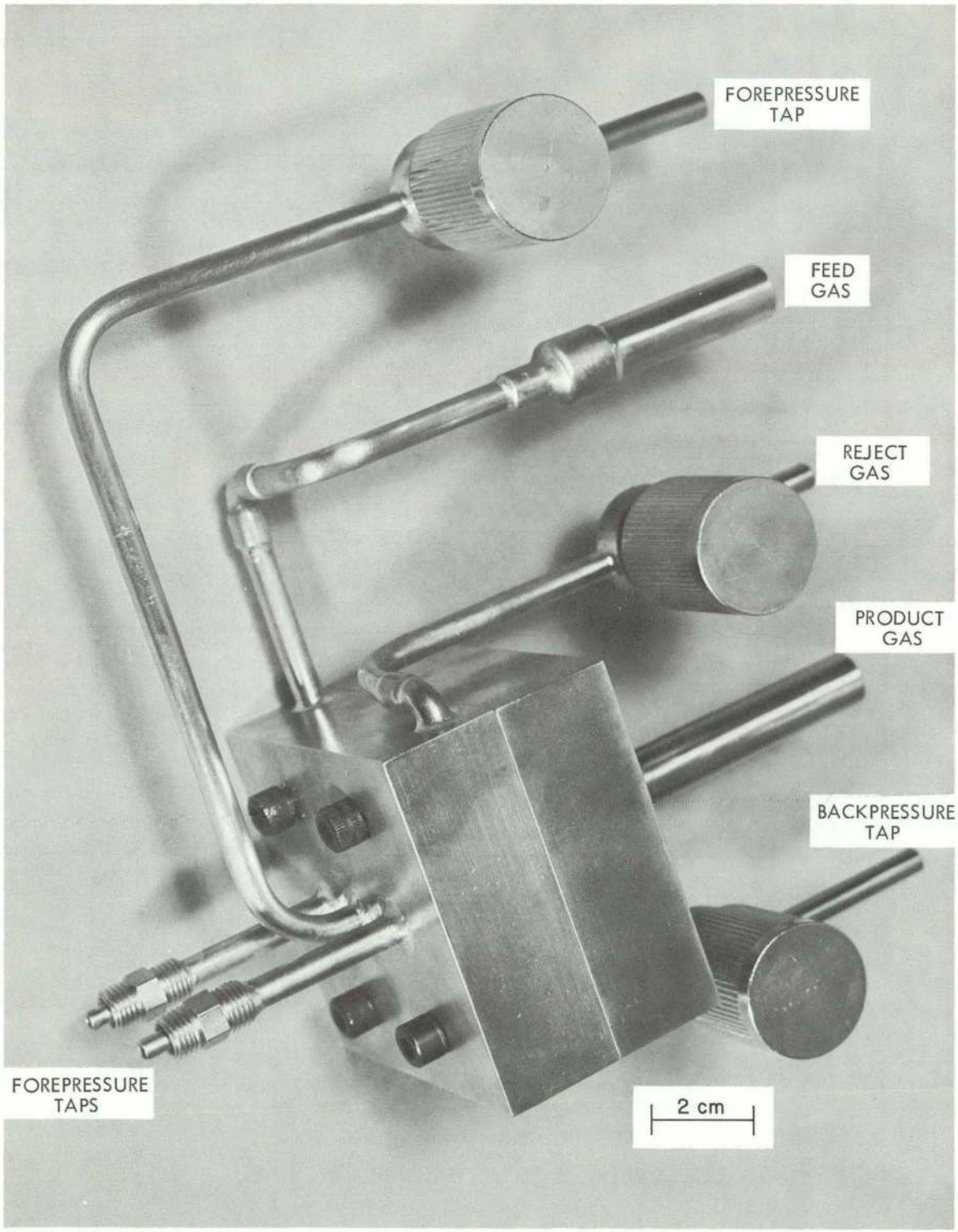

Figure 20
COMPLETE HOLDER ASSEMBLY

unsuccessful. As a last resort, the neon product sample was collected in a liquid helium dewar. This proved to be so satisfactory that all measurements were made in this manner. The product samples were collected with relatively low helium loss, and the cost of liquid helium to freeze out the neon samples was a small part of the overall effort. From the known flow rates through the test sample, the run times could be adjusted so that when the sample tubes were removed from the helium dewar, the sample pressures would be about 10 cm Hg. This technique provided a means of maintaining a very low pressure on the downstream side of the sample during the entire time required for the test. Most of the separation measurements were made with a high side-to-low side pressure ratio of between 100 and 1000. Since the test samples had different flow rates and a wide range of pressures was used in the measurements, several different sizes of product gas sampling tubes were used to avoid excessively short or long run times. Test sample forepressure varied from one atmosphere down to as low as about 0.5 mm Hg. Feed samples were always easily collected at the required 10-cm Hg pressure.

The sample to be tested was mounted in the separation sample holder using 0.05-in.-thick rubber gaskets on each side, and the two pieces of the holder were bolted together to compress the gasket and seal the sample. After the holder was mounted on the system, the system was evacuated and leak checked. The system was then filled with neon to an absolute pressure corresponding to the pressure necessary to permit a test to be made at a given pressure. Usually the high pressure measurements were made first to conserve neon.

There were two methods of operation: one in which the system operated as a closed loop where the gas was recirculated, and the other where the reject gas was exhausted to atmosphere. In the first method the first step was to circulate the gas. Next, the feed and product sample tubes were evacuated to a pressure of 10 μ Hg or less. A feed sample was taken by adjusting the feed line pressure to 10 cm Hg absolute and circulating the gas past the feed sample tube with the sample tube open for approximately 30 seconds. The valves on the line to the feed gas sample tube were then closed to return the feed gas to the test sample holder.

In the second method of operation the circulating pumps were not used. The feed gas sample was taken in the same manner but at a higher pressure. After sampling, the pressure was adjusted to the required 10 cm Hg. Since the depleted gas was not being recirculated, feed samples were not taken each time. In this method of operation the feed gas came directly from the supply cylinder to the system and the reject gas was exhausted through a pump to atmosphere; therefore, the feed gas always had the same concentration. This second method was used only at the lower pressures where the flow rates were very small and recirculation was difficult with the dry head piston pumps used for recirculation. A 20-liter buffer volume in the feed line was used as a reservoir so that pressures would not change rapidly. A Granville-Phillips automatic pressure controller which uses a servo-driven variable leak valve was used in the feed line to maintain a constant pressure on the high pressure side of the test sample.

In both methods of operation, after the product sample tube was evacuated, the valve was closed and the sample tube was immersed in a dewar of liquid helium. The pressure conditions for the test were set by regulating the feed throttle valve and the reject throttle valve. The product line was opened to the vacuum pump to start the flow through the test sample and reduce the backpressure as much as possible. After the pressure was reduced and sufficient time was given for reaching an equilibrium flow condition, the product sample tube valve was opened and the valve to the vacuum pump was closed. The length of time for the test was determined by the flow rate at the particular test conditions and the size of the sample tube being used. Enough neon was collected in the sample tube to give a pressure of at least 10 cm Hg absolute when the tube was at ambient temperature conditions. Exception was made when the run times required to collect neon at a pressure of 10 cm Hg exceeded six hours. In these cases only enough neon to give 5 cm Hg was collected. In these latter cases the separation results are somewhat less reliable, since pressures lower than 5 cm Hg absolute in the smallest sample tubes did not provide enough neon to obtain very reliable measurements from the spectrometer. During the test the forepressure, backpressure, and feed flow rate readings were recorded. After the test was complete, the product sample tube valve was closed and the sample tube removed from the liquid helium. It was allowed to warm to ambient conditions, and then the degree of separation achieved was measured with the double-collector mass spectrometer.

Figure 21 shows the separation apparatus and associated instruments.

SEPARATION EFFICIENCY CALCULATION METHOD

When a binary isotopic gas mixture is diffused through an appropriate test sample, the light component diffuses more rapidly than the heavy component so that the diffused mixture is enriched in the light component. When the diffusion occurs through an ideal Knudsen barrier with zero backpressure, the ratio of the flow of the light component to the heavy component is given by

$$\frac{F_1}{F_2} = \frac{k\bar{v}_1 N P_f}{k\bar{v}_2 (1 - N) P_f} = \frac{f^* N}{(1 - N)} \tag{29}$$

where

$$f^* = \frac{\bar{v}_1}{\bar{v}_2} = \sqrt{\frac{m_2}{m_1}} .$$

Also,

$$\frac{F_1}{F_2} = \frac{N_1 F}{(1 - N_1) F} = \frac{N_1}{1 - N_1} ; \tag{30}$$

therefore,

$$\frac{f^* N}{1 - N} = \frac{N_1}{1 - N_1} . \tag{31}$$

PHOTO NO. PH-71-665

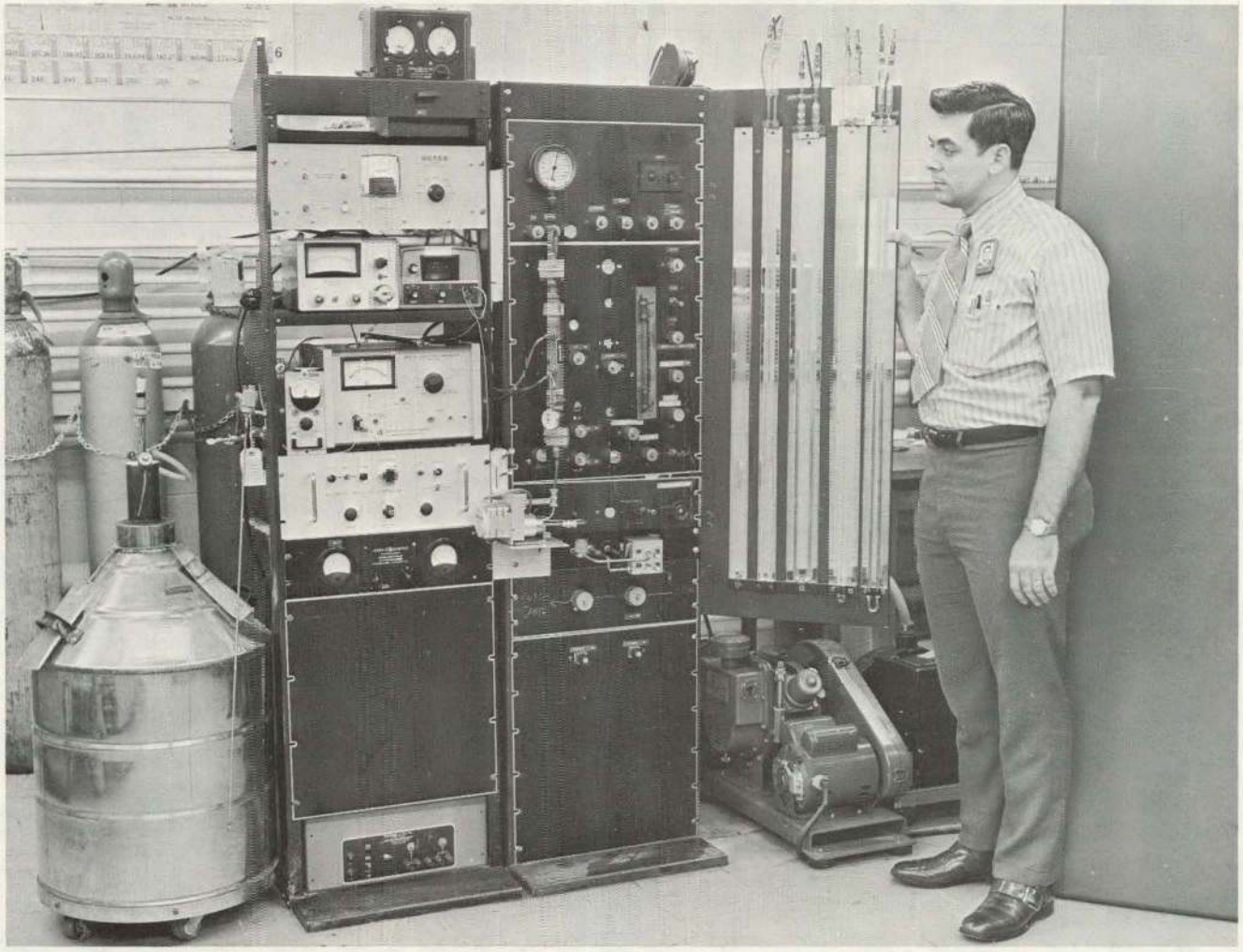

Figure 21
INERT GAS SEPARATION SYSTEM

Then for a given product mole fraction N_1 the ideal feed mole fraction would be

$$N^* = \frac{N_1}{N_1 + f^*(1 - N_1)} . \tag{32}$$

Then the ideal enrichment produced by an ideal barrier is

$$\delta^* = N^* - N_1 . \tag{33}$$

For a non-ideal barrier where the enrichment is

$$\delta = N - N_1 , \tag{34}$$

the separation efficiency is defined as

$$Z = \frac{\delta}{\delta^*} . \tag{35}$$

For an ideal barrier operating at finite backpressures the flow ratio is

$$\frac{F_1}{F_2} = \frac{k\bar{v}_1}{k\bar{v}_2} \frac{(NP_f - N_1P_b)}{(1 - N)P_f - (1 - N_1)P_b} . \tag{36}$$

From this it can be shown that the ideal enrichment is

$$\delta^o = \delta^*(1 - w) \tag{37}$$

where $w = P_b/P_f$. Then the separation efficiency for an ideal barrier operating at any pressure ratio is

$$Z = \frac{\delta^o}{\delta^*} = 1 - w . \tag{38}$$

The separation efficiency ratio, $Z/(1-w)$, is then the ratio of the separation efficiency of a diffusion barrier to that of an ideal diffusion barrier. Deviation of the separation efficiency ratio from unity represents deviations from ideal behavior.

A mass spectrometer can be used to measure the ratio of mole fractions of a binary mixture. The separation factor, f, measured with a mass spectrometer, is defined as

$$f = \frac{N'/(1 - N')}{N/(1 - N)} . \tag{39}$$

It can be shown that equation (35) can also be written as

$$Z = \left[N + (1 - N) \frac{f^*}{f}\right] \frac{f - 1}{f^* - 1} . \tag{40}$$

In the case of neon isotopes, Z can be approximated by neglecting the term in brackets in equation (40). The value of this term varies from unity for high separation factors to 1.004 for the lowest separation factors. Thus, the problem of not knowing the exact value of the feed mole fraction introduces a negligible error. Then, since f* = 1.04881 for neon isotopes,

$$Z = \frac{f - 1}{f^* - 1} = \frac{f - 1}{0.04881} , \tag{41}$$

where f is the value for the separation factor or ratio of mole fraction ratios as measured with a double-collector mass spectrometer.

In order to obtain an accurate separation efficiency, consideration needs to be given to the effect of the gas depletion or cut (ratio of product flow to feed flow) and to the effect of concentration gradients in front of the sample. The separation tests were made with a turbulent holder and at very low cuts to avoid a concentration gradient. However, this point was investigated on several occasions by varying the cut with all other conditions held constant. This was never a problem except at the lowest operating pressures. A correction was calculated for each test to account for the finite amount of gas removed from the stream by using the Rayleigh distillation correction:

$$\frac{\theta}{(1 - \theta)\ ln\ [1/(1 - \theta)]}$$

where θ is the cut or ratio of the product flow to the feed flow. Generally, this value deviated from unity by less than 1%. The separation efficiency is given by

$$Z = \left(\frac{f - 1}{f^* - 1}\right) \frac{\theta}{(1 - \theta)\ ln\ [1/(1 - \theta)]} . \tag{42}$$

Other factors which affect the separation efficiency are the forepressure, P_f, and the backpressure, P_b. All of the measurements were made at a room temperature of about 25°C; the small variations in room temperature have a negligible effect on the results.

DISCUSSION OF RESULTS

All of the separation data that were taken on all of the samples which were tested are shown in Appendix B. Graphs of separation efficiency ratio, $Z/(1-w)$, vs. pressure difference across the sample, ΔP, are shown for each of the samples investigated in figures 22 to 29. For some of the data a larger variance in the low pressure region is due to an early problem of measuring the backpressure accurately. During the study, improvements were made in measuring the backpressure that eliminated this source of error. It is also believed that the lower pressure data tend to be biased low and have a larger variance because of the accumulation of larger amounts of air in the sampling tube with the longer times required to collect a gas sample. The presence of air in the mass spectrometer causes errors due to varying amounts of beam dispersion. There was also another problem at the lowest pressure relative to the fraction of the feed gas withdrawn as product which will be discussed later. The problem of long sampling times could be reduced if the test samples contained more capillaries. Sample 212 was the first sample tested. Since the sample had the highest flow rate of any of the samples tested, significantly better data might have been obtained with this sample if the separation measurements had been repeated later after all the improvements were made.

The data for sample number 838 shown in figures 23 and the data for sample number 924 shown in figure 24 appear to have somewhat more scatter in the higher pressure region than for other samples. It is believed that this increased variance was related to system problems and temporary problems with the mass spectrometer. The mass spectrometer analysis was the main source of test variance. The standard deviation per measurement should have been about ± 0.009. A discussion of the mass spectrometer variance is given in Appendix C.

The primary purpose of this study was to obtain experimental data of a quality that could be used to evaluate any theory for the separation of a binary gas mixture of isotopes. No attempt has been made to obtain a least squares fit of the experimental data with an analytic expression to obtain an interpolation formula. Instead, an empirical modification of the Present and deBethune equations has been made which appears to represent the data quite well and may be used as an interpolation formula for the data. Table 3 gives some combinations of constants used in the modified Present and deBethune equation to show the sensitivity of the fits to variations in the constants as indicated by a calculated standard deviation. The best trial and error fit of the data is indicated by the lowest standard deviation.

It is easily recognized from the PBM theory that the primary variable is the product of the characteristic dimension of the geometry being tested, which from these data appears to be the hydraulic radius as suggested by Present and deBethune, and the pressure difference across the test sample. If that product is also divided by the product of the gas viscosity and the mean molecular velocity, a unique parameter is obtained which will allow all separation data to be plotted on the same scale.

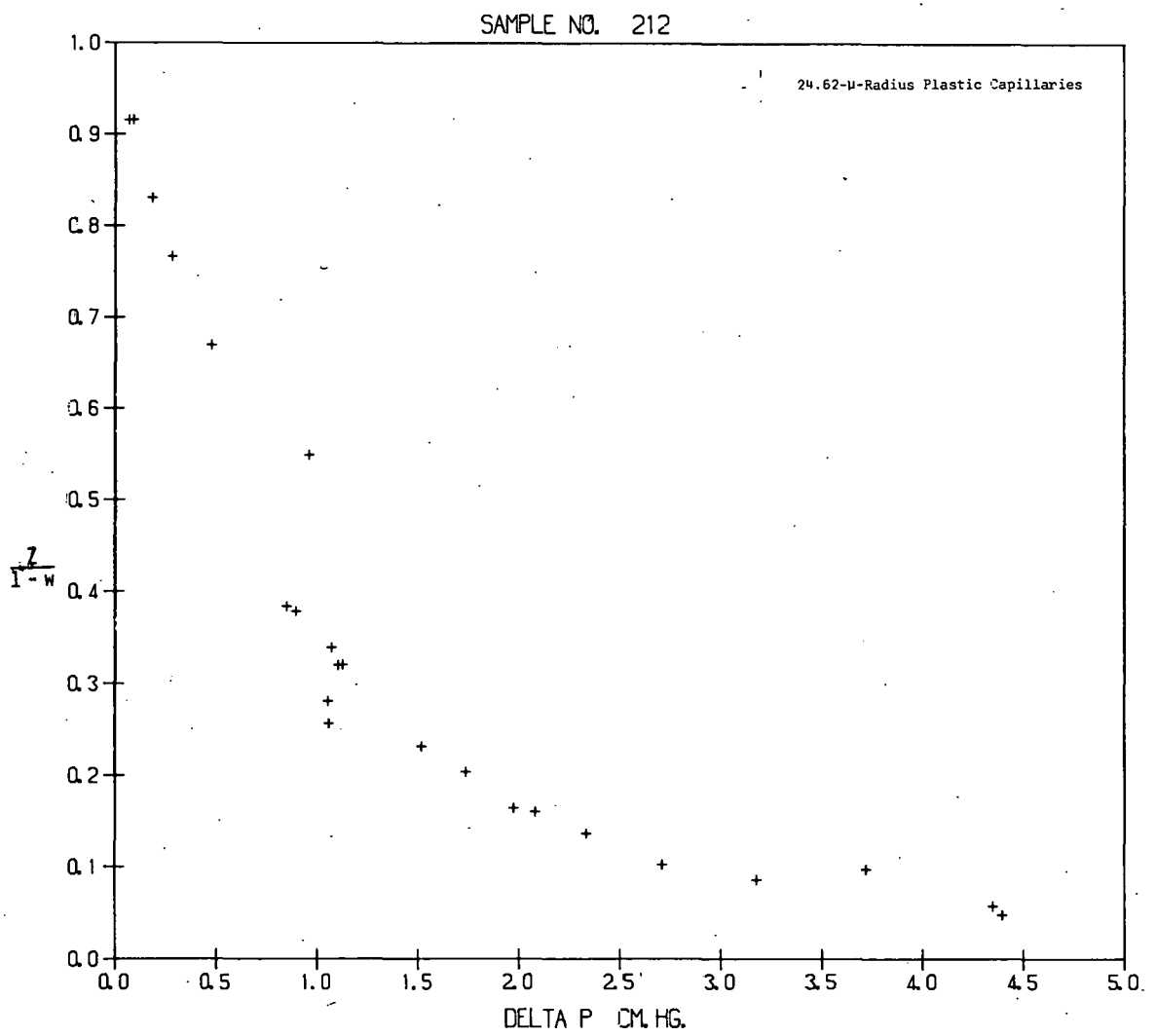

Figure 22

EXPERIMENTAL SEPARATION DATA FOR SAMPLE 212

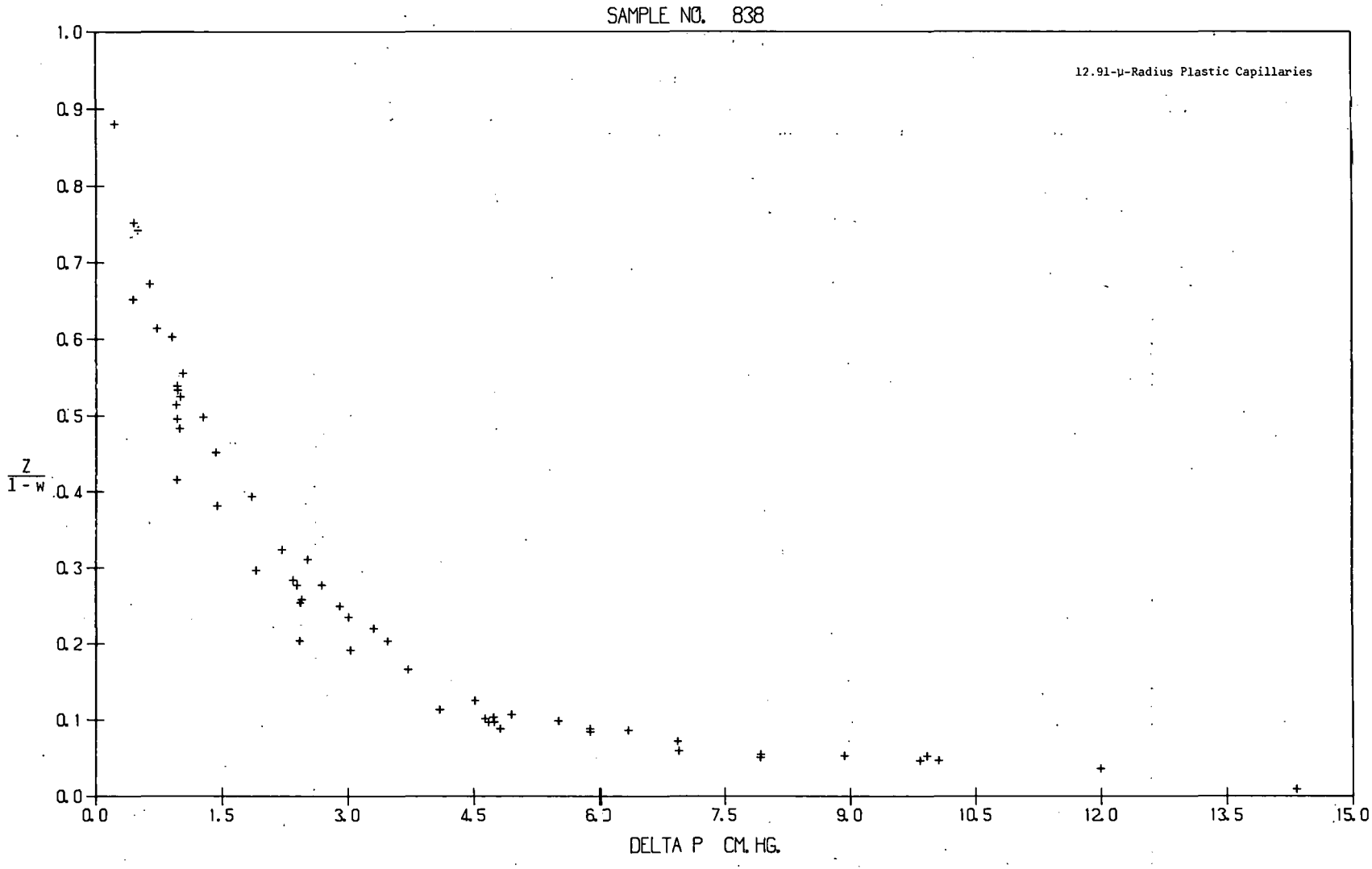

Figure 23

EXPERIMENTAL SEPARATION DATA FOR SAMPLE 838

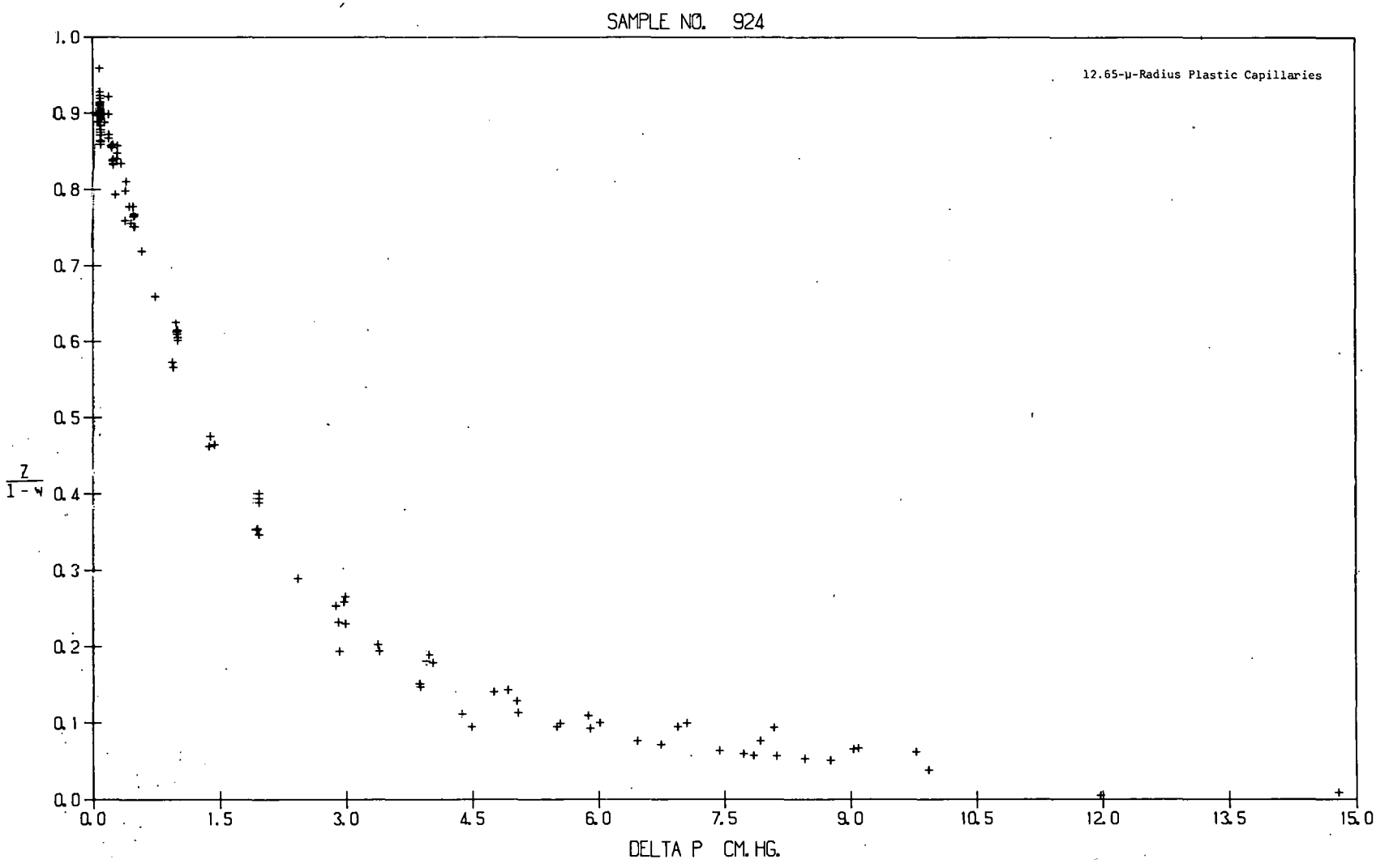

Figure 24

EXPERIMENTAL SEPARATION DATA FOR SAMPLE 924

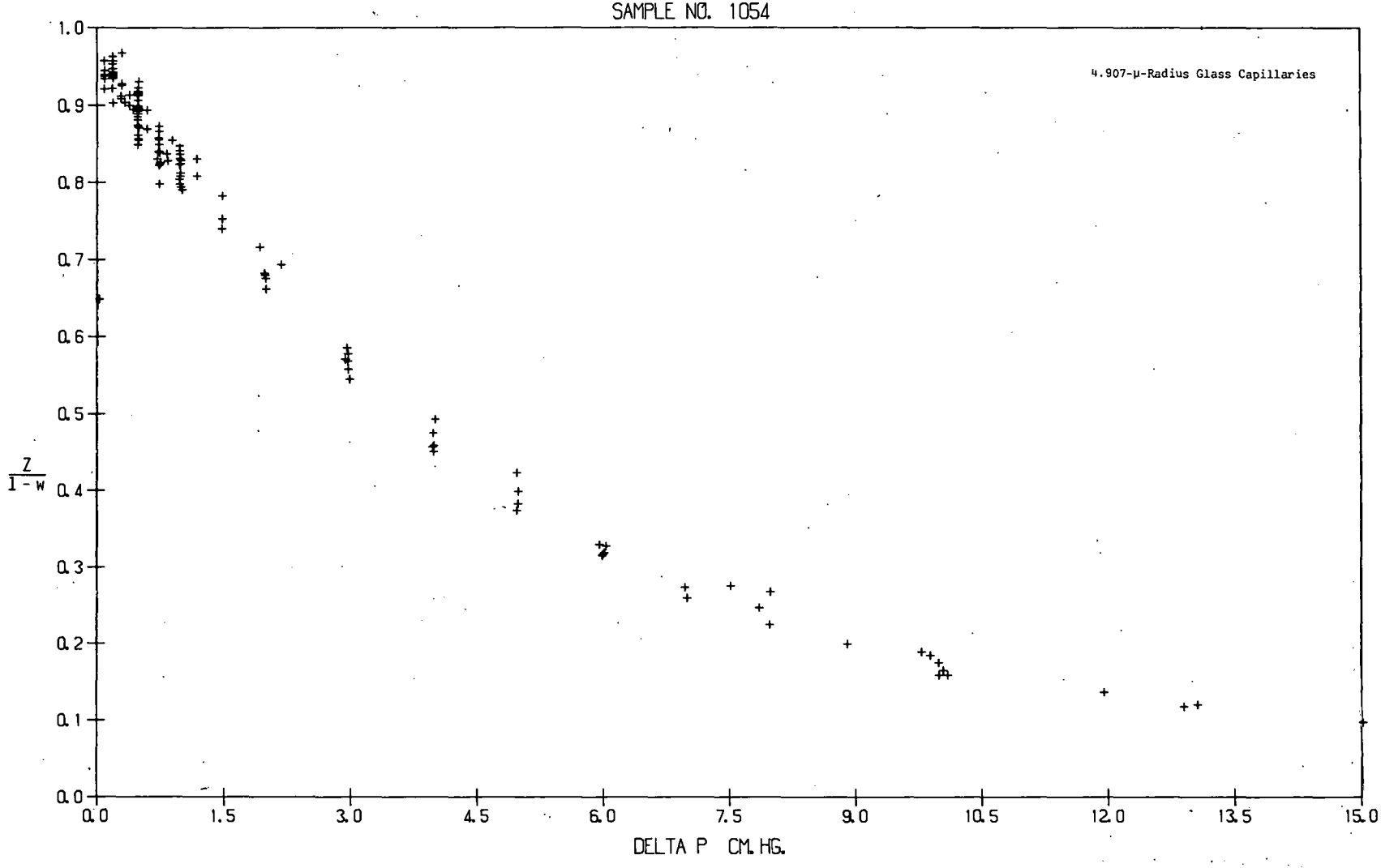

Figure 25

EXPERIMENTAL SEPARATION DATA FOR SAMPLE 1054

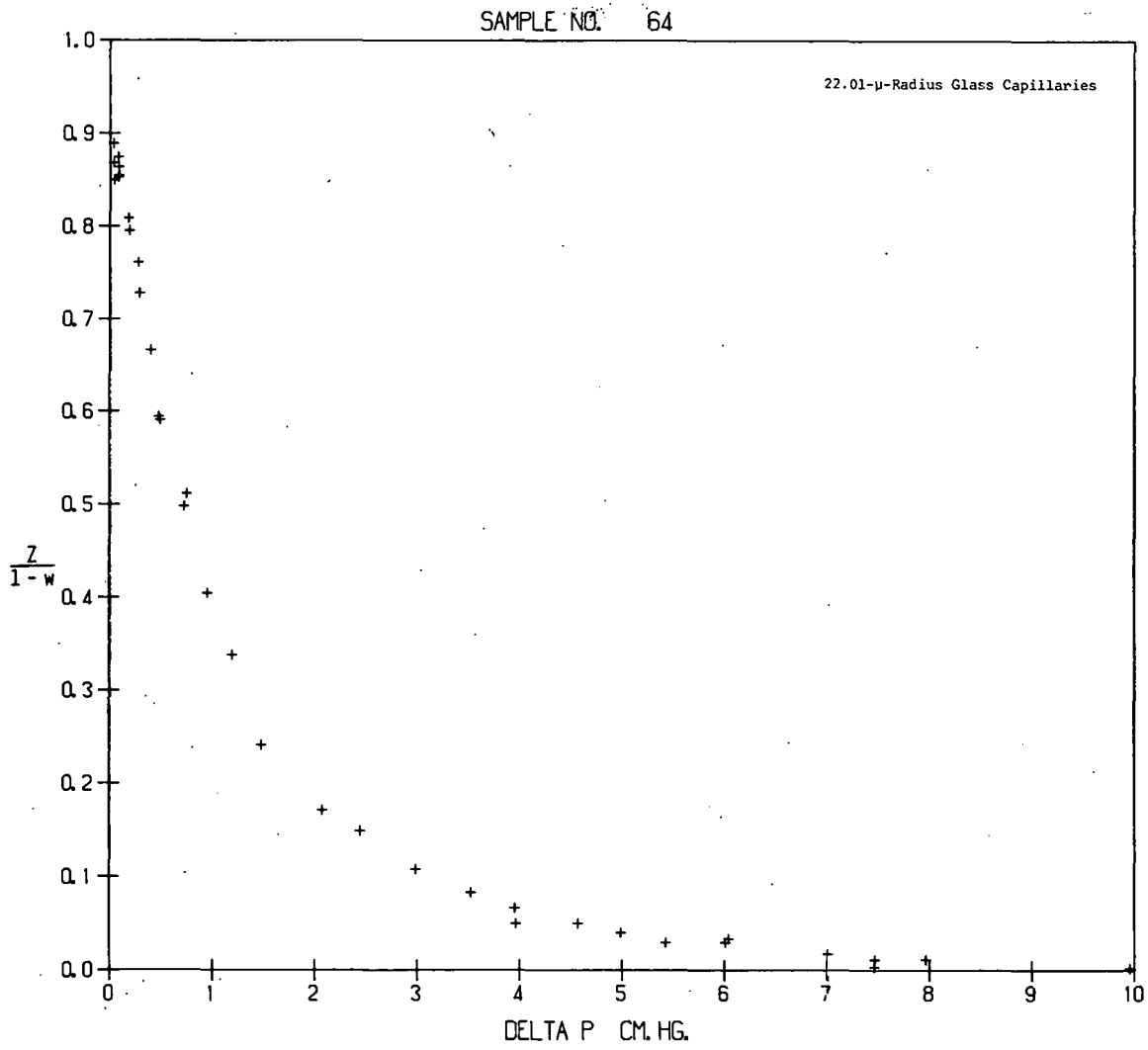

Figure 26

EXPERIMENTAL SEPARATION DATA FOR SAMPLE 64

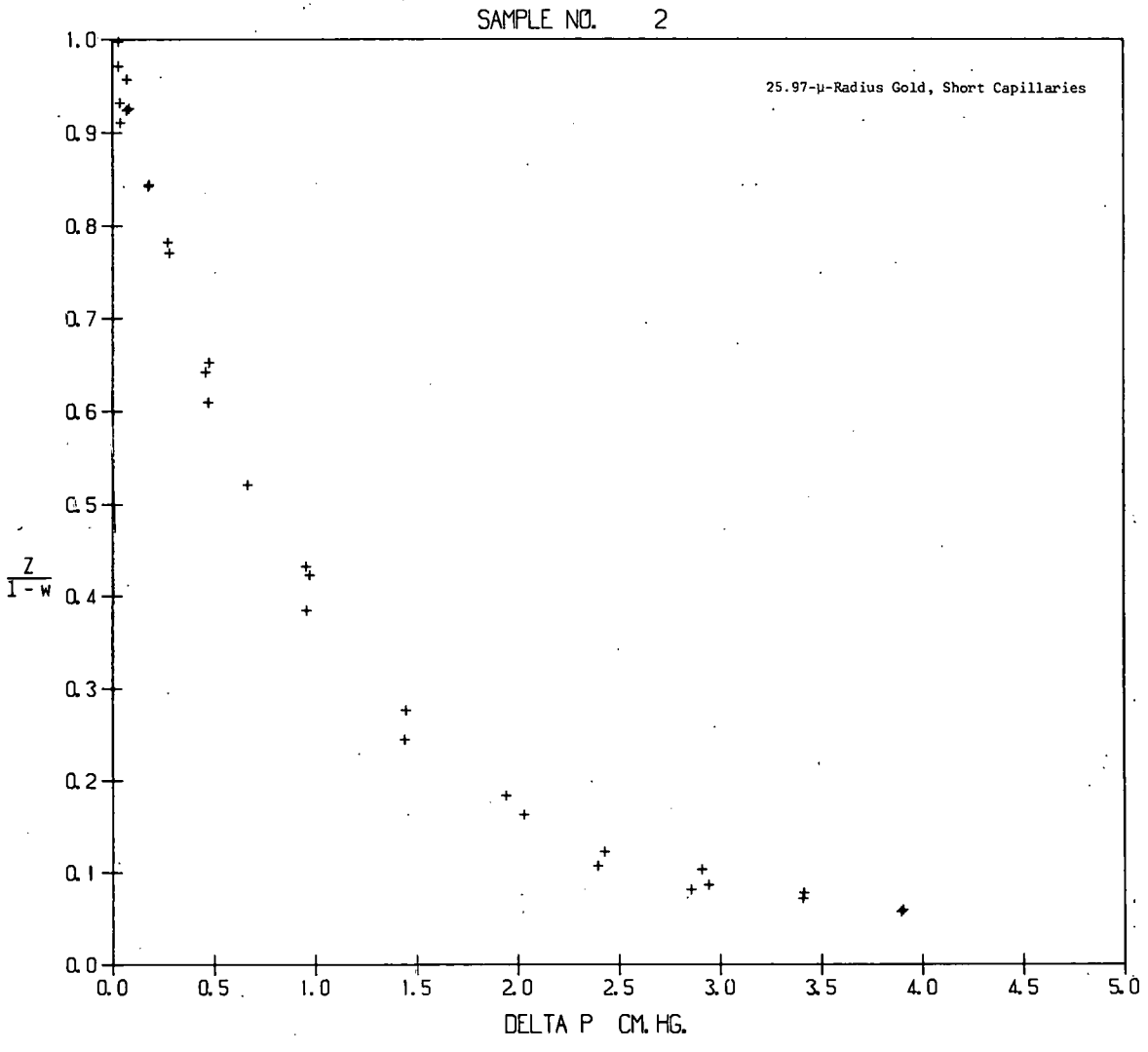

Figure 27

EXPERIMENTAL SEPARATION DATA FOR SAMPLE 2

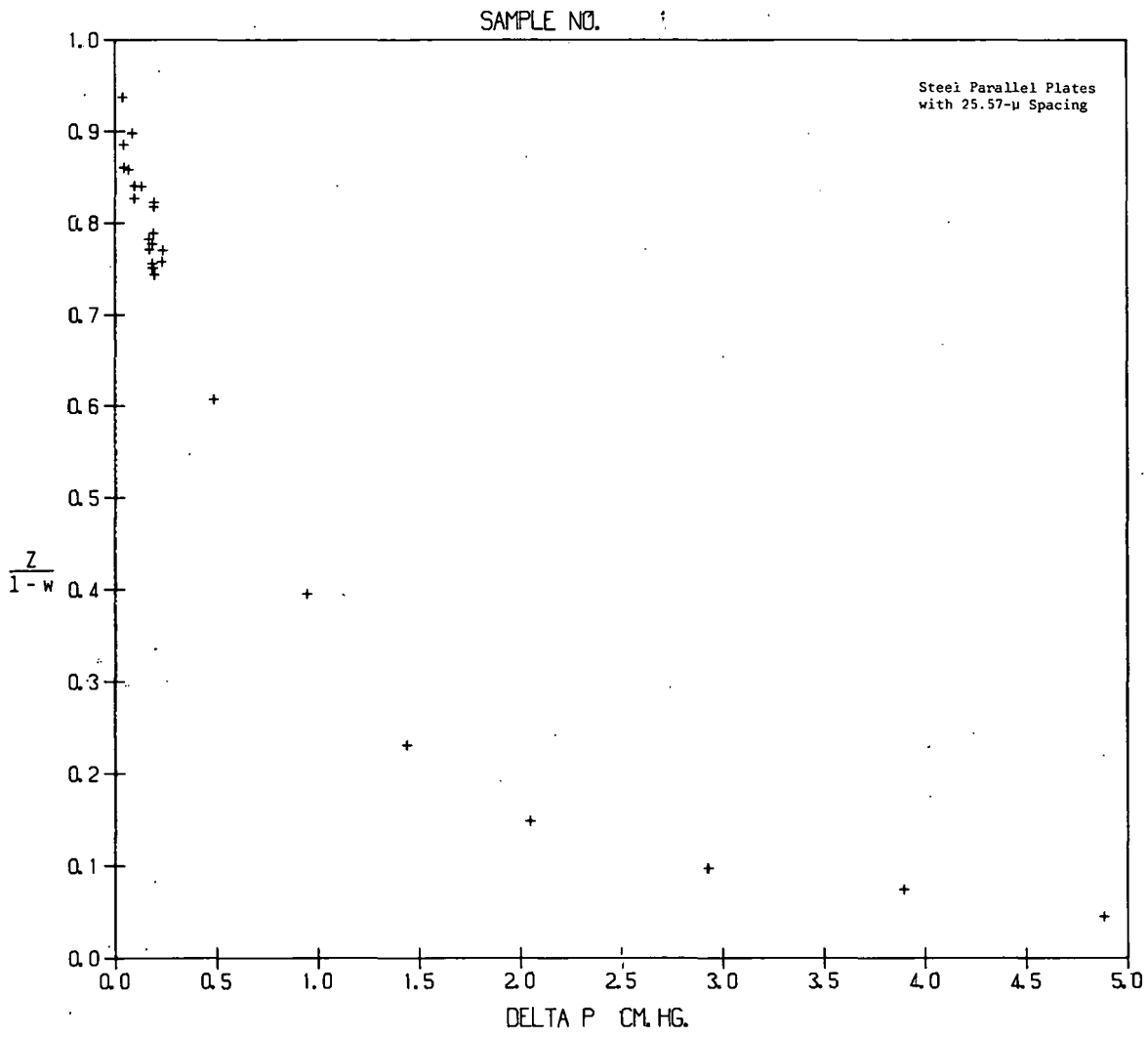

Figure 28

EXPERIMENTAL SEPARATION DATA FOR SAMPLE 1

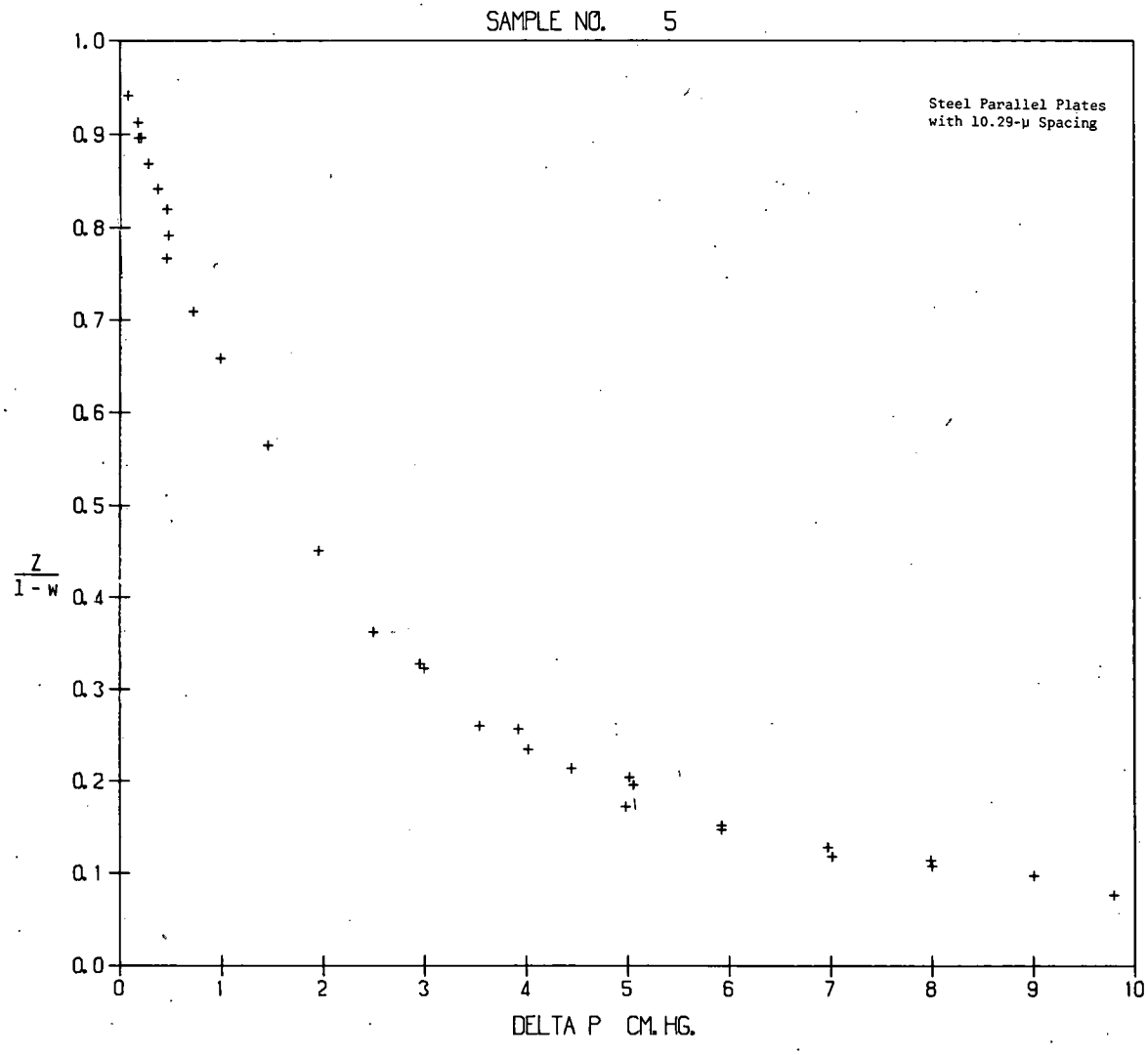

Figure 29

EXPERIMENTAL SEPARATION DATA FOR SAMPLE 5

Table 3

CONSTANT FOR THE MODIFIED PRESENT AND deBETHUNE MODEL

Sample	K	w_m/w_K	B	K'	s*
212	1.05	1.00	3	1	0.0695
	0.85	1.00	3	1	0.0492
	0.85	0.75	3	1	0.0335
	0.85	0.70	3	1	0.0319
	0.75	0.75	3	1	0.0306
	0.75	0.70	3	1	0.0301
838	0.75	0.85	3	1	0.0315
	0.75	0.75	1	1	0.0309
	0.75	0.85	1	1	0.0292
	0.70	0.85	1	1	0.0291
924	0.75	0.85	3	1	0.0367
	0.75	0.75	1	1	0.0366
	0.70	0.75	1	1	0.0360
	0.70	0.85	1	1	0.0362
	0.70	0.85	3	1	0.0358
1054	0.85	0.75	3	1	0.0306
	0.85	0.70	3	1	0.0280
	0.75	0.75	3	1	0.0268
	0.75	0.70	3	1	0.0256
64	0.75	0.70	1	1	0.0235
	0.85	0.70	3	1	0.0228
	0.85	0.70	1	1	0.0213
	0.85	0.75	1	1	0.0221
	1.05	0.70	3	1	0.0225
2	0.67	1.00	1	0.78	0.0335
	0.50	1.00	1	0.78	0.0182
	0.40	1.00	1	0.78	0.0158
	0.40	0.70	1	0.78	0.0161
	0.50	0.70	1	0.78	0.0156
1	1.178	0.50	1.5	0.67	0.0377
	1.178	0.60	1.5	0.67	0.0344
	1.178	0.70	1.5	0.67	0.0328
	1.178	0.70	2.0	0.67	0.0338
5	0.88	0.50	1.5	0.67	0.0284
	0.88	0.70	1.5	0.67	0.0215
	1.178	0.70	1.5	0.67	0.0249
	1.178	0.60	1.5	0.67	0.0180
	1.178	0.50	1.5	0.67	0.0176
	1.178	0.50	2.0	0.67	0.0192

*s is the standard deviation of experimental values from the calculated values.

$$Y = \frac{r\Delta P}{\bar{\eta}\bar{v}} . \tag{43}$$

Most of the data were obtained with very low backpressure; for cases when $P_b \to 0$,

$$Y = \frac{rP_f}{\bar{\eta}\bar{v}} = \frac{\pi r}{2\bar{\lambda}} \tag{44}$$

where $\eta = \frac{1}{2}\bar{\rho}\bar{v}\lambda$ defines the mean free path λ at the average pressure. This parameter Y emphasizes the relationship between the gas mean free path and the dimensions of the flow channel and provides a good scale to indicate the separation efficiency in relation to the ratio of the radius to mean free path. However, it must be emphasized that the important parameter is pressure difference and not pressure level. This correspondence follows only when the backpressure is small compared to the forepressure.

Figure 30 shows the data obtained with five different samples plotted as a function of Y. An initial examination of these data appears to indicate that there is no fundamental difference in the pressure dependence of the separation efficiency in these different geometries in contrast to the large differences in the pressure dependence of the transmission ratio in these same geometries. However, on closer examination it can be noted that the data band is relatively wider at the left- and right-hand sides of figure 30 than it is in the midrange. The parallel plate data are at the lower side of the data band on the left-hand side and at the higher side of the data band on the right-hand side of the figure. There are also pattern deviations in the data for the other samples which reveal significant information about the individual test samples. These pattern deviations are most easily observed in terms of the parameters required to fit the separation data with the PBFM as shown in table 3. The implications of the parameters will be discussed later.

Sample number 1054 is the sample with the smallest capillary radius, and for that reason more data were obtained with this sample than with any of the others. Figure 31 is a plot of these experimental data compared with four mathematical model calculations. These calculated curves were obtained using the measured values of the parameters required in the models and the parameters which gave the best fit for those which were not measured. It is quite clear that GCM using the average pressure weighting does not fit the data well. The GCM using local pressure weighting fits the data significantly better but still does not fit the data over the entire curve. The PBM calculations are too low over the entire range of the data, but the PBFM calculations fit the data well over the entire range of the measured separation efficiencies.

As is shown by equations (13) and (14), analytical expressions in terms of the capillary radius can be obtained for the initial slope of the separation efficiency vs. the pressure difference curve from the PBM. Because of the poorer reliability of the lower pressure data, the initial

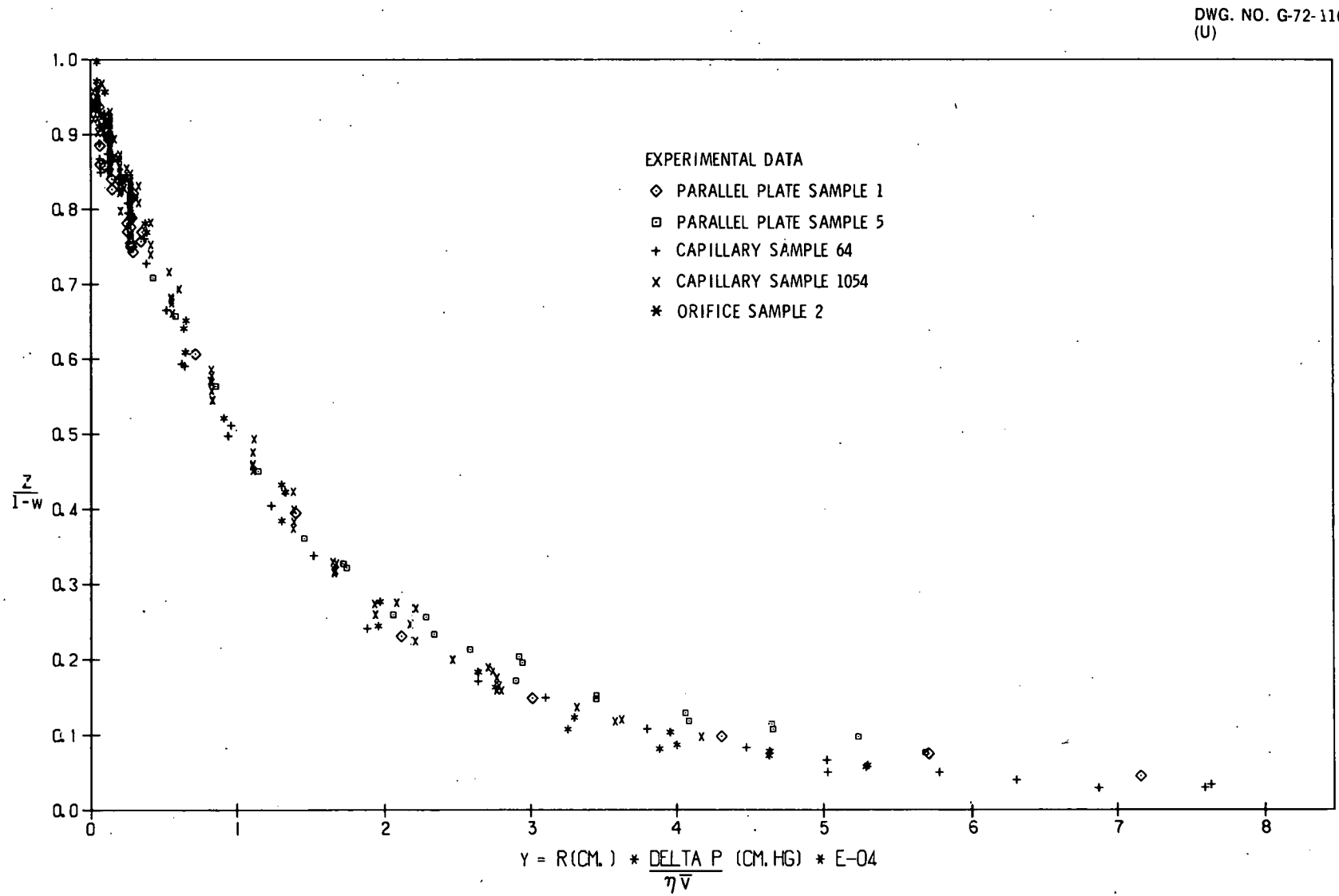

Figure 30

EFFECTIVE PRESSURE PARAMETER FOR SEPARATION

DWG. NO. G-70-953
(U)

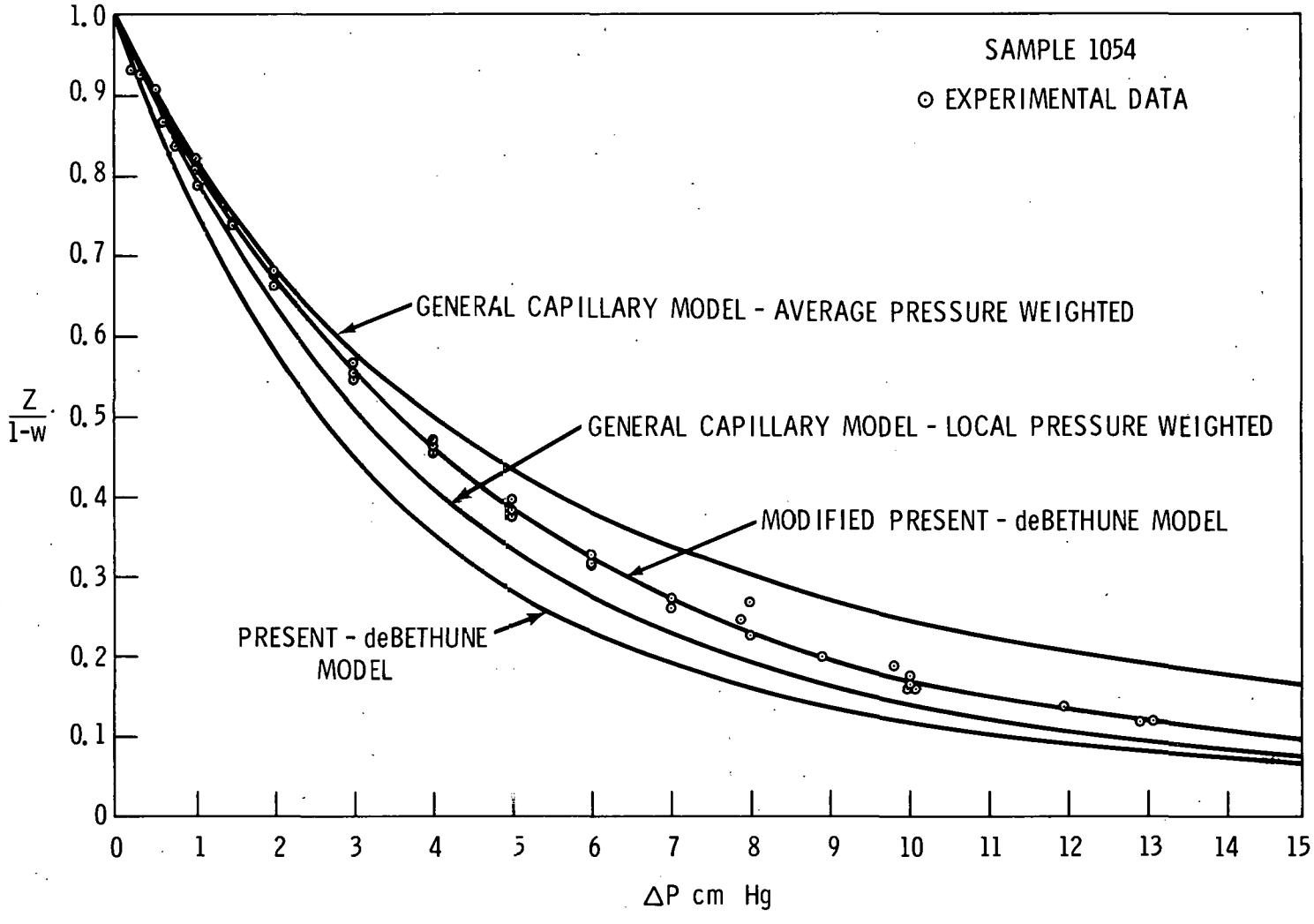

Figure 31

SEPARATION EFFICIENCY OF 4.907-MICRON-RADIUS GLASS CAPILLARY SAMPLE

slope for sample 1054, as well as that for all the other samples, was estimated by calculating the slope required to give the average experimental point at a separation efficiency of 0.85. This calculation was made by using the first three terms in the expansion of the analytical expressions (13) or (14). This approximation is in good agreement with the values obtained from the full calculation either with or without viscous flow. The capillary radii determined in this way for all of the samples are shown in table 4 compared with the radii determined from the measurement of Poiseuille flow through the samples. The ratios of these radii are used to estimate the deviations in the wall scattering law required by each of the models to produce the measured initial slope. These are shown in table 5, which also shows the scattering law deviations inferred from the flow measurements.

Table 4

MEASURES OF CAPILLARY RADIUS

Sample Number	R_1	R_2/R_1	R_3/R_1	R_4/R_1	R_5/R_1	R_6/R_1
212	24.7	-	0.98	0.93	0.81	0.96
838	12.9	-	-	0.89	0.78	0.96
924	12.7	1.04	0.99	0.91	0.79	0.98
1054	4.9	1.02	1.03	0.78	0.68	0.93
64	22.0	1.12	0.99	1.04	0.91	1.13
2	26.0	1.00	1.00	1.34	1.16	0.79
1	25.5	-	1.075	0.61	0.53	1.55
5	10.3	0.71	0.78	0.35	0.30	1.44

R_1 = capillary radius from Poiseuille flow.

R_2 = capillary radius from free molecule flow.

R_3 = capillary radius from slip flow (Maxwell model).

R_4 = capillary radius from initial slope of separation curve using the Present and deBethune separation theory (PBM) with no viscous flow.

R_5 = capillary radius from initial slope of separation curve using the Present and deBethune separation theory (PBM) with viscous flow.

R_6 = capillary radius from initial separation curve using the general capillary model (GCM).

Note: All the radii were calculated assuming completely diffuse reflection and the appropriate factor for the Clausing transmission probability.

Table 5

DEVIATIONS FROM DIFFUSE WALL SCATTERING
IMPLIED BY MEASUREMENTS

Sample Number	Measurements		Present and deBethune Model				General Capillary Model		Modified Present and deBethune	
			No Viscous Flow		Viscous Flow					
	α	f	α	f	α	f	α	f	α	f
212	-	-	0.962	-	0.895	-	0.89	-	0.86	-
838	-	-	0.942	-	0.873	-	0.67	-	0.82	-
924	-	0.94	0.951	-	0.881	-	0.63	-	0.82	-
1054	-	0.97	0.876	-	0.809	-	0.80	-	0.86	-
64	-	0.83	-	0.980	0.952	-	0.50	-	0.92	-
2	-	1.00	-	0.854	-	0.936	1	-	0.91	-
1	-	-	0.759	-	-	0.695	-	-	-	0.86
5	0.83	-	0.519	-	-	0.467	-	-	-	1

α = fraction of diffuse reflection when backscattering is present.

f = fraction of diffuse reflection when specular reflection is present.

Sample 1054 is also of particular interest because there were some changes in the physical characteristics of the sample during the period when it was being tested. Flow measurements were made on the sample (1) before the initial separation measurements, (2) after the first set of separation measurements, and (3) after the second set of separation measurements. The flow measurements indicated that between the first and second set of measurements there was a change in either the number of capillaries, the capillary radius, the surface scattering law, or some combination of these. After the second set of separation measurements, the sample was cleaned with a solution of a commercial cleaning agent called Decontam. Flow measurements after the cleaning indicated flow character essentially the same as that of the original flow measurements. Although it is less certain, there also could have been a decrease of as much as 20% in the initial slope between the first and second sets of separation measurements. This is less certain because the sample characteristics were probably changing during the separation tests which occurred over a period of over six months. The measured parameters at the different times are shown in table 6.

Analysis of all the parameters involved indicates that the most probable explanation is that an oil film with a thickness of between 1000 and 2000 A was adsorbed on the walls of the capillaries, which in turn affected the surface scattering law. A silane wetting agent was used on the outside of

Table 6

VARIATION IN FLOW PARAMETERS
FOR SMALLEST GLASS CAPILLARIES

Sample Number	$S \times 10^{-4}$ (cm^{-1} Hg)	$w_o \times 10^{-4}$	$w_m \times 10^{-4}$	R_1	R_2	R_3
1054[a]	2.17	--	25.87	4.907	--	5.065
1054[b]	1.91	28.0	21.85	4.749	4.839	4.788
1054[c]	2.36	36.0	26.90	5.007	5.262	5.132

R_1 = capillary radius from Poiseuille flow.

R_2 = capillary radius from free molecule flow.

R_3 = capillary radius from slip flow.

[a]Before first set of separation measurements.

[b]After first set of separation measurements.

[c]After cleaning.

the capillaries to assure good adhesion between the glass and the epoxy bonding agent. This silane could have migrated to the inside of the capillaries. Because of the small change in the capillary radius as indicated by Poiseuille flow in comparison with the larger changes in the slip and free molecule transport ratios, the data are more consistent with a decrease in specular reflection due to the oil adsorption rather than the alternative explanation which would require that the adsorbed oil film produce an increase in backscattering. The data appear to indicate no change in the number of capillaries which would have required that the capillary radius calculated from the free molecule and slip transport ratios increase more than that calculated from Poiseuille flow. It would also require no change in the initial slope of the separation curve. This conclusion is also supported by the fact that the sample was easily cleaned. It is doubtful that such small capillaries could be cleaned if they were completely plugged.

Figure 32 shows a comparison of the data obtained on sample 1054 with a curve calculated from PBM with the capillary radius arbitrarily adjusted to give the best fit of the data. The best fit of adjusted parameters for the GCM is also shown. With arbitrarily adjusted parameters the data are fairly well represented over the full range of the data. This shows that the PBM and the GCM can be made to be virtually identical with appropriate selection of parameters.

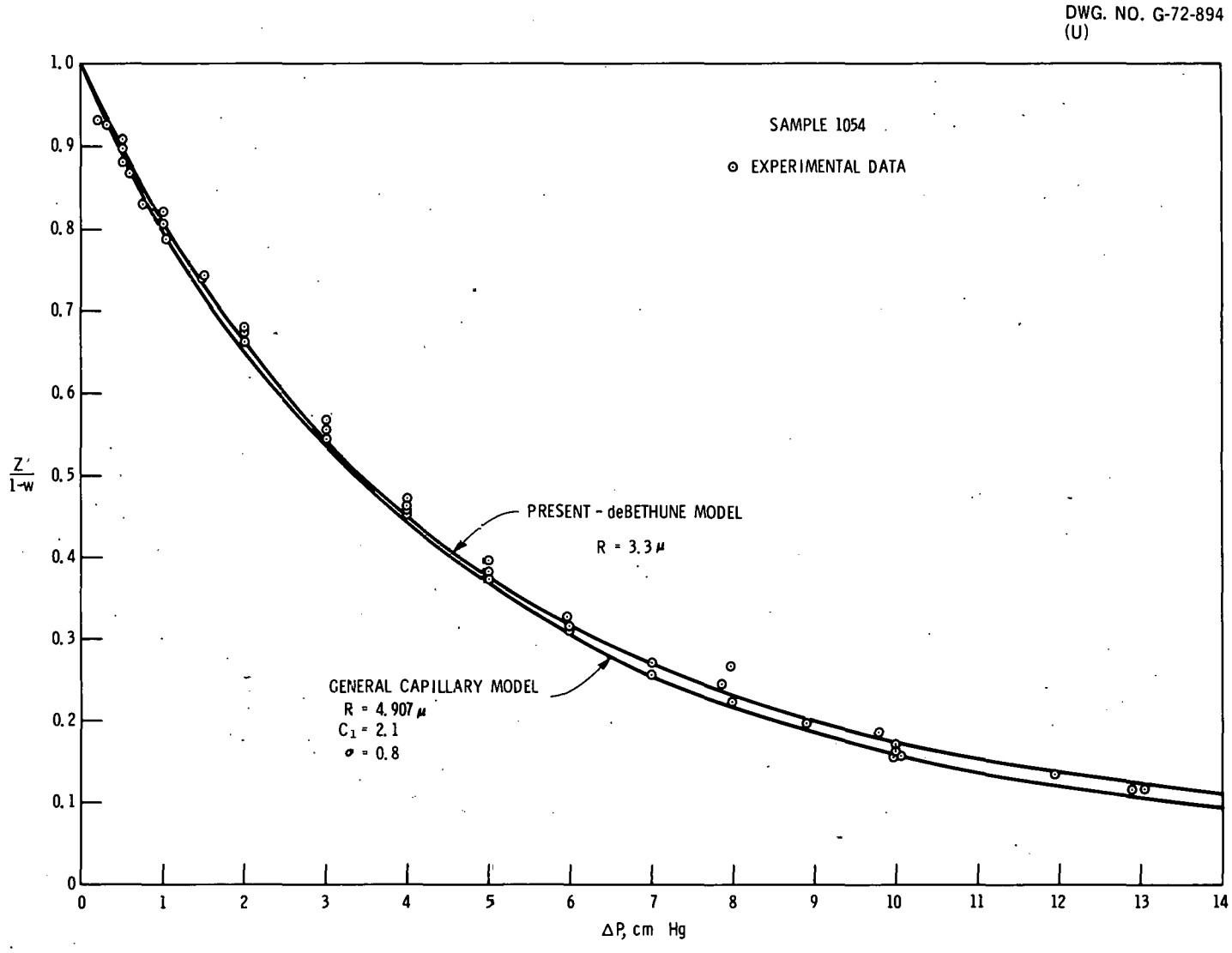

Figure 32

BEST AGREEMENT BETWEEN EXPERIMENTAL DATA AND THEORETICAL CURVES USING ADJUSTED PARAMETERS

As shown in table 5, the capillary radius from PBM and the C value from GCM both indicate backscattering. However, both the C and σ required to fit the separation data are quite different from the range of values measured by Lund and Berman and, in fact, are quite different from the approximated C and σ obtained from flow measurements on these samples. The values from the flow and separation measurements are approximate because least squares curves have not been obtained. Table 7 compares the C and σ values obtained from flow measurements with several combinations of C and σ used to fit the separation data for all the test samples. This shows the sensitivity of the fits of the data to variations in the constants C and σ by the variation in the calculated standard deviations.

Variations in the surface scattering law should have different effects in the two separation theories. If the appropriate correction is made in the PBM to account for the effect of scattering law deviations on free molecule flow, then this theory predicts that the effect will be to change the slope of the separation curve by the same fraction as the change in the free molecule transport ratio. However, in the GCM the effect is different from that obtained in the PBM. If the Maxwell calculation of the variation of C and σ with specular reflection or backscattering as given on pages 34 and 35 is assumed, then very little effect on the initial slope of the separation curve is produced by scattering law deviations. If the relation between C and σ observed by Lund and Berman, which is different from the variation predicted by Maxwell, is assumed, then the effect is to make a fractional change in the initial slope of the separation curve by about one-third of the fractional change in the free molecule transport ratio. All of the theories indicate that the initial slope of the separation curve should be proportional to the hydraulic radius. Therefore, the ratio of the initial slopes of the separation curves to the hydraulic radius for similar geometry test samples should have the same value. Experimentally, variations of the initial slopes of the separation curves due to variations in the wall scattering law can be observed by variations in the slope-to-radius ratio. Table 8 shows at least 20% variation in the measured ratios of slope-to-radius ratios. This is about the variation observed in the flow data, which is also presumably due to scattering law variations. This slope variation appears to be larger than can be accounted for by the measured range of C and σ variations using the GCM, but is within the range of accountability for the modified PBM.

Qualitatively, this difficulty can be seen in the following way. In the PBM form, the effect of specular reflection or backscattering is in direct proportion to the increase or decrease in gas velocity. The momentum exchange between unlike molecules is proportional to the difference in average velocity. An increase in average velocity increases the momentum exchange between unlike molecules and therefore increases the slope of the separation curve. In the GCM, an increase in the free molecule diffusion rate caused by specular reflection tends to decrease the initial slope of the separation curve since this increases the amount of separative flow. An increase in the slip transport ratio from the same cause will tend to increase the initial slope of the separation curve since this increases

Table 7

COMPARISON OF GCM PARAMETERS OBTAINED FROM FLOW MEASUREMENTS WITH THOSE NEEDED TO FIT THE SEPARATION DATA

Sample Number	Flow Measurements		Separation Measurements		
	c	σ	c	σ	s
212	-	1.77	1.00	1.85	0.0353
			1.50	1.00	0.0342
			1.25[a]	1.25	0.0314
838	-	-	1.00	1.85	0.0353
			1.50	1.00	0.0438
			1.25	1.25	0.0406
			2.00[a]	1.00	0.0275
			2.00	0.75	0.0397
			2.20	0.80	0.0295
924	0.878	1.80	1.00	1.85	0.0404
			1.50	1.00	0.0390
			2.00	1.00	0.0356
			1.75	1.00	0.0345
			2.20[a]	0.80	0.0336
1054	0.945	1.90	1.00	1.85	0.0333
			1.50[a]	1.00	0.0231
			1.33	0.925	0.0325
			1.25	1.25	0.0275
64	0.712	2.03	1.00	1.85	0.0258
			1.50	1.00	0.0331
			2.00	1.00	0.0203
			2.00	1.25	0.0328
			3.00	0.75	0.0341
			3.00[a]	0.50	0.0194
2	1.00	1.84	1.00	1.84	0.0567
			1.00[a]	1.00	0.0215
			1.00	0.75	0.0226
			0.75	1.00	0.0260
			1.33	1.00	0.0367
1	-	2.28	-	-	-
5	-	0.86	-	-	-

[a]Smallest Standard Deviation.

Table 8

SEPARATION EFFICIENCY INITIAL SLOPE RATIOS
COMPARED WITH RADIUS RATIOS

Sample Numbers	Initial Slope Ratio	Hydraulic Radius Ratio	Slope Ratio / Radius Ratio	
			Measured	Clausing
212/1054	5.22	5.039	1.036	0.982
838/1054	2.75	2.633	1.033	0.997
924/1054	2.72	2.580	1.054	0.994
64/1054	5.43	4.488	1.210	0.994
2/1054	4.65	5.506	0.844	0.550
1/1054	6.52	5.200	1.254	2.202
5/1054	2.45	2.092	1.171	2.544
1/5	2.66	2.485	1.070	0.866

the nonseparative flow. If the C and σ are both affected by the same fractional change, as is expected from the Maxwell theory, then the two effects almost cancel each other and result in no change in the initial slope. There will be a decrease in separation efficiency at the higher pressures, however, because of the increase in σ. Since Lund and Berman have observed that the magnitude of σ changes more rapidly than C, this type of change because of specular reflection causes a net increase in the initial slope, but by a smaller magnitude than that predicted by the modified Present and deBethune theory.

Because of this effect, the PBFM and the GCM should more closely correspond to each other when pure diffuse reflection is observed. Qualitatively, the two theories appear to fit the data better for sample 1054 than for any of the other samples, even though the C value required by the GCM indicates relatively less backscattering than for the other samples, and the capillary radius required by PBM indicates relatively more backscattering than for the other samples. In contrast, the C's and σ's inferred from the flow data imply the least deviation from diffuse reflection for sample 1054, with increasing amounts of specular reflection for the other samples. Although there are some serious questions concerning the level of the flow data, they do indicate the relative value and relative ordering of all the test samples.

Figures 33 through 35 show the experimental data obtained on samples 838, 924, and 64, compared with three of the mathematical models. In each case the calculations using the PBM are lower than the experimental data over the entire range of pressures when the measured capillary radius with the

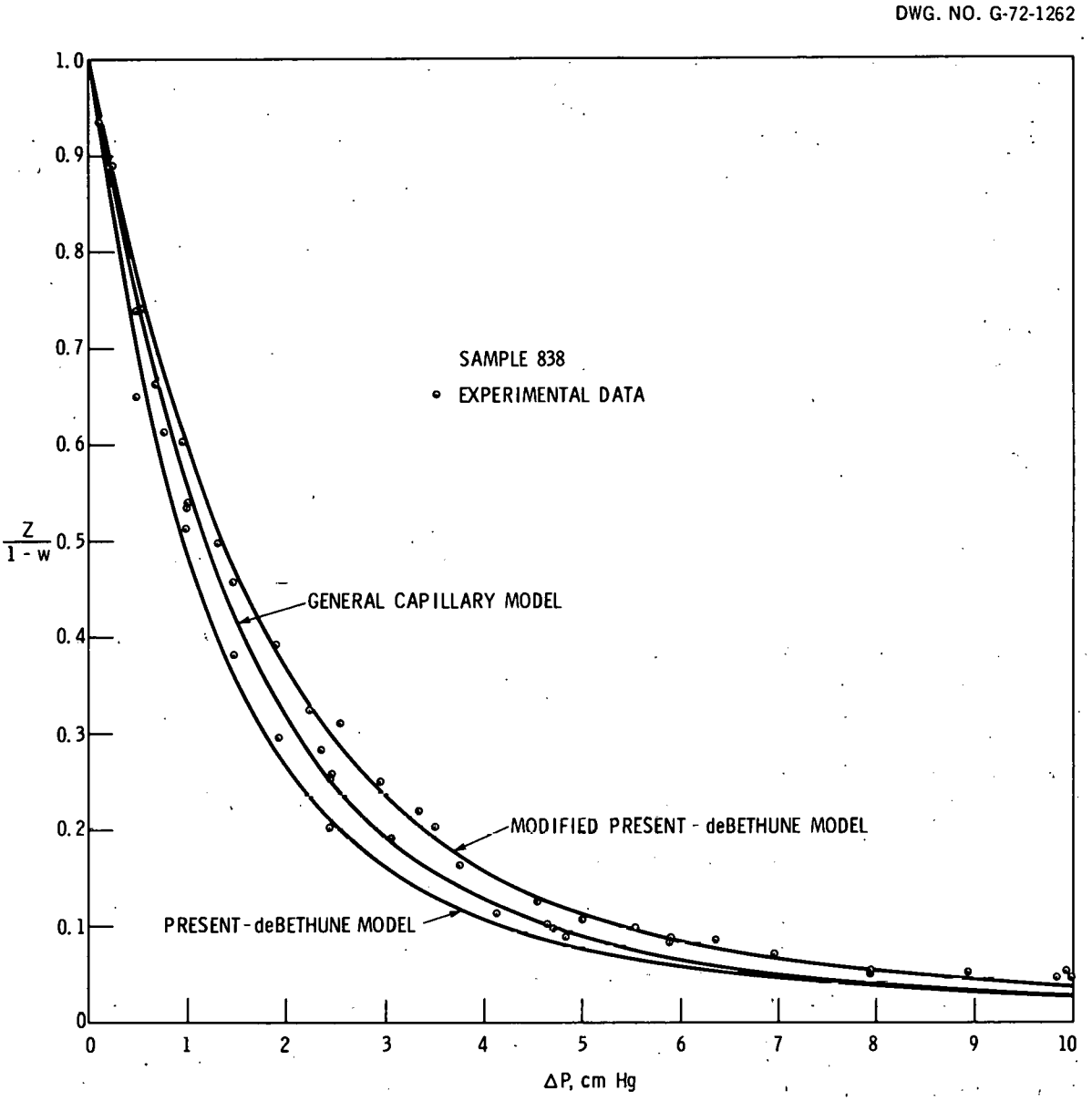

Figure 33

SEPARATION EFFICIENCY OF 12.91-MICRON-RADIUS PLASTIC CAPILLARY SAMPLE

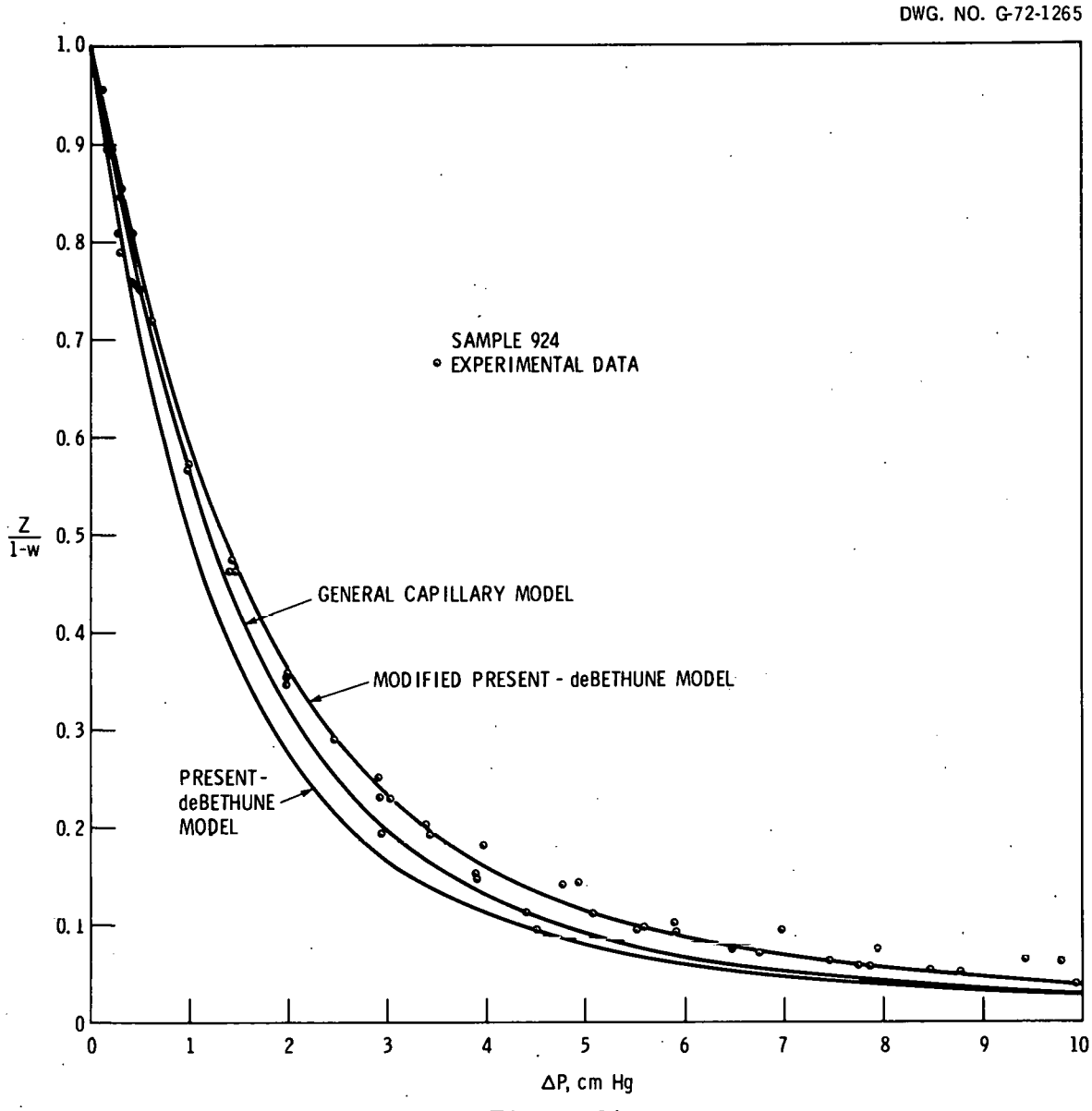

Figure 34

SEPARATION EFFICIENCY OF A 12.65-MICRON-RADIUS PLASTIC CAPILLARY SAMPLE

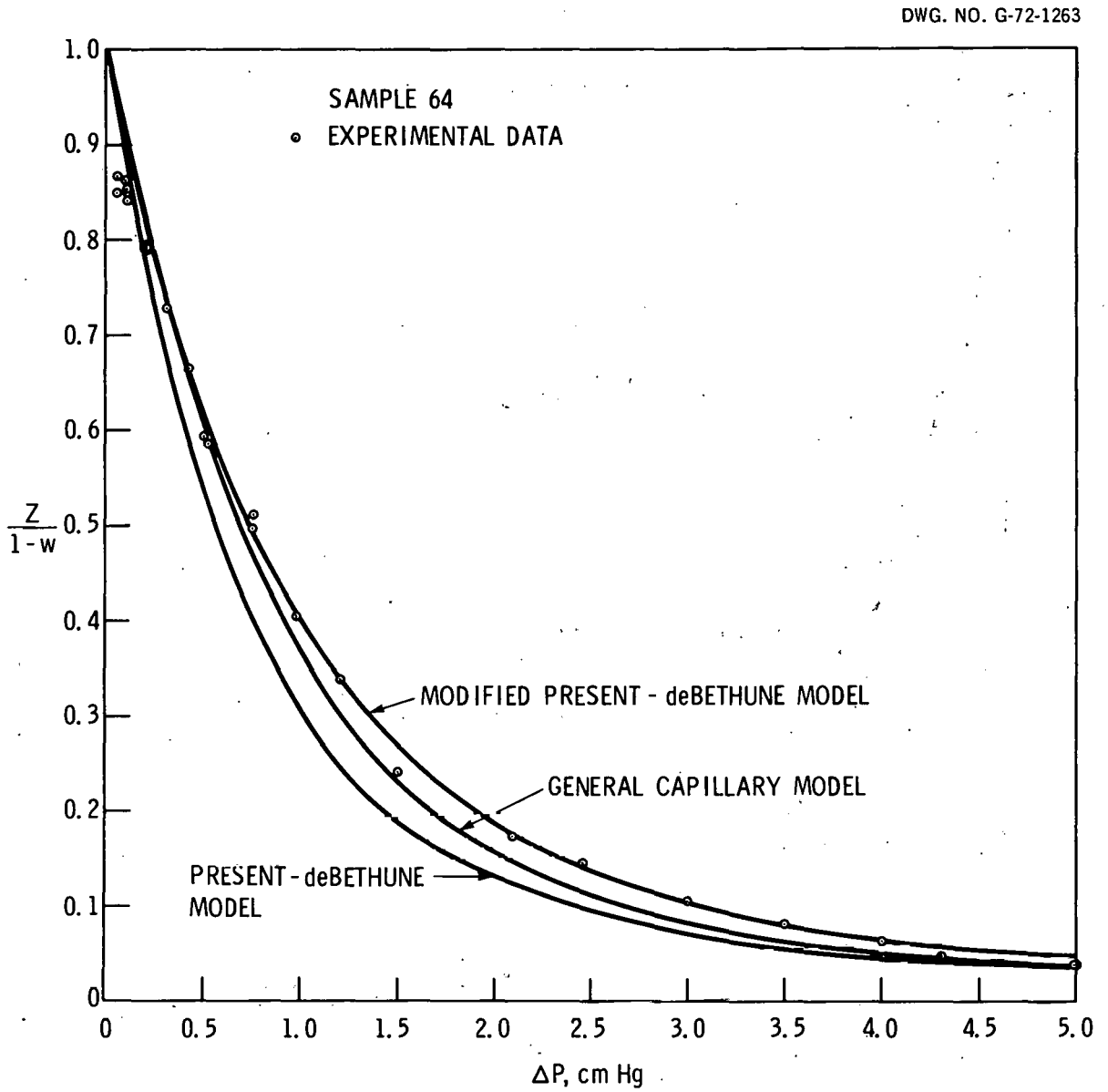

Figure 35

SEPARATION EFFICIENCY OF 22.01-MICRON-RADIUS GLASS CAPILLARY SAMPLE

appropriate Clausing factor is used. The GCM calculations are also lower than the experimental data in every case when the measured capillary radius is used with nominal values of C and σ. Again, the arbitrary modifications in the PBFM calculations produce a good fit of the experimental data in each case. Table 9 gives a comparison of the standard deviations on the fits for all the samples with the different calculations.

Table 9

COMPARISON OF THE STANDARD DEVIATION OF THE EXPERIMENTAL DATA OBTAINED WITH THE DIFFERENT MODELS

Sample Number	PBM	GCM[a]	GCM[b]	PBFM
212	0.0647	0.0353	0.0314	0.0301
838	0.0500	0.0316	0.0275	0.0291
924	0.0557	0.0404	0.0336	0.0358
1054	0.0617	0.0333	0.0231	0.0256
64	0.0421	0.0258	0.0203	0.0213
2	0.0855	0.0567	0.0226	0.0158
1	0.0486	0.0670	--	0.0328
5	0.0722	0.0355	--	0.0176

[a]Standard values of the constants C and σ.

[b]The constants C and σ were varied to give approximately minimum variance.

The deviations in scattering law inferred from each of the assumed models are given in table 5. The PBM implies that backscattering is present, but that the pattern of changes is consistent with the pattern of changes inferred from the flow measurements. The GCM using only the initial slope is also consistent with this ordering as indicated by R_6/R_1. However, the full GCM fits show a pattern of change opposite to that inferred from the flow measurements. The best agreement is obtained with sample 1054 which shows the smallest deviations in the scattering law, and the poorest agreement is with sample 64 which shows the largest deviation in the scattering law. The pattern of change in the C constant opposite to that indicated by the flow data implies that the GCM is not capable of accounting for deviations caused by specular reflections or backscattering. In addition, the values of the constant σ required to fit the separation data are consistently lower than those required to fit the flow data. The PBFM fits all of the data equally well and, therefore, apparently more accurately accounts for these anomalies.

The best experimental indication of the scattering law deviations is given by the ratios of the measured initial slopes of the separation curves to the capillary radius as shown in table 8. The deviations of the initial slope ratios from the capillary radius ratio could be simply due to inaccuracies in estimating the initial slopes, but these deviations are most likely due to the variations in the scattering law for molecules on the different surfaces, since they are consistent with the variations inferred from the flow measurements. It was shown that a fraction of molecules specularly reflected from a surface increases the effective radius of the capillary for free molecule flow and increases the initial slopes of the separation curve through the K constant in the PBM and the PBFM. According to the data of Lund and Berman [3], free molecule flows are usually less than those predicted by the Clausing theory and must be explained by a mechanism similar to the backscattering suggested by Berman. Backscattering will decrease the initial slope of the separation curve since it corresponds to an effective decrease in the capillary radius. The ratios of slope ratios to radius ratios given in table 8 imply either more specular reflection for sample 64 or more backscattering for sample 1054. Since sample 64 was fire polished, the former is more likely. If specular reflection is present, then this implies that a scaling factor to reduce the capillary radius is needed in both theories. This could mean that the Clausing factor as used by Present and deBethune does not give the correct relative momentum transfer to the walls, and therefore the proportionality constant for momentum exchange between molecules is incorrect. Of course, it could also mean that the calculation of momentum exchange between molecules is incorrect. But if the latter is the correct interpretation, the same error in the proportionality constant should be in effect for all geometries. Table 8 shows the calculated ratio of the slope ratio to the radius ratio for the indicated test samples assuming that the initial slope is proportional to the Clausing factor for each sample. There does not appear to be a consistent proportionality constant between the measured ratio of slope ratio to radius ratio and that calculated from the Clausing factors for the different geometries. This tends to imply that the problem is associated with the use of the Clausing factor rather than an error in the calculation of momentum exchange between molecules.

The experimental separation data generally became rather unreliable for forepressure of 2 mm or lower. It is believed that this effect and the scatter in the data are a result of a cut effect problem and air contamination because of the required long sampling times. Detailed cut curves were obtained on samples 924 and 1054, and the curves shown in figures 36 and 37 illustrate this point. The cut is varied by adjusting the reject flow. Separation data were taken over a range of cuts to determine if there were any losses in separation efficiency due to a concentration gradient in front of the sample. These data were plotted and extrapolated to zero cut. At zero cut no concentration gradient should exist. When the measurements can be made at a low enough cut so that there is no discernable difference between the measured value and the extrapolated value, then cut curves are not needed for each test. Measurements at pressures above 5 mm Hg showed that the cut effect could properly be accounted for by the correction given on page 13 for cuts existing below approximately $\theta = 0.05$. Most measurements were made at cuts of 0.001 or less where a

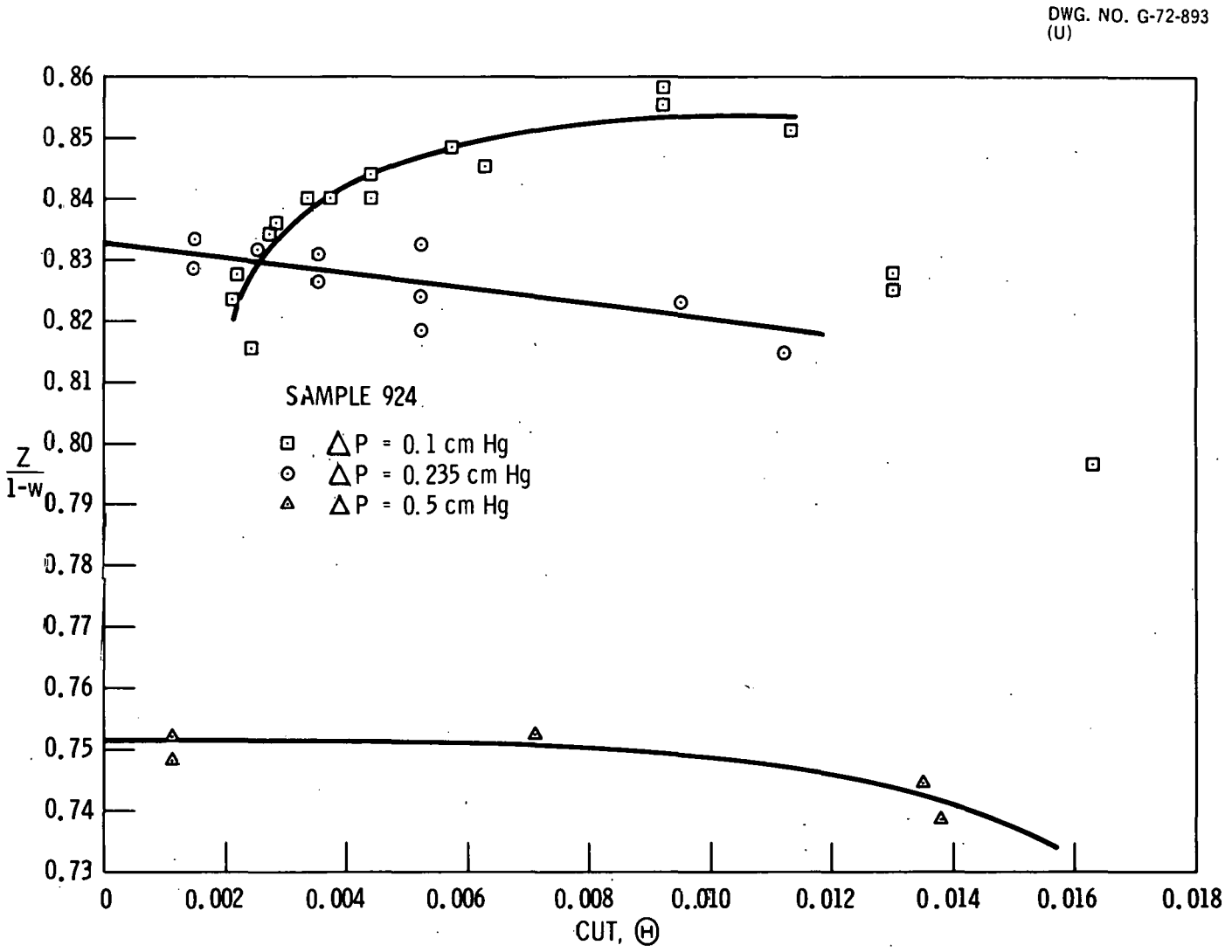

Figure 36

CUT CURVES FOR A 12.65-MICRON-RADIUS PLASTIC CAPILLARY SAMPLE

DWG. NO. G-70-948
(U)

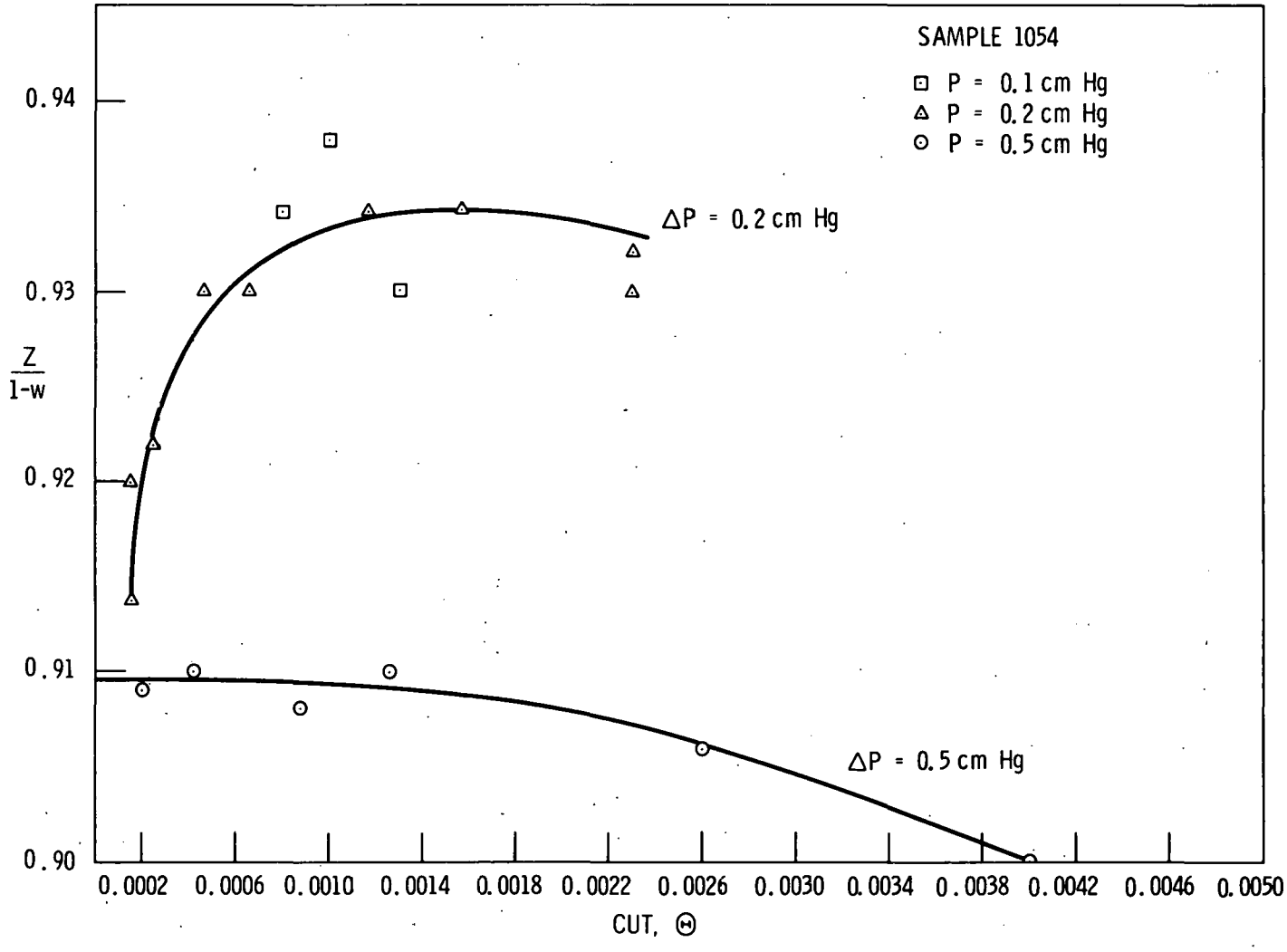

Figure 37
CUT CURVES FOR A 4.907-MICRON GLASS CAPILLARY SAMPLE

correction was unnecessary. A very unusual cut effect was observed at pressures of 2 mm Hg and lower. A decrease in separation efficiency is observed as the cut is decreased. This occurs when the velocity of the feed gas is about 0.01 or greater times that of sound. It is possible that the high velocity of the feed gas produces a perturbation in the velocity distribution function which causes this effect. From experience, it is concluded that the highest measured separation efficiencies at these pressure levels are the most representative of the sample, and that generally all of these lower pressure data are biased low.

Figures 38 and 39 show the lowest pressure data obtained with samples 1054 and 924. As indicated above, the data at pressures of 2 mm Hg or lower are less reliable and tend to be low because of the cut effect. These two figures also show the three model calculations and more accurately indicate how they compare at these lower pressures.

Comparison of the experimental data obtained on a long glass capillary, an orifice, and a parallel plate is shown in figures 40 and 41. The radius of the capillary samples and the height of the parallel plate samples are not identical, but they are close enough to make a good comparison of the separation efficiency obtained on the different geometries. These two figures emphasize the small differences in experimental data which can result in significant differences in the parameters required by the PBFM to obtain a good fit of the data.

A large difference in the initial slope of the separation curve between the long capillary and the parallel plate having the same radius and plate spacing is predicted by PBM when the appropriate Clausing factors are used. As is seen in figures 40 and 41, this is not experimentally observed. The length-to-plate spacing ratio for the parallel plate and, to a lesser extent, the length-to-radius ratio for a capillary have an effect on the initial slope of the separation curves. Table 10 shows the calculated effect for the test samples used in this study. The data may not be accurate enough to make a definite conclusion, but the data are more consistent with the hypothesis that the length-to-spacing ratio for parallel plates does not affect the initial slope of the separation curve to the extent predicted and that it should be proportional only to the plate spacing. As seen in table 9, the ratio of the initial slope of the separation curves for the two parallel plate samples tested is different from the ratio of the plate spacing, but not as predicted by the Clausing correction to the Present and deBethune theory. There is an indication from the flow data that there is more specular reflection with test sample 1 than with test sample 5, which would account for this deviation in the separation slope. Again, this is an important point because this also implies that the Clausing factor is not the appropriate coefficient to indicate the correct momentum transfer to the wall. However, additional data are needed for confirmation.

Figure 42 shows the separation data for the short capillary test sample 2 compared with the calculated curves. In this case the PBM, using the appropriate Clausing factor with the capillary radius and the appropriate

DWG. NO. G-72-1264

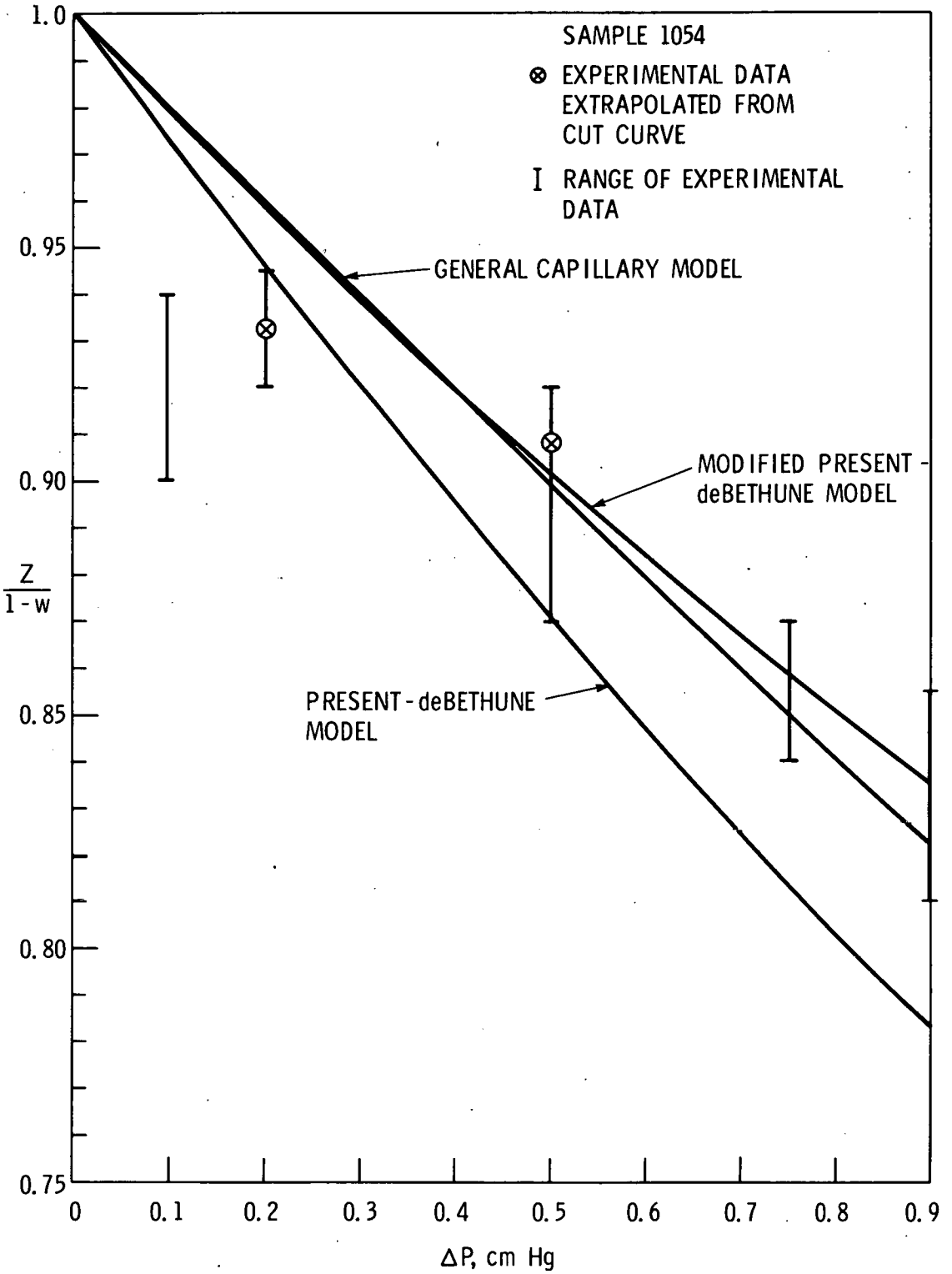

Figure 38

LOW PRESSURE SEPARATION EFFICIENCY DATA FOR 4.907-MICRON-RADIUS GLASS CAPILLARY SAMPLE

DWG. NO. G-70-949-R
(U)

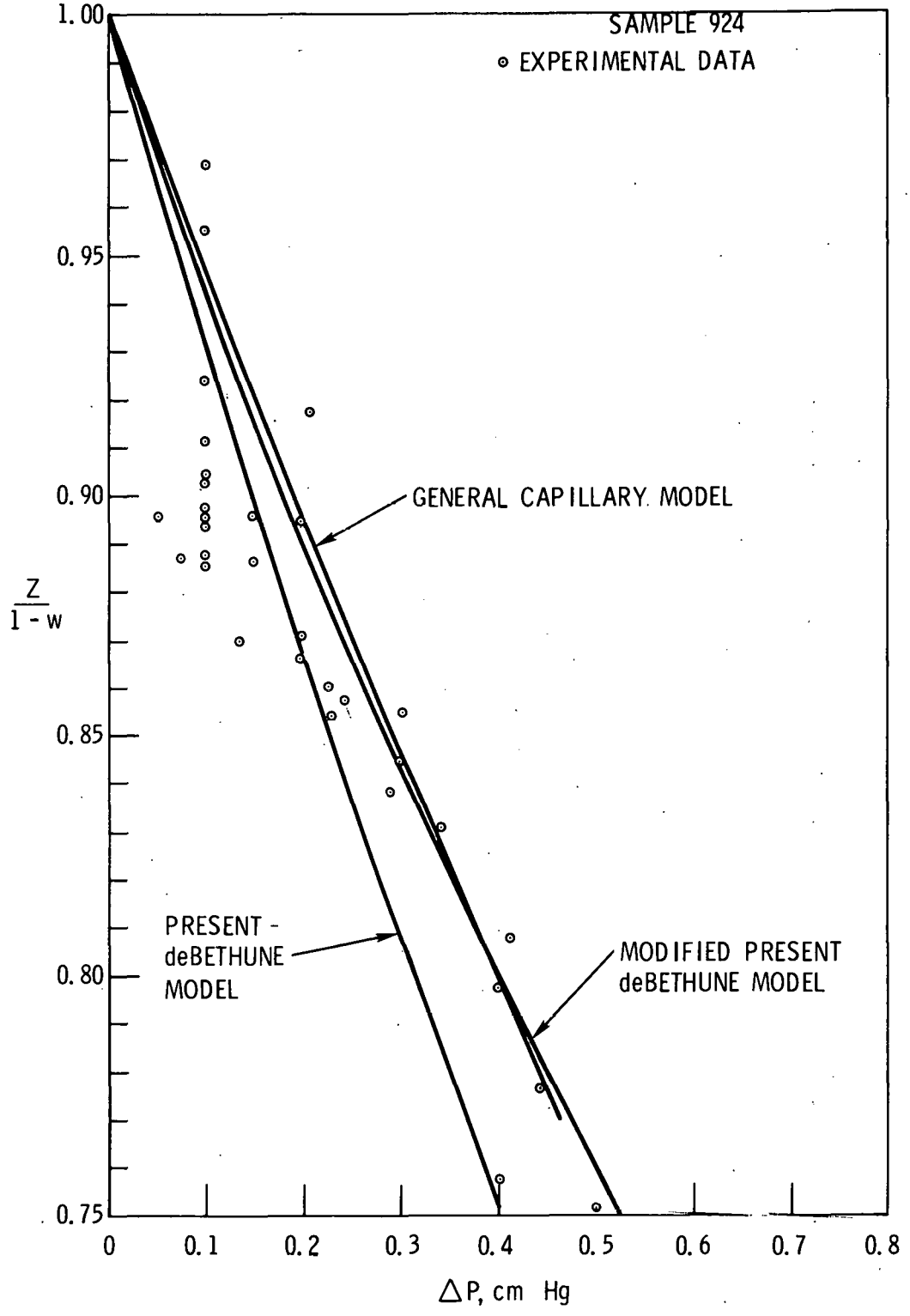

Figure 39

LOW PRESSURE SEPARATION EFFICIENCY DATA FOR 12.65-MICRON-RADIUS PLASTIC CAPILLARY SAMPLE

DWG. NO. G-72-895
(U)

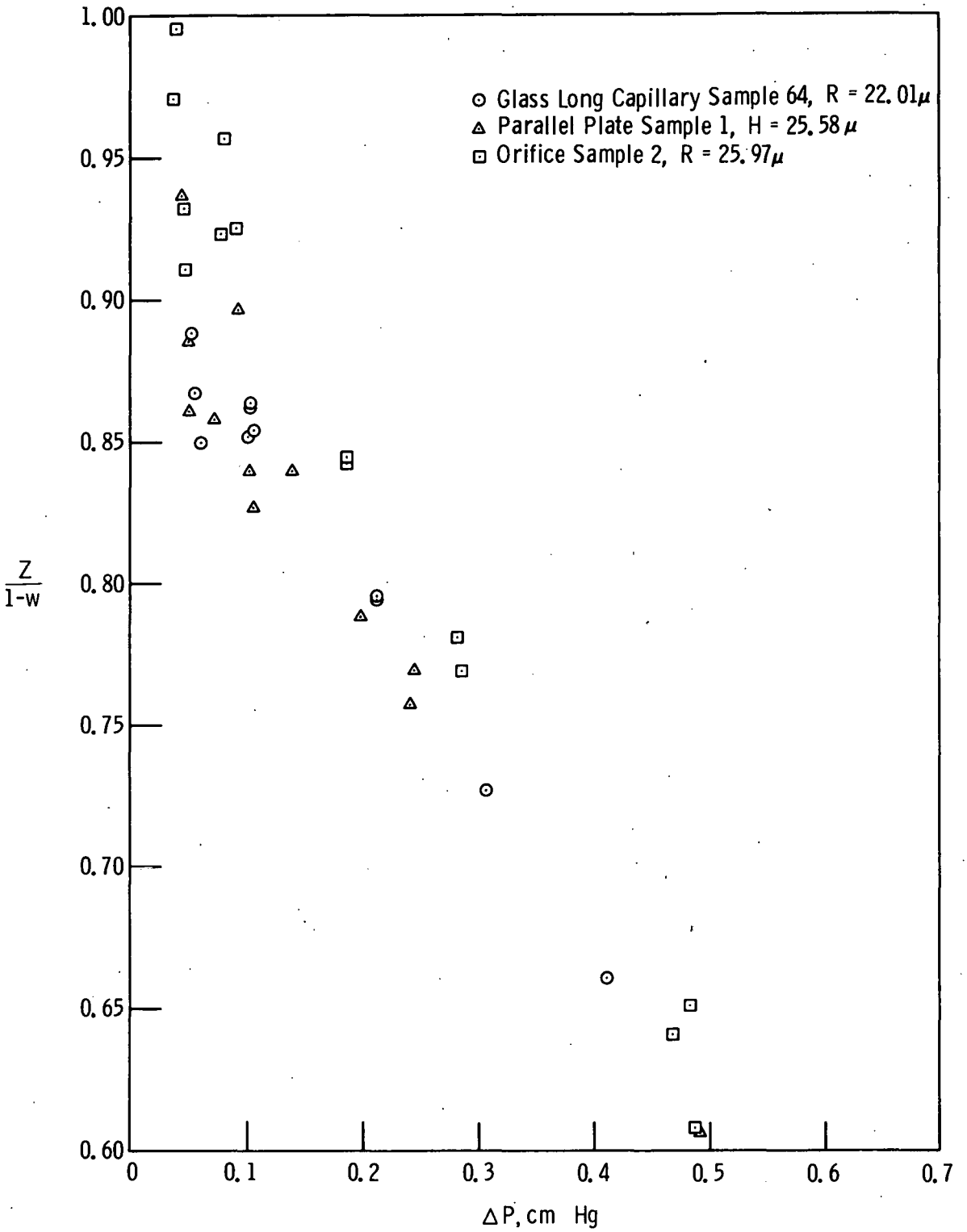

Figure 40

COMPARISON OF GLASS LONG CAPILLARY, ORIFICE, AND PARALLEL PLATE DATA IN LOW PRESSURE REGION

DWG. NO. G-70-952
(U)

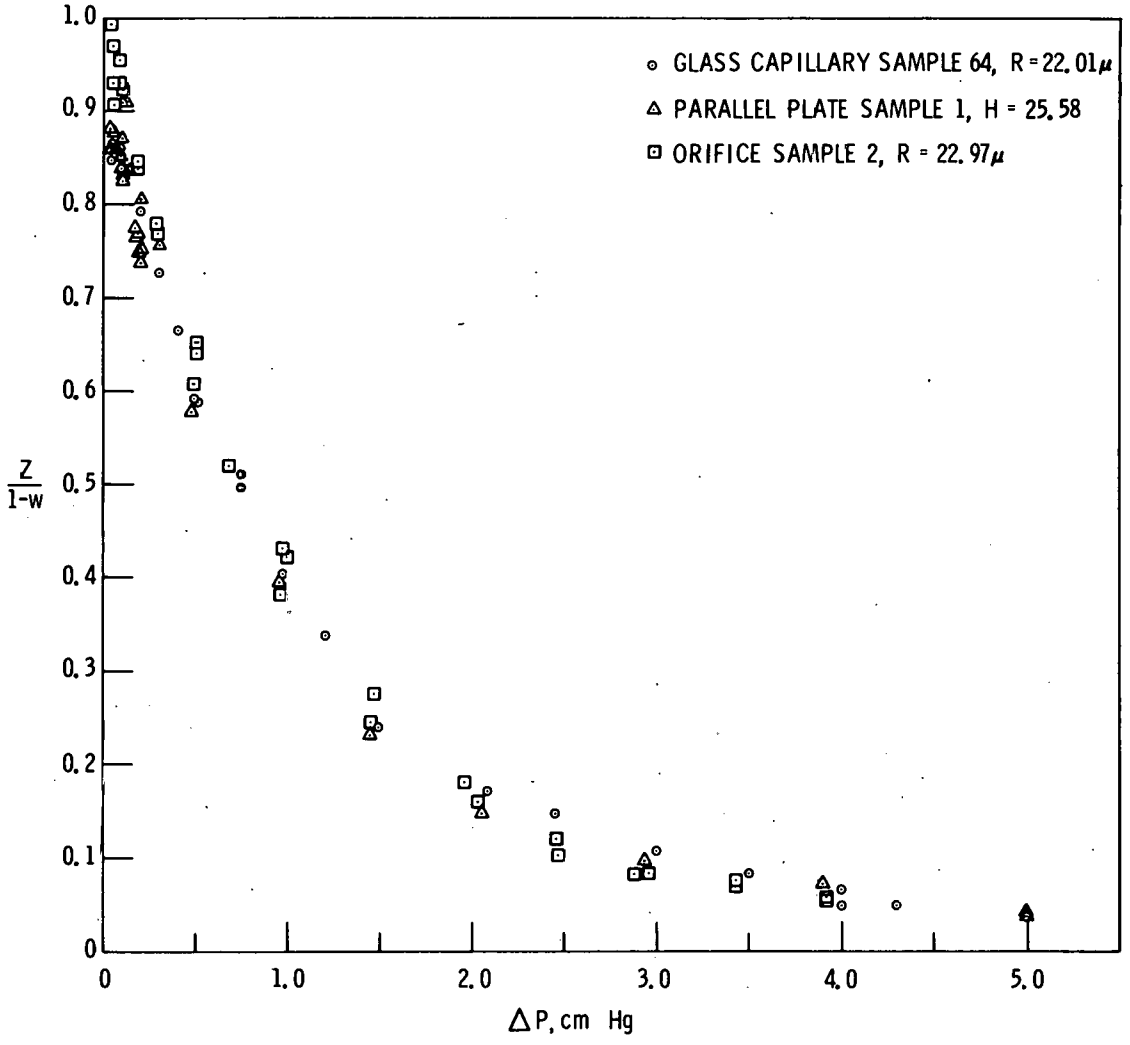

Figure 41

COMPARISON OF SEPARATION EFFICIENCY OF LONG CAPILLARY, ORIFICE, AND PARALLEL PLATE

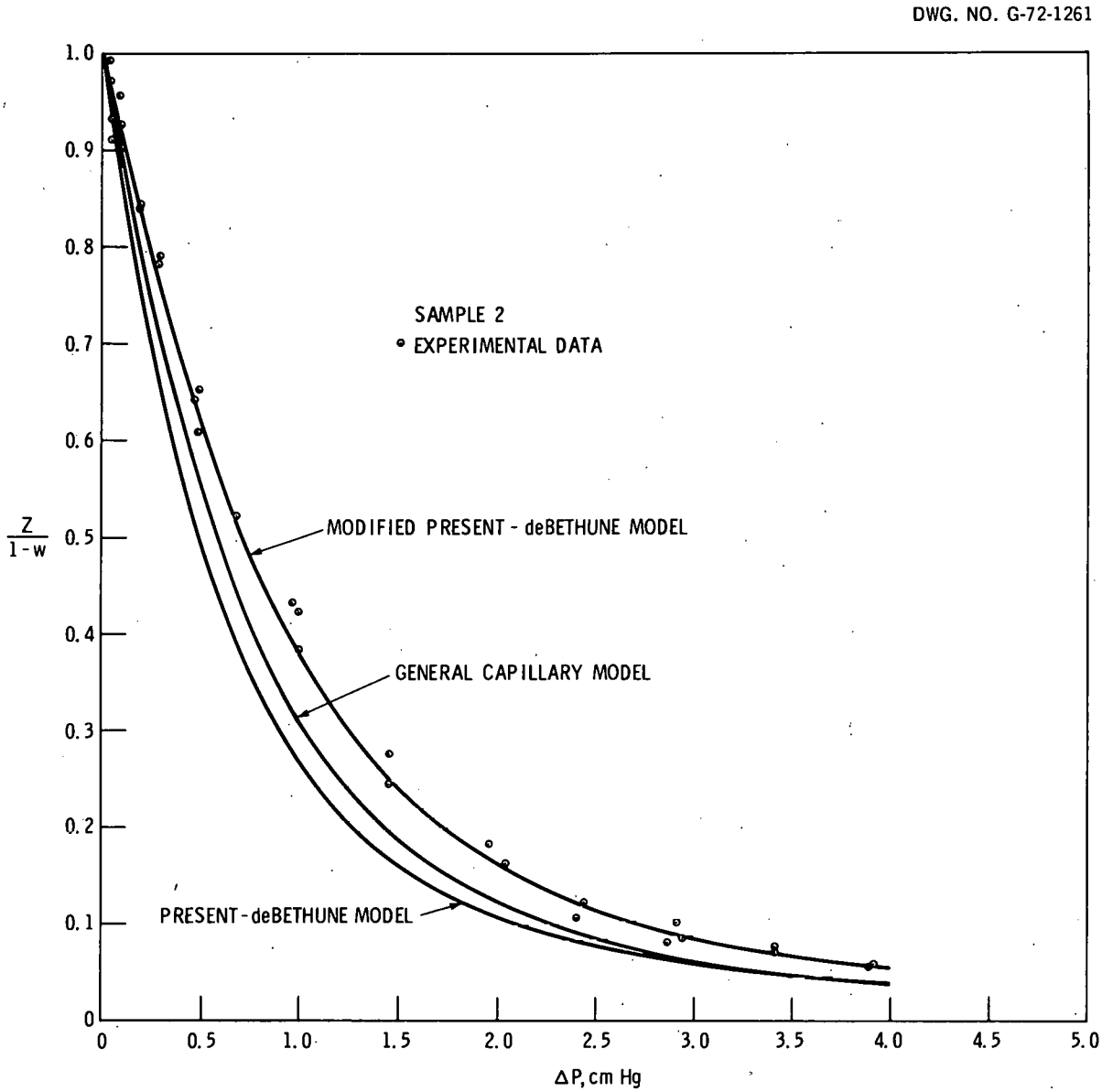

Figure 42

SEPARATION EFFICIENCY OF 25.97-MICRON-RADIUS GOLD ORIFICE SAMPLE

Table 10

THE MODIFICATION CONSTANT K FOR THE PRESENT AND deBETHUNE MODEL FOR DIFFERENT GEOMETRIES AND CALCULATION METHODS

Sample Number	Clausing Free Molecule Flow		Slip Flow	Momentum Transfer
	Infinite Length	Finite Length	Infinite Length	Infinite Length
212	1	0.974	0.76	1.178
838	1	0.989	0.76	1.178
924	1	0.986	0.76	1.178
1054	1	0.992	0.76	1.178
64	1	0.986	0.76	1.178
2	1	0.550	0.76	--
1	2.203	--	0.76	1.178
5	2.544	--	0.76	1.178

K' constant taking proper account of viscous flow for the short capillary, represents the data better than the GCM with nominal values of C and σ. This result perhaps should not be too surprising since the transmission ratio for this test sample is linear with average pressures as was assumed in the Present and deBethune theory. A somewhat better fit is obtained with the PBFM using an arbitrary value of the constant K which is again smaller than that calculated from the Clausing factor. The best fit with PBFM was obtained with a value of $W_m/W_K = 1$ corresponding to a transmission ratio, linear with average pressure, which is consistent with the intent of the modification of the PBM. A good fit is obtained with the GCM when a smaller than nominal value of σ is used.

Figures 43 and 44 show the separation data for the parallel plate test sample 1 and 5 compared with the model calculations. In this case, the calculation for PBM using the Clausing factor was so poor that a calculation using the spacing itself as the dimension parameter was made. This calculation corresponds to using the hydraulic radius as was suggested by Present and deBethune. However, this suggestion is inconsistent with the change to the Clausing factor which was made by Present and deBethune for the capillary. The use of the hydraulic radius in the PBM produced calculated values of the separation efficiency ratio which were much higher, but still lower than the experimental data. The GCM using nominal C and σ gives results significantly higher than the data in the low pressure region and significantly lower than the data in the high pressure region. The calculated slope-to-spacing ratio for the GCM is about 50% less than the measured slope-to-spacing ratio. Again, both the PBM and GCM give poor representation of the experimental data for the parallel plate data.

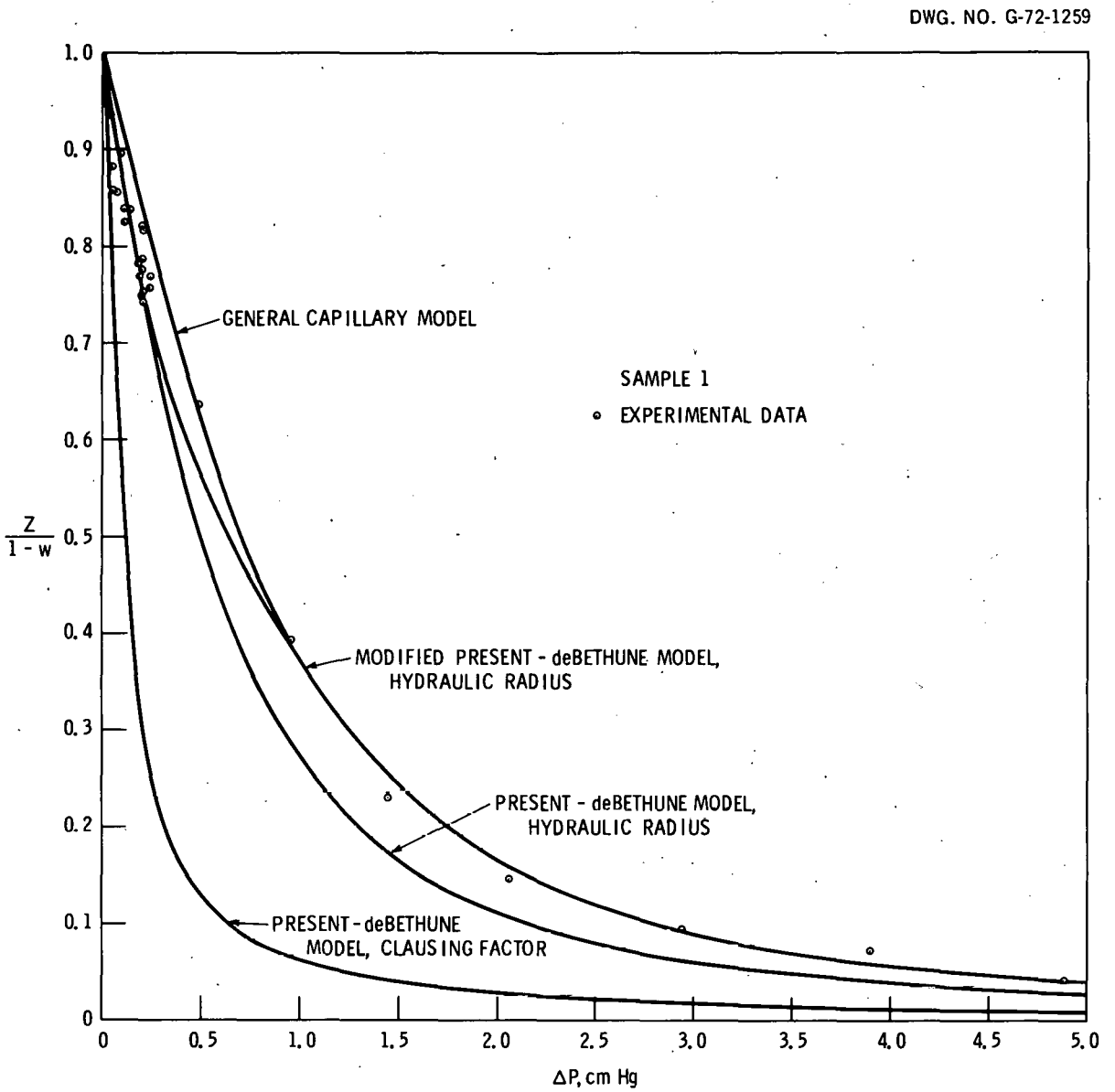

Figure 43

SEPARATION EFFICIENCY OF STEEL PARALLEL PLATE SAMPLE WITH PLATE SPACING OF 25.58 MICRONS

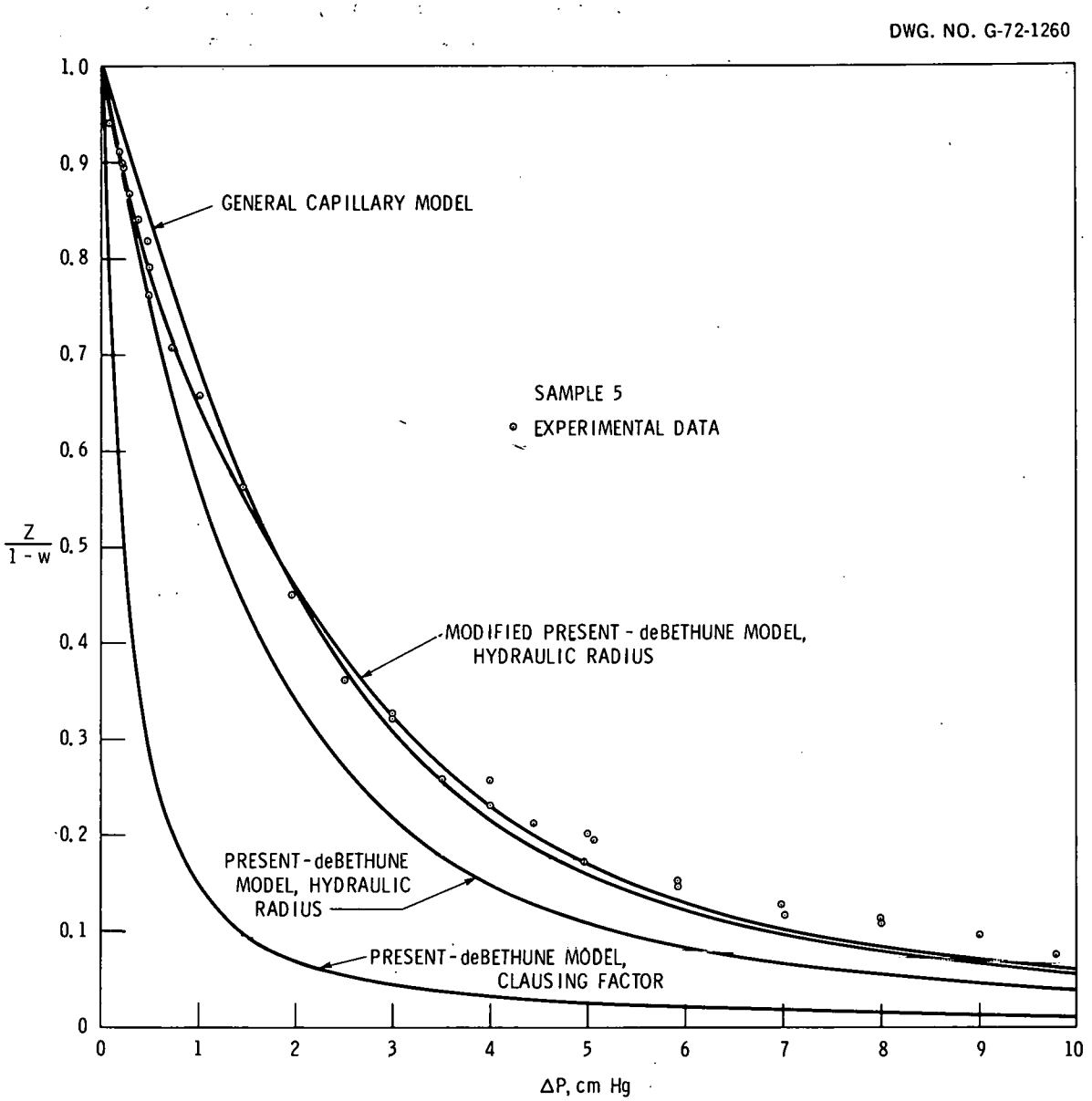

Figure 44

SEPARATION EFFICIENCY OF STEEL PARALLEL PLATE SAMPLE WITH PLATE SPACING OF 10.29 MICRONS

Because of the pattern of deviations from the experimental data, it would be particularly difficult to fit the experimental data with the GCM even with completely unreasonable C and σ. The PBFM fits the experimental data fairly well with parameters consistent with the intent of the model when the hydraulic radius is used to represent the free molecule flow component, but not when the Clausing factor is used for that purpose.

CONCLUSIONS

A large body of accurate data showing the pressure dependence of the separation of neon isotopes by diffusion with a pressure gradient through different regular geometries is presented. The geometries investigated include long and short capillaries and parallel flat plates. The test samples were prepared with different materials such as glass, plastic, and metals. Consistent differences in the separation data were observed. Some of the differences in the separation data can be attributed to the geometric differences among the test samples and others can be attributed to the differences in the material used to prepare the test samples. The differences in the separation data produced by the materials used to prepare the test samples are presumably due to differences in the law of scattering of the molecules from these surfaces. Such deviations in the scattering law have been well documented as previously indicated.

Isotopes were chosen for this study to try to avoid discrepancies which would result if the anomaly produced by variations in the surface scattering law were different for the two gas species in the binary mixture. This appears to have been a fortunate choice, since both the flow and separation data show large anomalies presumably due to variations in the surface scattering law. However, as expected, the separation data show the anomaly to be the same for both isotopes, since the separation efficiency approaches that for ideal free molecule flow in every case. The variation in the anomaly due to surface scattering law deviations as indicated by both flow and separation measurements was about 30%. This variation is only slightly larger than that which was reported by Lund and Berman [3].

There was very good correspondence between the capillary radii and the plate spacings as determined by optical measurements and by flow measurements. In general, the flow measurements were more precise than the optical measurements. The best agreement between flow and optical measurements was obtained when a similar sample was metallographically polished before the optical measurements were made. Most of the optical measurements were obtained on the as-made samples with their rough, poorly defined edges. For this reason, the capillary radii and plate spacings determined from the flow measurements were considered to be the more accurate.

Even though the approaches to a theory for separation are grossly different in character, the theory of Present and deBethune, PBM, and the result obtained by Malling using the Lund and Berman flow equations, GCM, are quite similar in character and calculation. The GCM should be more accurate because it specifically provides for variations in free molecule flow as well as for slip flow. Also, the pressure weighting is slightly different because of the independent variation in slip and free molecule flow. However, the coefficients of free molecule and slip flow required to fit the separation data are quite different from those measured by Lund and Berman or those indicated by the flow measurements on the test samples used in this study. The pattern of changes in the initial slope of the

separation curves between test samples also seems contrary to the flow measurements. This discrepancy appears to be caused by the way the free molecule and slip flow anomalies are introduced into the theory. In the GCM there are only separative and nonseparative terms which are influenced independently by the anomalies. There is no interaction term. In the PBM the whole problem is an interaction term through the momentum exchange calculation. The momentum exchange is proportional to the free molecule flow level which is constant. The PBFM allows the interaction term to be scaled to vary from the free molecule flow level to the slip flow level with appropriate influence from the flow anomalies in both cases. This approach appears to have a particularly favorable effect in allowing fits of the data for all geometries. This is most clearly demonstrated in the case of the parallel plates which exhibit such large variations between the free molecule and slip flow levels. The PBFM is purely an interpolation equation and seems to represent the data exceptionally well. It was derived from physical arguments and therefore can be given a physical interpretation, but only in a qualitative sense. The PBFM approach gives the PBM the same kind of flexibility that the Lund and Berman equations gives to the GCM. It should be clear that the refinements required to represent the separation data do not have to be nearly as accurate as those required to fit the flow data. However, they must account for the interaction between molecules.

In their theory, Present and deBethune derived equations for a capillary only. Initially, they calculated the free molecule flow for a capillary using the calculation technique of momentum transfer to the wall. However, this did not agree with the free molecule flow calculation of Knudsen, Clausing and others, so they introduced a correction factor to make their calculation agree with the Knudsen and Clausing value. In their paper, they indicated that the capillary radius should be replaced with the hydraulic radius (ratio of cross-sectional area to perimeter) for other geometries. However, to be consistent, it should be concluded that the appropriate Clausing factor which would define the free molecule transmission probability, for whatever geometry is considered, would be the appropriate value to use in the equations.

The GCM does use the appropriate Clausing factor with the capillary radius for capillaries and fairly well approximates that value at finite pressures for the parallel plate. The Hiby and Pahl interpolation is used for the parallel plate.

In the PBFM, the hydraulic radius is used and an appropriate constant is determined to fit the data. The constant which is determined should provide some implication as to what value is correct. The constants determined for the PBFM and the arbitrary constants used with the GCM to obtain the best fits indicate that the Clausing factor is not the best value to indicate the relative amount of momentum transferred to the walls. Both sets of constants imply that there is a smaller amount of momentum loss to the walls per unit of drift velocity than is indicated by the Clausing factor for the transmission probability. For the capillaries, this might be interpreted as being due to scattering law deviations which

result in a preponderance of backscattering. For test sample 1054, this would require 15 to 20% backscattering, which seems to be a rather large amount for what should be a smooth glass surface. An alternative explanation would be that the constant of proportionality for momentum exchange between molecules is not correct. A decrease of about 25 to 30% in the constant of proportionality could change the inferred backscattering to specular reflection, with near perfect diffuse reflection for sample 1054 and 15 to 20% specular reflection for sample 64. However, this does not correct the discrepancy observed for the short capillary and the parallel plates.

The constants obtained with the parallel plate data are simply too small to be accounted for by scattering law deviation. The constants are, however, compatible with the original calculation of momentum loss to the wall by Present and deBethune or to the use of the hydraulic radius. Since the capillary data are not consistent with the original calculation of momentum loss to the walls, and neither the capillary nor the parallel plate is completely compatible with the Clausing factor, there is at present no satisfactory explanation for the experimental variation of the separation data with geometry.

The effects produced by surface scattering law variations are well represented with the long capillaries. The large plastic capillaries, 212, and the small plastic capillaries, 838 and 924, showed approximately the same constants with both flow and separation measurements. The small glass capillaries, 1054, showed constants significantly lower than the plastic capillaries and the larger glass capillaries, 64, showed constants significantly larger than the plastic capillaries. The flow measurements implied specular reflection in varying degrees for all of the capillaries, but the separation measurements implied backscattering for all samples except 64 when the Clausing factor, as suggested by Present and deBethune, is used in the separation equations. If the characteristic constant relating the momentum loss to the wall to the average drift velocity were about 0.75 times the Clausing factor, then the constants determined from the separation measurements would all imply about the same amount of specular reflection as is indicated by the flow measurements.

Regardless of what the appropriate constant of proportionality is, the variation in the initial slope of the separation curve with surface scattering law deviations is more consistent with the PBFM than with the GCM. This is true not only in connection with the initial slope, but also in terms of the resulting fit patterns. Since the representation of the separation data by the GCM with arbitrary constants is better over the full range of pressure and requires smaller changes in C and σ, it might be concluded that the scattering law is more nearly diffuse for sample 1054 than for any of the other samples. As has already been indicated, this conclusion is consistent with the results of the flow measurements. This conclusion is also supported by the fits obtained with the PBM by changing the apparent capillary radius. Sample 1054 gives the best fit from this simple change in the PBM.

The same sort of fit pattern variance is shown to an even larger extent with the parallel plate data, where the large Clausing factor relative

to the capillary Clausing factor produces a large increase in the initial slope of the separation curve for the PBFM, but a large decrease in slope for the GCM. It would seem to be indicated that while the GCM might be modified to account accurately for separation data in capillaries when only diffuse wall reflections are present, it is doubtful that in its present form it can properly account for anomalies due to scattering law variation or for extremes in geometry such as parallel plates.

The PBFM generally does an excellent job of fitting all the experimental data; however, even it shows some small fit pattern variances in the range of separation efficiencies below 40% for the short capillary and for the parallel plates. While the pattern variances are small, they serve to emphasize that the PBFM is an empirical modification and that a better theory is needed for a complete description.

There is at least an implication from this study that the theoretical equations for free molecule flow predict flow ratios which are too large for both the capillary and the parallel plate. The K-factors obtained from the PBFM and the C values from the GCM suggest that the flow rate for long capillaries should be perhaps as much as 0.75 times that predicted by Clausing and for a parallel plate as much as 0.5 times that predicted by Clausing. This study also implies that most calculations of the slip coefficient could also be too large. Both PBFM and GCM suggest that the ratio of the slip coefficient, as interpreted from these data, to the slip coefficient calculated from most other methods is about 0.6.

This work has shown that separation data can be obtained with sufficient accuracy to allow significant interpretations regarding geometry, surface scattering law deviations, and possibly constants relative to the ratio of the average drift velocity to the momentum loss to the wall. It has been shown that when real gas flow characteristics are taken into account in a logical way, the Present and deBethune separation theory can accurately represent separation produced by gaseous diffusion of a binary mixture of isotopes. It has raised some important and serious questions relative to the momentum transfer to the walls or mean flow velocity under free molecule conditions for all geometries, but especially for the parallel plate. Further work with parallel plate geometries with different length-to-spacing ratios and with different surfaces such as fire-polished glass and metal could be helpful in answering some of the questions raised by this work. Flow data only should be sufficient to answer the question concerning the dependence of the free molecule transmission ratio on length-to-spacing ratio. This type of measurement represents a significant means of studying the relative interaction of different molecules with surfaces as well as molecule-molecule scattering. Thus, further measurements should be made with other isotopes and nonisotopic gas pairs.

ACKNOWLEDGMENTS

A study of this magnitude would have been very difficult without the variety of comprehensive services which are available at the Oak Ridge Gaseous Diffusion Plant. Numerous physical and analytical services of the Gaseous Diffusion Development Division, the Laboratory Division, and the Computer Sciences Division are gratefully acknowledged. In particular, the mass spectrometer analyses provided by the Isotopic Analysis Department and the metallurgical and analytical services provided by the Metallurgical Services Section were invaluable.

Special credit should go to W. H. Harber who made all of the flow measurements with the special volumetric flow measurement system. The consultation and calculations provided by G. F. Malling have also contributed much to the study. Thanks also to R. D. Bundy, L. M. Lund, and particularly R. M. McGill for their review and discussion of the report.

/jg

BIBLIOGRAPHY

1. Present, R. D., and deBethune, A. J., Phys. Rev., 75, 1050 (1949).

2. Malling, G. F., Union Carbide Corporation, Nuclear Division, Oak Ridge Gaseous Diffusion Plant, Private Communication.

3. Lund, L. M., and Berman, A. S., J. Appl. Phys., 37, 2489 and 2496 (1966).

4. Clausius, R., Die Kinetische Theorie der Gase, F. Vieweg und Sohn, Braunschweig (1889).

5. Maxwell, J. C., Scientific Papers, W. D. Niven, ed., Cambridge University Press, Cambridge (1890).

6. Boltzmann, L., Vorlesungen über die Gase Theorie, Johann Ambrosius Barth, Leipzig (1910).

7. Graham, T., Phil. Mag., 2, 175, 269, 351 (1833). Reprinted in Graham, T., Chemical and Physical Researches, Edinburgh University Press, pp. 44-70 (1876).

8. Aston, J. G., Phil. Mag., 39, 449 (1920).

9. Kundt and Warburg, Phil. Mag., 50, 53 (1875); Pogg. Ann., 155, 337, 525 (1875).

10. Knudsen, M., Ann. Physik, 28, 75 (1909).

11. Gaede, W., Ann. Physik, 41, 289 (1913).

12. Adzumi, H., Bull. Chem. Soc. Japan, 12, 292; 14, 343 (1939).

13. Pollard, W. G., and Present, R. D., Phys. Rev., 73, 762 (1948).

14. Visner, S., Gaseous Self-Diffusion and Flow in Capillaries at Low Pressures (U), Union Carbide Corporation, Nuclear Division, Oak Ridge Gaseous Diffusion Plant, May 9, 1951 (K-688). Phys. Rev., 82, 297 (1951).

15. Hiby, J. W., and Pahl, M., Z. Naturforsch., 7A, 542 (1952).

16. Weber, S., "Kgl. Danske Videnskab. Selskab," Mat. Fys. Medd., 28, No. 2 (1954).

17. Albertoni, S., Cercignani, C., and Gotusso, L., Phys. Fluids, 6, 993 (1963).

18. Berman, A. S., and Maegley, W. J., Phys. Fluids, 15, 780 (1972).

19. Scott, D. S., and Dullien, F. A. L., AIChE Journal, 8, 293 (1962).

20. Fryer, G. M., Proc. Roy. Soc., A293, 329 (1966).

21. Barrer, R. M., and Nicholsen, D., Brit. J. Appl. Phys., 17, 1091 (1966).

22. Hertz, G. L., Z. Phys., 79, 108 (1932).

23. Woolridge, D. E., and Smythe, W. R., Phys. Rev., 50, 233 (1936).

24. Bosanquet, C. H., British TA Report Br-507, September 27, 1944.

25. Huggill, J. A. W., Proc. Roy. Soc. (London), A212, 123 (1952).

26. Kennard, E. H., Kinetic Theory of Gases, McGraw Hill Book Co., Inc., New York, p. 294ff (1938).

27. Hanks, R. W., and Weissberg, H. L., J. Appl. Phys., 35, 142 (1964).

28. Berman, A. S., Internal Rarefied Gas Flows with Backscattering - Part 1: The Backscattering Boundary Condition and Free Molecule Flow in a Long Capillary; Part 3: Kramer's Problem--The Effect of Backscattering on Slip (U), Union Carbide Corporation, Nuclear Division, Oak Ridge Gaseous Diffusion Plant, June 16, 1971 (K-1798, Parts 1 and 3).

29. Von Smoluchowski, M., Ann. Physik, 33, 1559 (1910).

30. Clausing, P., Ann. Physik, 12, 961 (1932).

31. DeMarcus, W. C., The Problem of Knudsen Flow - Part 3: Solutions for One-Dimensional Systems (U), Union Carbide Corporation, Nuclear Division, Oak Ridge Gaseous Diffusion Plant, March 19, 1957 (K-1302, Part 3).

32. Berman, A. S., J. Appl. Phys., 36, 3356 (1965).

APPENDIX A - NOMENCLATURE

A^*	Collision integral parameter
b	$(8Kr/3\pi)(kT/2m^+)^{1/2}\ [\langle m^{1/2}\rangle_N/(m_1 + m_2)^{1/2}](1/pD_{12})$, constant in the PBM
b_m	Modified b constant
c	Clausing transmission ratio divided by measured transmission ratio at zero pressure
D_{12}	Coefficient for mutual diffusion
d_{12}	$(d_1 + d_2)/2$, average molecular diameter
E_1	Exponential integral
F	Correction function for the Bosanquet diffusion coefficient
f	$[\nu(1 - N)]/[N(1 - \nu)]$, separation factor
$\overline{f}$	Mole fraction averaged separation factor
f^*	Ideal separation factor
G	Transport, pressure-volume per unit time
G_1	Molecular transport of gas 1
h	Plate separation on parallel plate sample
K	Ratio of free molecule flow for any geometry to the ideal free molecule flow for an infinitely long capillary
K'	Ratio of Poiseuille flow for any geometry to that for a capillary
k	Boltzmann's constant
L	Capillary length-to-radius ratio
M_{12}	Momentum transferred per unit time per unit volume from gas 1 to gas 2
m	Molecular mass
m^+	Reduced mass of a binary pair
$\langle m^{1/2}\rangle_N$	$Nm_1^{1/2} + (1 - N)m_2^{1/2}$, mole fraction averaged mass

N_o	Mole fraction of gas 1
N_1	Mole fraction of gas 1 in product stream
n	Molecule number density, number of molecules per unit volume
P	Pressure
P_b	Backpressure, pressure on the exit side area open to flow
P_f	Forepressure, pressure on the entrance side area open to flow
r	Capillary radius
T	Absolute temperature
u	Mean drift velocity at a point
u_c	Drift velocity of center of mass
$\bar{v}$	Mean molecular velocity $= \sqrt{RT/\pi M}$
W_K	Zero pressure intercept from low pressure flow data, Knudsen flow intercept
W_M	Zero pressure intercept extrapolated from high pressure flow data, as calculated by Maxwell.
w	P_b/P_f, pressure ratio
X	$R\Sigma P/\eta\bar{v}$, a correlation parameter proportional to r/λ
Z	Separation efficiency

Greek Symbols

ΔP	Forepressure minus backpressure
η	Gas viscosity
λ	Mean free path of molecule
ν_g	Contribution to collision frequency from molecules leaving another molecule
ν_w	Contribution to collision frequency from molecules leaving another wall
ΣP	Sum of forepressure and backpressure
σ	"Constant" related to the slip coefficient for a long capillary.

APPENDIX B - COMPILATION OF DATA

The following table lists all of the data which were obtained on all of the test samples. The test sample number is given at the top of the page. The first column lists an individual test point identification number. The second column lists the high side pressure, PF, in cm Hg. The third column lists the low side pressure, PB, in cm Hg. The fourth column lists the ratio of the mole fraction ratio in the product stream to the mole fraction ratio feed stream as measured by the mass spectrometer. The fifth column lists the cut. The sixth column lists the pressure ratio, PB/PF. The seventh column lists the pressure difference across the test sample. The eighth column lists the separation efficiency, Z, and the ninth column lists the separation efficiency ratio, Z/(1-w).

NEON SEPARATION DATA
SAMPLE NUMBER 212

RUN	PF	PB	RATIO	CUT	R	DELTA P	Z	Z/1-W
1005	4.6370	0.28000	1.00250	0.0684	0.06038	4.357	0.05308	0.05649
1006	2.5040	0.15900	1.00600	0.0748	0.06350	2.345	0.12783	0.13650
1007	1.1650	0.09300	1.01100	0.0819	0.07983	1.072	0.23527	0.25568
1010	1.2020	0.08500	1.01390	0.0785	0.07072	1.117	0.29674	0.31932
1011	1.1660	0.08200	1.01470	0.0827	0.07033	1.084	0.31455	0.33834
1012	2.2130	0.12500	1.00710	0.0724	0.05648	2.088	0.15107	0.16011
1013	3.3740	0.19100	1.00380	0.0672	0.05661	3.183	0.08062	0.08546
1014	4.6510	0.25100	1.00210	0.0689	0.05397	4.400	0.04460	0.04714
1015	2.0140	0.03000	1.00760	0.0731	0.01490	1.984	0.16176	0.16421
1022	1.6350	0.10600	1.01010	0.0791	0.06483	1.529	0.21569	0.23064
1023	3.9420	0.21600	1.00430	0.0761	0.05479	3.726	0.09168	0.09699
1024	2.8880	0.16750	1.00450	0.0786	0.05800	2.720	0.09607	0.10199
1025	1.8660	0.11850	1.00890	0.0786	0.06350	1.747	0.19002	0.20290
1026	1.2260	0.08750	1.01390	0.0791	0.07137	1.138	0.29684	0.31965
1027	0.9320	0.07050	1.01660	0.0770	0.07564	0.861	0.35410	0.38307
1029	1.1410	0.07650	1.01190	0.1312	0.06705	1.064	0.26178	0.28059
1031	0.9759	0.07040	1.01640	0.0795	0.07214	0.906	0.35031	0.37754
1787	1.0000	0.02970	1.02580	0.0121	0.02970	0.970	0.53181	0.54809
1788	0.5020	0.01610	1.03140	0.0124	0.03207	0.486	0.64733	0.66877
1789	0.3030	0.01100	1.03580	0.0118	0.03630	0.292	0.73782	0.76561
1790	0.2000	0.00776	1.03870	0.0113	0.03880	0.192	0.79737	0.82956
1791	0.0880	0.01020	1.03940	0.0037	0.11591	0.078	0.80870	0.91472
1792	0.1100	0.01132	1.04000	0.0036	0.10291	0.099	0.82097	0.91515

NEON SEPARATION DATA
SAMPLE NUMBER 838

RUN	PF	PB	RATIO	CUT	R	DELTA P	Z	Z/1-W
1032	5.0794	0.10300	1.00510	0.0006	0.02028	4.976	0.10451	0.10668
1033	7.1031	0.13670	1.00280	0.0006	0.01925	6.966	0.05738	0.05851
1034	10.2530	0.18460	1.00220	*0.0007	0.01800	10.068	0.04509	0.04591
1035	4.2107	0.09170	1.00540	0.0005	0.02178	4.119	0.11066	0.11313
1036	3.1280	0.07200	1.00910	0.0005	0.02302	3.056	0.18649	0.19088
1039	4.8476	0.09540	1.00480	0.0539	0.01968	4.752	0.10112	0.10315
1040	4.8650	0.09840	1.00460	0.0102	0.02023	4.767	0.09473	0.09668
1041	4.7930	0.09540	1.00460	0.0010	0.01990	4.698	0.09429	0.09621
1042	1.0130	0.02690	1.01970	0.0010	0.02655	0.986	0.40381	0.41482
1043	1.0130	0.02690	1.02340	0.0096	0.02655	0.986	0.48173	0.49487
1044	1.0830	0.02850	1.02560	0.0551	0.02632	1.054	0.53964	0.55423
1045	2.4938	0.05770	1.00970	0.0005	0.02314	2.436	0.19878	0.20349
1046	1.9690	0.04770	1.01410	0.0005	0.02423	1.921	0.28896	0.29613
1047	1.4990	0.03850	1.01810	0.0006	0.02568	1.460	0.37093	0.38071
1048	4.7404	0.09540	1.00480	0.0213	0.02012	4.645	0.09941	0.10145
1049	1.0085	0.03420	1.02410	0.0095	0.03391	0.974	0.49612	0.51353
1050	2.5038	0.06000	1.01210	0.0005	0.02396	2.444	0.24797	0.25405
1051	1.0415	0.02650	1.02280	0.0122	0.02544	1.015	0.46999	0.48226
1052	0.4800	0.01690	1.03060	0.0019	0.03521	0.463	0.62753	0.65043
1053	1.0100	0.02920	1.02550	0.0008	0.02891	0.981	0.52264	0.53820
1055	1.0138	0.02920	1.02520	0.0048	0.02880	0.985	0.51753	0.53288
1056	1.0446	0.02770	1.02460	0.0244	0.02652	1.017	0.51026	0.52416
1057	0.7661	0.02070	1.02910	0.0013	0.02702	0.745	0.59657	0.61314
1058	2.5200	0.05850	1.01230	0.0005	0.02321	2.461	0.25206	0.25805

RUN	PF	PB	RATIO	CUT	R	DELTA P	Z	Z/I-W
1059	3.5540	0.07540	1.00970	0.0005	0.02122	3.479	0.19878	0.20309
1060	6.0176	0.11850	1.00400	0.0005	0.01969	5.899	0.08197	0.08362
1061	8.0800	0.15000	1.00240	0.0006	0.01856	7.930	0.04919	0.05012
1062	9.1000	0.16600	1.00250	0.0007	0.01824	8.934	0.05124	0.05219
1063	10.1000	0.17920	1.00250	*0.0007	0.01774	9.921	0.05124	0.05216
1064	0.5400	0.02000	1.03480	0.0017	0.03704	0.520	0.71357	0.74102
1067	0.2485	0.01000	1.04110	0.0049	0.04024	0.238	0.84412	0.87952
1069	0.2461	0.01000	1.04750	0.0190	0.04063	0.236	0.98258	1.02419
1071	8.0800	0.14460	1.00260	0.0006	0.01790	7.935	0.05328	0.05426
1072	7.0800	0.13070	1.00340	0.0006	0.01846	6.949	0.06968	0.07099
1073	6.0200	0.11530	1.00420	0.0006	0.01915	5.905	0.08607	0.08775
1074	5.6300	0.10530	1.00470	0.0006	0.01870	5.525	0.09632	0.09815
1075	4.6200	0.08920	1.00600	0.0005	0.01931	4.531	0.12296	0.12538
1078	14.5900	0.25460	1.00040	*0.0008	0.01745	14.335	0.00820	0.00834
1080	3.4030	0.07460	1.01050	0.0006	0.02192	3.328	0.21518	0.22000
1081	2.9920	0.06600	1.01190	0.0006	0.02206	2.926	0.24387	0.24937
1082	2.6030	0.06000	1.01480	0.0006	0.02305	2.543	0.30330	0.31046
1083	1.9340	0.05690	1.01860	0.0006	0.02942	1.877	0.38118	0.39273
1084	1.3330	0.03620	1.02360	0.0007	0.02716	1.297	0.48369	0.49719
1085	0.9577	0.02770	1.02850	0.0011	0.02892	0.930	0.58423	0.60163
1087	2.2807	0.05380	1.01540	0.0006	0.02359	2.227	0.31560	0.32323
1088	3.8100	0.08300	1.00790	0.0006	0.02178	3.727	0.16190	0.16551
1089	12.2200	0.22200	1.00170	0.0008	0.01817	11.998	0.03484	0.03549
1090	4.9350	0.10080	1.00420	0.0006	0.02043	4.834	0.08607	0.08787

RUN	PF	PB	RATIO	CUT	R	DELTA P	Z	Z/1-W
1091	10.0200	0.18080	1.00220	0.0007	0.01804	9.839	0.04509	0.04592
1092	6.4900	0.12620	1.00410	0.0006	0.01945	6.364	0.08403	0.08569
1093	1.4890	0.04150	1.02140	0.0006	0.02787	1.447	0.43856	0.45113
1094	0.4862	0.01690	1.03530	0.0027	0.03476	0.469	0.72420	0.75028
1095	0.6800	0.02150	1.03170	0.0012	0.03162	0.658	0.64986	0.67108
1096	2.4177	0.06000	1.01350	0.0005	0.02482	2.358	0.27666	0.28370
1098	2.4615	0.05540	1.01320	0.0005	0.02251	2.406	0.27051	0.27674
1099	2.7630	0.06380	1.01320	0.0005	0.02309	2.699	0.27051	0.27691
1100	3.0880	0.06770	1.01120	0.0005	0.02192	3.020	0.22952	0.23467

NEON SEPARATION DATA
SAMPLE NUMBER 924

RUN	PF	PB	RATIO	CUT	R	DELTA P	Z	Z/1-W
1101	5.0690	0.12300	1.00680	0.0007	0.02427	4.946	0.13937	0.14284
1102	6.0400	0.14230	1.00520	0.0008	0.02356	5.898	0.10658	0.10915
1103	2.9869	0.08153	1.01200	0.0007	0.02730	2.905	0.24594	0.25285
1104	4.0676	0.10307	1.00860	0.0007	0.02534	3.965	0.17626	0.18084
1105	7.1200	0.16077	1.00450	0.0008	0.02258	6.959	0.09223	0.09436
1106	8.1200	0.17846	1.00360	0.0009	0.02198	7.942	0.07379	0.07545
1107	9.2400	0.19769	1.00310	0.0009	0.02140	9.042	0.06354	0.06493
1108	10.0100	0.21923	1.00290	0.0010	0.02190	9.791	0.05944	0.06077
1110	1.0092	0.03615	1.02660	0.0011	0.03582	0.973	0.54527	0.56553
1119	2.0077	0.05923	1.01670	0.0007	0.02950	1.948	0.34227	0.35267
1120	3.4777	0.09153	1.00960	0.0010	0.02632	3.386	0.19678	0.20210
1121	4.6169	0.11460	1.00450	0.0009	0.02482	4.502	0.09223	0.09458
1122	5.6460	0.13230	1.00450	0.0008	0.02343	5.514	0.09223	0.09445
1123	6.6230	0.15000	1.00360	0.0008	0.02265	6.473	0.07379	0.07550
1124	7.6200	0.17080	1.00300	0.0009	0.02241	7.449	0.06149	0.06290
1125	8.6500	0.18846	1.00250	0.0009	0.02179	8.462	0.05124	0.05238
1126	12.2200	0.24300	1.00020	0.0011	0.01989	11.977	0.00410	0.00418
1127	15.1000	0.30540	1.00040	*0.0012	0.02023	14.795	0.00820	0.00837
1128	1.4554	0.04846	1.02240	0.0008	0.03330	1.407	0.45912	0.47493
1129	0.2992	0.01461	1.03670	0.0046	0.04883	0.285	0.75362	0.79231
1130	0.2654	0.01307	1.03850	0.0080	0.04925	0.252	0.79195	0.83297
1131	0.4954	0.03000	1.03460	0.0019	0.06056	0.465	0.70956	0.75530
1132	2.0277	0.05923	1.01640	0.0007	0.02921	1.968	0.33612	0.34624
1167	6.0500	0.13900	1.00440	0.0009	0.02298	5.911	0.09019	0.09231

RUN	PF	PB	RATIO	CUT	R	DELTA P	Z	Z/1-W
1168	7.9100	0.17900	1.00280	0.0010	0.02263	7.731	0.05739	0.05872
1169	4.8800	0.10700	1.00670	0.0010	0.02193	4.773	0.13733	0.14041
1170	8.9600	0.19300	1.00240	0.0010	0.02154	8.767	0.04920	0.05028
1171	6.9200	0.15700	1.00340	0.0009	0.02269	6.763	0.06969	0.07131
1172	4.0000	0.09900	1.00700	0.0009	0.02475	3.901	0.14348	0.14712
1174	3.0100	0.06900	1.00920	0.0008	0.02292	2.941	0.18856	0.19298
1175	2.0200	0.05300	1.01680	0.0008	0.02624	1.967	0.34433	0.35360
1177	3.0900	0.08200	1.01090	0.0007	0.02654	3.008	0.22339	0.22948
1178	2.5200	0.07200	1.01370	0.0007	0.02857	2.448	0.28078	0.28904
1181	10.1400	0.20800	1.00180	0.0010	0.02051	9.932	0.03690	0.03767
1182	8.0400	0.17800	1.00270	0.0009	0.02214	7.862	0.05534	0.05659
1183	3.9900	0.09900	1.00720	0.0007	0.02481	3.891	0.14756	0.15132
1184	1.5100	0.04800	1.02190	0.0008	0.03179	1.462	0.44886	0.46359
1185	3.0000	0.07800	1.01100	0.0007	0.02600	2.922	0.22545	0.23146
1187	1.4400	0.04600	1.02180	0.0008	0.03194	1.394	0.44682	0.46156
1188	0.9931	0.03538	1.02690	0.0010	0.03563	0.958	0.55140	0.57176
1189	0.4300	0.01923	1.03770	0.0032	0.04472	0.411	0.77364	0.80986
1190	0.7780	0.02980	1.03090	0.0012	0.03830	0.748	0.63344	0.65867
1191	0.2392	0.01080	1.03980	0.0062	0.04515	0.228	0.81794	0.85662
1194	3.4920	0.09100	1.00920	0.0007	0.02606	3.401	0.18855	0.19360
1195	4.5000	0.11100	1.00530	0.0007	0.02467	4.389	0.10862	0.11137
1196	5.1800	0.12400	1.00540	0.0007	0.02394	5.056	0.11067	0.11339
1197	5.6880	0.13120	1.00470	0.0008	0.02307	5.557	0.09633	0.09860
1198	0.6220	0.02360	1.03370	0.0014	0.03794	0.598	0.69093	0.71818

RUN	PF	PB	RATIO	CUT	R	DELTA P	Z	Z/1-W
1199	0.4168	0.01780	1.03540	0.0025	0.04271	0.399	0.72616	0.75855
1200	0.5172	0.02140	1.03510	0.0017	0.04138	0.496	0.71974	0.75081
1201	0.3152	0.01370	1.03990	0.0041	0.04346	0.302	0.81914	0.85636
1203	0.2124	0.01028	1.04260	0.0079	0.04840	0.202	0.87622	0.92079
1204	0.3120	0.01400	1.03940	0.0039	0.04487	0.298	0.80878	0.84678
1205	0.2072	0.00980	1.04160	0.0072	0.04730	0.197	0.85538	0.89785
1206	0.1520	0.00732	1.04160	0.0060	0.04816	0.145	0.85485	0.89810
1207	0.0980	0.00488	1.04430	0.0058	0.04980	0.093	0.91026	0.95797
1419	0.1010	0.00232	1.04280	0.0015	0.02297	0.099	0.87753	0.89816
1420	0.2020	0.00428	1.04160	0.0012	0.02119	0.198	0.85279	0.87125
1421	0.0520	0.00120	1.04270	0.0019	0.02308	0.051	0.87566	0.89634
1422	0.0772	0.00160	1.04240	0.0019	0.02073	0.076	0.86948	0.88788
1423	0.1010	0.00236	1.04260	0.0016	0.02337	0.099	0.87348	0.89438
1424	0.2000	0.00460	1.04130	0.0012	0.02300	0.195	0.84666	0.86659
1425	0.2940	0.00680	1.04000	0.0011	0.02313	0.287	0.81994	0.83935
1426	0.4020	0.00540	1.03840	0.0009	0.01343	0.397	0.78709	0.79781
1427	0.1500	0.00300	1.04240	0.0014	0.02000	0.147	0.86929	0.88703
1428	0.2500	0.00570	1.04090	0.0011	0.02280	0.244	0.83841	0.85797
1429	0.3480	0.00800	1.03970	0.0010	0.02299	0.340	0.81376	0.83290
1430	0.4500	0.00960	1.03710	0.0009	0.02133	0.440	0.76043	0.77701
1467	0.1008	0.00792	1.04100	0.0021	0.07857	0.093	0.84088	0.91258
1468	0.1000	0.00258	1.04220	0.0064	0.02580	0.097	0.86736	0.89033
1469	0.1000	0.00744	1.04000	0.0135	0.07440	0.093	0.82510	0.89142
1470	0.1020	0.00707	1.04100	0.0019	0.06931	0.095	0.84077	0.90339

RUN	PF	PB	RATIO	CUT	R	DELTA P	Z	Z/1-W
1472	0.1020	0.00702	1.04110	0.0031	0.06882	0.095	0.84336	0.90569
1473	0.1020	0.00703	1.04070	0.0018	0.06892	0.095	0.83459	0.89637
1474	0.1020	0.00700	1.04160	0.0078	0.06863	0.095	0.85562	0.91867
1475	0.1020	0.00700	1.04120	0.0050	0.06863	0.095	0.84620	0.90855
1477	0.0990	0.00690	1.04060	0.0019	0.06970	0.092	0.83258	0.89495
1478	0.1020	0.00744	1.04180	0.0071	0.07294	0.095	0.85943	0.92705
1479	0.1020	0.00708	1.04090	0.0065	0.06941	0.095	0.84070	0.90341
1488	0.1020	0.00700	1.04080	0.0069	0.06863	0.095	0.83880	0.90061
1489	0.1020	0.00680	1.04020	0.0020	0.06667	0.095	0.82442	0.88331
1490	0.1020	0.00690	1.04100	0.0036	0.06765	0.095	0.84149	0.90255
1491	0.1050	0.00240	1.04140	0.0058	0.02286	0.103	0.85067	0.87057
1492	0.1020	0.00690	1.04180	0.0083	0.06765	0.095	0.85996	0.92236
1496	0.1020	0.00708	1.04040	0.0021	0.06941	0.095	0.82858	0.89038
1497	0.1020	0.00700	1.04080	0.0027	0.06863	0.095	0.83703	0.89871
1498	0.1020	0.00240	1.04100	0.0033	0.02353	0.100	0.84140	0.86168
1499	0.1020	0.00670	1.04120	0.0042	0.06569	0.095	0.84585	0.90532
1500	0.1020	0.00690	1.04130	0.0059	0.06765	0.095	0.84866	0.91023
1502	0.1050	0.00666	1.04160	0.0083	0.06343	0.098	0.85584	0.91380
1503	0.1020	0.00768	1.03980	0.0022	0.07529	0.094	0.81632	0.88279
1504	0.1020	0.00276	1.04070	0.0029	0.02706	0.099	0.83505	0.85828
1505	0.1020	0.00690	1.04100	0.0042	0.06765	0.095	0.84174	0.90281
1506	0.1020	0.00760	1.04030	0.0124	0.07451	0.094	0.83081	0.89770
1510	0.2500	0.02020	1.03830	0.0014	0.08080	0.230	0.78524	0.85426
1523	0.2500	0.00480	1.03970	0.0055	0.01920	0.245	0.81561	0.83158

RUN	PF	PB	RATIO	CUT	R	DELTA P	Z	Z/1-W
1524	0.2500	0.01480	1.03820	0.0115	0.05920	0.235	0.78717	0.83670
1526	0.2500	0.00460	1.04010	0.0029	0.01840	0.245	0.82274	0.83816
1527	0.2500	0.00440	1.04020	0.0014	0.01760	0.246	0.82420	0.83897
1528	0.1020	0.00198	1.04160	0.0114	0.01941	0.100	0.85718	0.87415
1529	0.1020	0.00180	1.04190	0.0087	0.01765	0.100	0.86221	0.87770
1530	0.5100	0.00840	1.03580	0.0138	0.01647	0.502	0.73858	0.75094
1531	0.5000	0.00840	1.03660	0.0072	0.01680	0.492	0.75258	0.76544
1533	0.5000	0.01260	1.03610	0.0135	0.02520	0.487	0.74466	0.76391
1534	0.5060	0.01260	1.03650	0.0011	0.02490	0.493	0.74821	0.76732
1535	0.5060	0.00840	1.03670	0.0011	0.01660	0.498	0.75231	0.76501
1536	0.1020	0.00740	1.04040	0.0124	0.07255	0.095	0.83288	0.89803
1537	0.5060	0.02540	1.03600	0.0021	0.05020	0.481	0.73833	0.77735
1539	0.1020	0.00710	1.03890	0.0155	0.06961	0.095	0.80324	0.86334
1541	1.0200	0.01520	1.02950	0.0013	0.01490	1.005	0.60479	0.61393
1542	1.0200	0.01060	1.02960	0.0017	0.01039	1.009	0.60694	0.61332
1543	1.0200	0.01060	1.02900	0.0026	0.01039	1.009	0.59492	0.60117
1544	1.0200	0.01820	1.02910	0.0068	0.01784	1.002	0.59822	0.60908
1545	1.0200	0.01860	1.02940	0.0026	0.01824	1.001	0.60312	0.61432
1546	1.0200	0.01060	1.02910	0.0068	0.01039	1.009	0.59823	0.60451
1547	1.0200	0.03160	1.02950	0.0026	0.03098	0.988	0.60517	0.62452
1548	1.0200	0.02500	1.02910	0.0027	0.02451	0.995	0.59699	0.61199
1549	2.0000	0.03040	1.01920	0.0037	0.01520	1.970	0.39410	0.40018
1550	2.0000	0.03100	1.01860	0.0062	0.01550	1.969	0.38226	0.38828
1551	2.0000	0.03040	1.01890	0.0015	0.01520	1.970	0.38750	0.39349

RUN	PF	PB	RATIO	CUT	R	DELTA P	Z	Z/1-W
1552	4.0400	0.05180	1.00910	0.0028	0.01282	3.988	0.18670	0.18913
1553	6.1000	0.07500	1.00480	0.0010	0.01230	6.025	0.09839	0.09962
1554	8.1600	0.06500	1.00450	0.0010	0.00797	8.095	0.09224	0.09298
1555	3.0400	0.02820	1.01280	0.0015	0.00928	3.012	0.26245	0.26490
1556	5.0800	0.04400	1.00620	0.0011	0.00866	5.036	0.12709	0.12820
1557	4.1000	0.05200	1.00860	0.0012	0.01268	4.048	0.17630	0.17856
1558	7.1200	0.05800	1.00480	0.0010	0.00815	7.062	0.09839	0.09920
1559	3.0400	0.04400	1.01240	0.0015	0.01447	2.996	0.25423	0.25797
1560	9.2000	0.10200	1.00320	0.0010	0.01109	9.098	0.06559	0.06633
1561	8.2000	0.06600	1.00270	0.0010	0.00805	8.134	0.05534	0.05579

NEON SEPARATION DATA
SAMPLE NUMBER1054

RUN	PF	PB	RATIO	CUT	R	DELTA P	Z	Z/1-W
1211	2.0360	0.01000	1.03210	0.0001	0.00491	2.026	0.65765	0.66090
1212	3.0040	0.01400	1.02760	0.0001	0.00466	2.990	0.56551	0.56816
1213	4.0180	0.01812	1.02190	0.0001	0.00451	4.000	0.44868	0.45071
1214	10.1400	0.04130	1.00770	0.0001	0.00407	10.099	0.15776	0.15841
1215	8.0320	0.03360	1.01090	0.0001	0.00418	7.998	0.22334	0.22428
1217	15.0800	0.05780	1.00470	*0.0001	0.00383	15.022	0.09631	0.09668
1218	8.9570	0.03720	1.00970	0.0001	0.00415	8.920	0.19874	0.19957
1219	7.0500	0.02940	1.01260	0.0001	0.00417	7.021	0.25814	0.25922
1228	12.0100	0.04760	1.00660	0.0001	0.00396	11.962	0.13522	0.13576
1229	13.1200	0.05040	1.00580	*0.0001	0.00384	13.070	0.11884	0.11930
1231	2.0120	0.01000	1.03310	0.0001	0.00497	2.002	0.67826	0.68165
1232	3.0060	0.01360	1.02710	0.0001	0.00452	2.992	0.55531	0.55784
1239	1.0304	0.00520	1.03830	0.0001	0.00505	1.025	0.78469	0.78867
1240	0.7336	0.00406	1.04030	0.0001	0.00553	0.730	0.82575	0.83035
1241	3.0130	0.01196	1.02650	0.0001	0.00397	3.001	0.54298	0.54515
1242	0.5003	0.00310	1.04270	0.0003	0.00620	0.497	0.87497	0.88042
1243	0.3028	0.00170	1.04420	0.0013	0.00561	0.301	0.90615	0.91127
1245	0.3116	0.00164	1.04490	0.0010	0.00526	0.310	0.92038	0.92525
1246	0.7524	0.00424	1.04070	0.0001	0.00564	0.748	0.83392	0.83864
1248	0.5060	0.00282	1.04360	0.0003	0.00557	0.503	0.89338	0.89839
1249	0.6100	0.00302	1.04220	0.0002	0.00495	0.607	0.86465	0.86895
1250	1.0012	0.00492	1.03920	0.0001	0.00491	0.996	0.80323	0.80719
1251	5.0000	0.01780	1.01820	0.0001	0.00356	4.982	0.37293	0.37426
1256	0.2060	0.00224	1.04610	0.0021	0.01087	0.204	0.94550	0.95589

RUN	PF	PB	RATIO	CUT	R	DELTA P	Z	Z/1-W
1267	0.5044	0.00257	1.04150	0.0002	0.00510	0.502	0.85032	0.85467
1268	0.2080	0.00246	1.04350	0.0003	0.01183	0.206	0.89138	0.90205
1269	1.0060	0.00530	1.04000	0.0002	0.00527	1.001	0.81958	0.82392
1271	0.7632	0.00360	1.04010	0.0002	0.00472	0.760	0.82166	0.82555
1272	0.3152	0.00306	1.04480	0.0003	0.00971	0.312	0.91797	0.92697
1276	0.5008	0.00246	1.04160	0.0002	0.00491	0.498	0.85237	0.85658
1277	0.7536	0.00388	1.03870	0.0001	0.00515	0.750	0.79293	0.79704
1278	0.3024	0.00140	1.04410	0.0012	0.00463	0.301	0.90406	0.90826
1281	0.4030	0.00408	1.04410	0.0004	0.01012	0.399	0.90370	0.91294
1282	0.7552	0.00395	1.04000	0.0001	0.00523	0.751	0.81960	0.82391
1283	1.0060	0.00498	1.03850	0.0001	0.00495	1.001	0.78880	0.79272
1284	1.4960	0.00698	1.03590	0.0001	0.00467	1.489	0.73562	0.73907
1285	0.4970	0.00550	1.04300	0.0016	0.01107	0.491	0.88166	0.89152
1286	12.9500	0.04600	1.00570	0.0001	0.00355	12.904	0.11679	0.11720
1287	9.8300	0.03580	1.00920	0.0001	0.00364	9.794	0.18852	0.18921
1288	7.9000	0.02960	1.01200	0.0001	0.00375	7.870	0.24585	0.24678
1289	6.0000	0.02380	1.01600	0.0001	0.00397	5.976	0.32780	0.32910
1290	4.0160	0.01420	1.02220	0.0001	0.00354	4.002	0.45489	0.45651
1291	3.0400	0.02200	1.02640	0.0001	0.00724	3.018	0.54093	0.54487
1292	4.0200	0.01440	1.02230	0.0001	0.00358	4.006	0.45693	0.45858
1293	6.0200	0.02400	1.01530	0.0001	0.00399	5.996	0.31349	0.31475
1294	5.0320	0.02040	1.01860	0.0001	0.00405	5.012	0.38108	0.38263
1295	10.0800	0.03640	1.00800	0.0001	0.00361	10.044	0.16392	0.16451
1298	6.0400	0.02400	1.01540	0.0001	0.00397	6.016	0.31552	0.31678

RUN	PF	PB	RATIO	CUT	R	DELTA P	Z	Z/1-W
1299	10.0300	0.03680	1.00770	0.0001	0.00367	9.993	0.15776	0.15835
1300	0.7512	0.00406	1.04160	0.0001	0.00540	0.747	0.85236	0.85699
1301	0.5024	0.00252	1.04120	0.0003	0.00502	0.500	0.84425	0.84850
1302	0.7488	0.00386	1.03990	0.0001	0.00515	0.745	0.81755	0.82179
1303	0.5030	0.00266	1.04180	0.0003	0.00529	0.500	0.85653	0.86108
1304	6.0400	0.02028	1.01550	0.0001	0.00336	6.020	0.31758	0.31865
1305	6.0680	0.02420	1.01590	0.0001	0.00399	6.044	0.32578	0.32709
1306	10.0200	0.03150	1.00850	0.0001	0.00314	9.988	0.17418	0.17473
1307	0.7564	0.00394	1.04120	0.0001	0.00521	0.752	0.84423	0.84865
1308	1.0050	0.00514	1.03940	0.0001	0.00511	1.000	0.80730	0.81145
1309	2.0160	0.00940	1.03280	0.0001	0.00466	2.007	0.67200	0.67514
1310	0.5060	0.00252	1.04230	0.0003	0.00498	0.503	0.86676	0.87110
1311	0.8506	0.00416	1.04020	0.0001	0.00489	0.846	0.82366	0.82771
1312	2.0080	0.00940	1.03300	0.0001	0.00468	1.999	0.67623	0.67941
1313	3.0120	0.01200	1.02650	0.0001	0.00398	3.000	0.54298	0.54515
1314	4.0040	0.01420	1.02310	0.0001	0.00355	3.990	0.47336	0.47505
1315	5.0200	0.01720	1.01940	0.0001	0.00343	5.003	0.39745	0.39882
1316	7.0040	0.02280	1.01330	0.0001	0.00326	6.981	0.27253	0.27342
1317	8.0200	0.02600	1.01300	0.0001	0.00324	7.994	0.26634	0.26721
1318	0.9980	0.00486	1.03900	0.0001	0.00487	0.993	0.79903	0.80294
1319	0.8448	0.00470	1.04060	0.0001	0.00556	0.840	0.83189	0.83654
1320	0.7512	0.00386	1.04080	0.0001	0.00514	0.747	0.83594	0.84026
1321	1.0000	0.00464	1.03870	0.0001	0.00464	0.995	0.79297	0.79667
1322	0.5140	0.00242	1.04230	0.0003	0.00471	0.512	0.86677	0.87087

RUN	PF	PB	RATIO	CUT	R	DELTA P	Z	Z/1-W
1325	0.5000	0.00276	1.04240	0.0003	0.00552	0.497	0.86883	0.87365
1326	0.6112	0.00296	1.04220	0.0002	0.00484	0.608	0.86463	0.86884
1327	0.4020	0.00252	1.04360	0.0007	0.00627	0.399	0.89355	0.89919
1328	0.4460	0.00222	1.04340	0.0004	0.00498	0.444	0.88937	0.89382
1329	0.3120	0.00168	1.04690	0.0023	0.00538	0.310	0.96198	0.96719
1330	0.3460	0.00198	1.04380	0.0012	0.00572	0.344	0.89788	0.90305
1562	0.5080	0.00300	1.04450	0.0002	0.00591	0.505	0.91180	0.91722
1563	0.5100	0.00320	1.04470	0.0009	0.00627	0.507	0.91621	0.92199
1564	0.5100	0.00090	1.04360	0.0018	0.00176	0.509	0.89406	0.89564
1565	0.5000	0.00300	1.04350	0.0044	0.00600	0.497	0.89318	0.89857
1567	0.5100	0.00300	1.04510	0.0009	0.00588	0.507	0.92443	0.92990
1568	0.5100	0.00300	1.04420	0.0026	0.00588	0.507	0.90674	0.91210
1570	0.5000	0.00300	1.04440	0.0013	0.00600	0.497	0.91022	0.91572
1571	0.5100	0.00300	1.04430	0.0009	0.00588	0.507	0.90801	0.91338
1572	0.5100	0.00300	1.04440	0.0004	0.00588	0.507	0.90986	0.91525
1573	0.2000	0.00156	1.04460	0.0002	0.00780	0.198	0.91379	0.92097
1574	0.2000	0.00132	1.04540	0.0005	0.00660	0.199	0.93038	0.93656
1575	0.2000	0.00150	1.04560	0.0012	0.00750	0.198	0.93478	0.94185
1576	0.2000	0.00090	1.04540	0.0023	0.00450	0.199	0.93122	0.93543
1578	0.2000	0.00108	1.04550	0.0023	0.00540	0.199	0.93327	0.93834
1579	1.0100	0.00560	1.04020	0.0001	0.00554	1.004	0.82374	0.82834
1580	0.2000	0.00100	1.04560	0.0015	0.00500	0.199	0.93496	0.93966
1582	0.6100	0.00372	1.04330	0.0007	0.00610	0.606	0.88744	0.89288
1583	0.7500	0.00450	1.04230	0.0011	0.00600	0.745	0.86711	0.87234

RUN	PF	PB	RATIO	CUT	R	DELTA P	Z	Z/1-W
1585	1.2000	0.00660	1.04030	0.0010	0.00550	1.193	0.82605	0.83062
1586	0.9060	0.00600	1.04140	0.0010	0.00662	0.900	0.84862	0.85428
1587	1.2000	0.00660	1.03920	0.0010	0.00550	1.193	0.80350	0.80795
1588	1.5000	0.00840	1.03790	0.0010	0.00560	1.492	0.77687	0.78125
1589	0.1000	0.00042	1.04560	0.0008	0.00420	0.100	0.93461	0.93856
1590	0.1000	0.00055	1.04580	0.0010	0.00550	0.099	0.93881	0.94400
1591	0.1000	0.00060	1.04540	0.0013	0.00600	0.099	0.93074	0.93636
1711	0.4986	0.00379	1.04340	0.0006	0.00760	0.495	0.88943	0.89624
1712	0.2030	0.00157	1.04520	0.0013	0.00773	0.201	0.92665	0.93387
1713	0.7508	0.00187	1.04080	0.0018	0.00249	0.749	0.83664	0.83873
1714	0.9994	0.00228	1.03950	0.0010	0.00228	0.997	0.80967	0.81152
1715	0.1012	0.00086	1.04450	0.0012	0.00850	0.100	0.91225	0.92006
1716	1.4946	0.00336	1.03660	0.0014	0.00225	1.491	0.75038	0.75207
1717	0.2001	0.00149	1.04580	0.0013	0.00745	0.199	0.93894	0.94598
1718	0.5010	0.00341	1.04390	0.0006	0.00681	0.498	0.89969	0.90585
1719	0.2026	0.00155	1.04540	0.0013	0.00765	0.201	0.93074	0.93792
1720	0.1004	0.00074	1.04520	0.0012	0.00737	0.100	0.92659	0.93347
1721	2.9760	0.00616	1.02850	0.0010	0.00207	2.970	0.58419	0.58540
1722	1.9520	0.01148	1.03470	0.0010	0.00588	1.941	0.71127	0.71548
1723	4.0240	0.00812	1.02400	0.0010	0.00202	4.016	0.49195	0.49294
1724	4.9900	0.00988	1.02060	0.0010	0.00198	4.980	0.42226	0.42309
1725	7.5340	0.01381	1.01340	0.0010	0.00183	7.520	0.27467	0.27518
1726	9.9000	0.01153	1.00900	0.0010	0.00116	9.888	0.18448	0.18470
1727	2.9720	0.00346	1.02780	0.0010	0.00116	2.969	0.56985	0.57051

RUN	PF	PB	RATIO	CUT	R	DELTA P	Z	Z/1-W
1803	1.0000	0.00889	1.03980	0.0004	0.00889	0.991	0.81557	0.82289
1804	0.7500	0.00656	1.04060	0.0010	0.00875	0.743	0.83221	0.83955
1805	0.5100	0.00413	1.04300	0.0010	0.00810	0.506	0.88142	0.88861
1806	0.2000	0.00205	1.04600	0.0008	0.01025	0.198	0.94281	0.95257
1807	0.5000	0.00428	1.04280	0.0010	0.00856	0.496	0.87731	0.88488
1808	0.2000	0.00192	1.04530	0.0008	0.00960	0.198	0.92845	0.93745
1809	0.7500	0.00563	1.04140	0.0010	0.00751	0.744	0.84862	0.85503
1810	1.0000	0.00755	1.04100	0.0010	0.00755	0.992	0.84042	0.84681
1811	0.1000	0.00120	1.04610	0.0010	0.01200	0.099	0.94495	0.95643
1812	1.0000	0.00776	1.04070	0.0010	0.00776	0.992	0.83426	0.84078
1813	2.2000	0.01370	1.03360	0.0010	0.00623	2.186	0.68874	0.69306
1814	3.0000	0.01850	1.02800	0.0010	0.00617	2.981	0.57394	0.57750
1815	0.7560	0.00580	1.04190	0.0010	0.00767	0.750	0.85887	0.86551
1816	0.5100	0.00429	1.04320	0.0010	0.00841	0.506	0.88552	0.89303
1817	0.5000	0.00411	1.04420	0.0010	0.00822	0.496	0.90601	0.91352
1818	0.2000	0.00186	1.04650	0.0008	0.00930	0.198	0.95304	0.96199
1819	1.0000	0.00755	1.04050	0.0010	0.00755	0.992	0.83017	0.83648
1820	1.0000	0.00755	1.04020	0.0010	0.00755	0.992	0.82402	0.83029

NEON SEPARATION DATA
SAMPLE NUMBER 64

RUN	PF	PB	RATIO	CUT	R	DELTA P	Z	Z/1-W
1384	0.9840	0.00600	1.01960	0.0006	0.00610	0.978	0.40168	0.40415
1385	2.1000	0.00740	1.00830	0.0003	0.00352	2.093	0.17008	0.17068
1386	0.5008	0.00400	1.02870	0.0012	0.00799	0.497	0.58836	0.59309
1387	0.5150	0.00320	1.02860	0.0012	0.00621	0.512	0.58629	0.58995
1388	0.2120	0.00138	1.03850	0.0005	0.00651	0.211	0.78898	0.79415
1389	0.3080	0.00150	1.03530	0.0007	0.00487	0.306	0.72346	0.72700
1390	0.2120	0.00100	1.03860	0.0005	0.00472	0.211	0.79101	0.79476
1391	0.1000	0.00040	1.04140	0.0007	0.00400	0.100	0.84848	0.85189
1392	0.0600	0.00018	1.04130	0.0009	0.00300	0.060	0.84650	0.84905
1393	0.1060	0.00120	1.04120	0.0007	0.01132	0.105	0.84439	0.85406
1394	0.1040	0.00200	1.04130	0.0007	0.01923	0.102	0.84644	0.86304
1395	0.7624	0.00420	1.02480	0.0005	0.00551	0.758	0.50823	0.51105
1396	0.4140	0.00200	1.03230	0.0007	0.00483	0.412	0.66199	0.66520
1397	1.5000	0.00780	1.01170	0.0009	0.00520	1.492	0.23982	0.24107
1398	0.1020	0.00046	1.04190	0.0007	0.00451	0.102	0.85874	0.86263
1399	0.0552	0.00040	1.04200	0.0008	0.00725	0.055	0.86084	0.86712
1400	0.0520	0.00136	1.04220	0.0009	0.02615	0.051	0.86495	0.88818
1401	1.2100	0.00700	1.01640	0.0005	0.00579	1.203	0.33607	0.33803
1402	2.4700	0.01460	1.00720	0.0003	0.00591	2.455	0.14753	0.14841
1403	3.0200	0.01720	1.00520	0.0003	0.00570	3.003	0.10655	0.10716
1404	3.5800	0.02100	1.00400	0.0003	0.00590	3.539	0.08196	0.08245
1405	0.7500	0.00440	1.02410	0.0017	0.00587	0.746	0.49417	0.49709
1406	4.0000	0.02120	1.00240	0.0003	0.00530	3.979	0.04918	0.04944
1407	4.6100	0.02680	1.00240	0.0003	0.00581	4.583	0.04918	0.04947

RUN	PF	PB	RATIO	CUT	R	DELTA P	Z	Z/1-W
1408	5.0300	0.02920	1.00190	0.0003	0.00581	5.001	0.03893	0.03916
1409	6.0400	0.02240	1.00140	*0.0003	0.00371	6.018	0.02869	0.02879
1410	7.0400	0.02660	1.00080	*0.0003	0.00378	7.013	0.01639	0.01645
1411	6.0900	0.03520	1.00160	*0.0003	0.00578	6.055	0.03278	0.03298
1412	8.0200	0.04580	1.00050	*0.0003	0.00571	7.974	0.01025	0.01030
1413	7.5200	0.04440	1.00010	*0.0003	0.00590	7.476	0.00205	0.00206
1414	5.4800	0.03160	1.00140	*0.0003	0.00577	5.448	0.02869	0.02885
1415	10.0000	0.03860	1.00005	*0.0004	0.00386	9.961	0.00102	0.00103
1416	4.0000	0.02240	1.00320	0.0003	0.00560	3.978	0.06557	0.06594
1417	7.5200	0.04320	1.00050	*0.0003	0.00574	7.477	0.01025	0.01030
1800	0.2120	0.00493	1.03850	0.0005	0.02325	0.207	0.78898	0.80776
1801	0.1020	0.00220	1.04170	0.0007	0.02157	0.100	0.85465	0.87349
1802	0.3000	0.00574	1.03640	0.0004	0.01913	0.294	0.74591	0.76046

NEON SEPARATION DATA
SAMPLE NUMBER 2

RUN	PF	PB	RATIO	CUT	R	DELTA P	Z	Z/1-W
1598	0.5000	0.03160	1.02930	0.0011	0.06320	0.468	0.60061	0.64113
1599	0.1000	0.00960	1.04080	0.0010	0.09600	0.090	0.83629	0.92510
1600	0.0500	0.00500	1.04090	0.0013	0.10000	0.045	0.83847	0.93164
1601	0.0508	0.00400	1.04090	0.0013	0.07874	0.047	0.83848	0.91014
1602	2.1000	0.06520	1.00770	0.0020	0.03105	2.035	0.15791	0.16297
1603	1.0200	0.04020	1.01980	0.0019	0.03941	0.980	0.40604	0.42270
1605	2.4600	0.06080	1.00510	0.0017	0.02472	2.399	0.10458	0.10723
1606	3.0200	0.07340	1.00410	0.0018	0.02430	2.947	0.08407	0.08617
1607	1.5000	0.04200	1.01310	0.0018	0.02800	1.458	0.26862	0.27636
1669	0.5020	0.02188	1.02840	0.0017	0.04359	0.480	0.58234	0.60888
1670	0.7000	0.02787	1.02440	0.0017	0.03981	0.672	0.50033	0.52107
1671	1.0010	0.03998	1.01800	0.0017	0.03994	0.961	0.36910	0.38445
1672	1.5000	0.05415	1.01150	0.0017	0.03610	1.446	0.23581	0.24464
1674	2.5040	0.07225	1.00580	0.0018	0.02885	2.432	0.11893	0.12247
1675	0.1000	0.02160	1.03530	0.0014	0.21600	0.078	0.72372	0.92311
1676	0.0502	0.01365	1.03540	0.0013	0.27191	0.037	0.72573	0.99676
1677	0.2020	0.01701	1.03770	0.0016	0.08421	0.185	0.77302	0.84410
1678	0.2988	0.01443	1.03570	0.0017	0.04829	0.284	0.73203	0.76918
1679	2.9900	0.12975	1.00380	0.0017	0.04339	2.860	0.07792	0.08145
1680	3.5000	0.08926	1.00340	0.0016	0.02550	3.411	0.06971	0.07154
1681	4.0000	0.10322	1.00270	0.0015	0.02580	3.897	0.05536	0.05682
1682	4.0280	0.12055	1.00280	0.0006	0.02993	3.907	0.05738	0.05915
1683	3.5160	0.09847	1.00370	0.0006	0.02801	3.418	0.07583	0.07801
1684	2.9940	0.07675	1.00490	0.0005	0.02563	2.917	0.10042	0.10306

RUN	PF	PB	RATIO	CUT	R	DELTA P	Z	Z/1-W
1685	2.0080	0.05730	1.00870	0.0005	0.02854	1.951	0.17829	0.18353
1686	0.9960	0.03258	1.02040	0.0005	0.03271	0.963	0.41804	0.43218
1687	0.5048	0.02038	1.03050	0.0005	0.04037	0.484	0.62505	0.65134
1688	0.3014	0.02141	1.03540	0.0006	0.07104	0.280	0.72548	0.78096
1689	0.1996	0.01598	1.03780	0.0007	0.08006	0.184	0.77470	0.84212
1690	0.0996	0.02125	1.03670	0.0008	0.21335	0.078	0.75220	0.95621
1691	0.0502	0.01288	1.03520	0.0010	0.25657	0.037	0.72151	0.97052

NEON SEPARATION DATA
SAMPLE NUMBER 1

RUN	PF	PB	RATIO	CUT	R	DELTA P	Z	Z/1-W
1338	5.0120	0.12200	1.00210	0.0015	0.02434	4.890	0.04306	0.04413
1339	2.1260	0.06570	1.00700	0.0015	0.03090	2.060	0.14352	0.14810
1341	0.9968	0.03820	1.01850	0.0022	0.03832	0.959	0.37944	0.39456
1342	1.5080	0.06000	1.01080	0.0017	0.03979	1.448	0.22146	0.23063
1343	3.0200	0.08460	1.00460	0.0015	0.02801	2.935	0.09431	0.09703
1344	4.0040	0.10400	1.00350	0.0014	0.02597	3.900	0.07176	0.07367
1349	0.2160	0.01280	1.03720	0.0258	0.05926	0.203	0.77218	0.82082
1350	0.2056	0.01420	1.03490	0.0192	0.06907	0.191	0.72200	0.77556
1357	0.2168	0.01480	1.03350	0.0154	0.06827	0.202	0.69168	0.74236
1361	0.2060	0.01430	1.03400	0.0147	0.06942	0.192	0.70178	0.75413
1362	0.2160	0.01490	1.03640	0.0353	0.06898	0.201	0.75933	0.81559
1366	0.1900	0.01320	1.03470	0.0148	0.06947	0.177	0.71625	0.76972
1367	0.1884	0.01310	1.03520	0.0147	0.06953	0.175	0.72653	0.78082
1368	0.2056	0.01400	1.03390	0.0118	0.06809	0.192	0.69868	0.74973
1372	0.1480	0.01100	1.03770	0.0105	0.07432	0.137	0.77647	0.83881
1373	0.1088	0.00420	1.03870	0.0032	0.03860	0.105	0.79414	0.82602
1374	0.2020	0.00688	1.03530	0.0026	0.03406	0.195	0.72414	0.74967
1375	0.0530	0.00210	1.04020	0.0039	0.03962	0.051	0.82519	0.85924
1376	0.1060	0.00420	1.03930	0.0032	0.03962	0.102	0.80645	0.83972
1377	0.0754	0.00320	1.04000	0.0035	0.04244	0.072	0.82094	0.85732
1378	0.0508	0.00209	1.04130	0.0039	0.04114	0.049	0.84780	0.88418
1756	0.2468	0.00936	1.03550	0.0022	0.03793	0.237	0.72811	0.75681
1757	0.2030	0.00745	1.03700	0.0024	0.03670	0.196	0.75896	0.78787
1758	0.1012	0.01039	1.03920	0.0031	0.10271	0.091	0.80437	0.89644

RUN	PF	PB	RATIO	CUT	R	DELTA P	Z	Z/1-W
1759	0.0505	0.00610	1.04010	0.0038	0.12070	0.044	0.82312	0.93610
1760	0.5048	0.01489	1.02870	0.0017	0.02951	0.490	0.58849	0.60638
1761	0.2512	0.00869	1.03620	0.0022	0.03459	0.243	0.74247	0.76908

NEON SEPARATION DATA
SAMPLE NUMBER 5

RUN	PP	PB	RATIO	CUT	R	DELTA P	Z	Z/1-W
1763	0.4018	0.01065	1.03990	0.0019	0.02651	0.391	0.81822	0.84050
1764	2.5200	0.01779	1.01730	0.0237	0.00706	2.502	0.35873	0.36128
1765	1.0244	0.02089	1.03140	0.0021	0.02039	1.004	0.64397	0.65738
1766	0.7566	0.01851	1.03370	0.0020	0.02446	0.738	0.69111	0.70844
1767	0.4918	0.01262	1.03890	0.0019	0.02566	0.479	0.79771	0.81872
1768	3.0180	0.01815	1.01540	0.0259	0.00601	3.000	0.31969	0.32162
1769	3.5700	0.02291	1.01240	0.0262	0.00642	3.547	0.25745	0.25912
1770	4.0440	0.01572	1.01120	0.0280	0.00389	4.028	0.23275	0.23365
1771	0.3058	0.00936	1.04100	0.0018	0.03061	0.296	0.84077	0.86732
1772	0.2300	0.00662	1.04240	0.0019	0.02878	0.223	0.86951	0.89528
1773	0.1004	0.00387	1.04410	0.0015	0.03855	0.097	0.90418	0.94043
1774	4.4780	0.02549	1.01020	0.0294	0.00569	4.453	0.21212	0.21334
1775	1.5008	0.02606	1.02700	0.0022	0.01736	1.475	0.55376	0.56355
1776	2.0000	0.03248	1.02160	0.0023	0.01624	1.968	0.44304	0.45035
1777	5.0180	0.02922	1.00820	0.0312	0.00582	4.989	0.17069	0.17169
1778	5.9680	0.03227	1.00700	0.0322	0.00541	5.936	0.14578	0.14658
1779	7.0580	0.03739	1.00560	0.0354	0.00530	7.021	0.11682	0.11745
1780	8.0360	0.02653	1.00510	0.0383	0.00330	8.009	0.10655	0.10691
1781	9.0380	0.02886	1.00460	0.0411	0.00319	9.009	0.09625	0.09656
1782	9.8340	0.03360	1.00360	0.0434	0.00342	9.800	0.07542	0.07567
1783	0.4916	0.01240	1.03620	0.0091	0.02522	0.479	0.74506	0.76434
1784	0.2086	0.00650	1.04220	0.0049	0.03116	0.202	0.86669	0.89456
1785	0.1992	0.00660	1.04300	0.0007	0.03313	0.193	0.88128	0.91148
1786	0.5020	0.01157	1.03770	0.0008	0.02305	0.490	0.77270	0.79093

RUN	PF	PB	RATIO	CUT	R	DELTA P	Z	Z/1-W
1793	5.1000	0.03361	1.00950	0.0006	0.00659	5.066	0.19470	0.19599
1794	5.1000	0.07290	1.00980	0.0031	0.01429	5.027	0.20109	0.20400
1795	6.0100	0.07400	1.00730	0.0032	0.01231	5.936	0.14980	0.15167
1796	7.0200	0.04110	1.00620	0.0033	0.00585	6.979	0.12723	0.12798
1797	8.0400	0.04628	1.00550	0.0038	0.00576	7.994	0.11290	0.11355
1798	3.0200	0.04788	1.01570	0.0025	0.01585	2.972	0.32206	0.32725
1799	4.0000	0.06407	1.01230	0.0028	0.01602	3.936	0.25235	0.25646

APPENDIX C - ACCURACY AND PRECISION

MASS SPECTROMETER MEASUREMENTS

A quality control test was conducted to monitor the performance of the mass spectrometer during the period of this study. Neon samples were prepared by collecting appropriately large samples from several of the separation tests. Ratios of the isotopic ratios were measured by the mass spectrometer by pairing together individual product samples with multiple feed samples and individual feed samples with multiple product samples. The ratio of the $^{22}Ne/(1 - {}^{22}Ne)$ for the product sample to the $^{22}Ne/(1 - {}^{22}Ne)$ for the feed sample was calculated to give a value, R, for the ratio of isotopic ratios.

Thirteen control samples with varying $^{22}Ne/(1 - {}^{22}Ne)$ were prepared and paired together to form 19 ratio pairs with R values ranging from 1.008 to 1.043. These paired control materials were analyzed from October 1967 to March 1970 for a total of 117 analyses. The following statistical estimates were obtained from the analyses:

Variance per individual (R - 1) result:	0.19×10^{-6}
Standard deviation per individual (R - 1) result:	$\pm 0.44 \times 10^{-3}$
95% confidence level per individual (R - 1) result:	$\pm 0.86 \times 10^{-3}$

There is no known bias associated with the measurements.

FLOW MEASUREMENTS

The flow measurements on all the test samples were made with the volumetric flow system described in the text. The precision of the volumetric system was checked by measuring flow rates through a jeweled orifice with a throat diameter of 0.001 in. Measurements were also made with the gravimetric flow system which was designed and constructed at ORGDP and has been compared with NBS standards.* Table C-1 shows a comparison between the measurements made with the gravimetric system and the volumetric system. Table C-2 shows results of viscosity ratios and slip intercepts with standard deviations obtained from measurements with different gases on the test sample 1054.

---

*Collins, W. T., and Selby, T. W., *Gravimetric Mass Flow Standard. Part 1: Design and Construction*, Union Carbide Corporation, Nuclear Division, Oak Ridge Gaseous Diffusion Plant, May 18, 1965 (K-1632, Part 1).

Collins, W. T., and Selby, T. W., *Gravimetric Mass Flow Standard. Part 2: Performance and Evaluation*, Union Carbide Corporation, Nuclear Division, Oak Ridge Gaseous Diffusion Plant, April 15, 1966 (K-1632, Part 2).

Table C-1

COMPARISON OF FLOW MEASUREMENTS FROM A VOLUMETRIC SYSTEM WITH THOSE FROM A GRAVIMETRIC SYSTEM

Gravimetric System

A fit of seven measurements gave:

F (std cc/min) = $0.07934\ P_f - 0.0992$

Standard deviation = 0.0179

Percent deviation at midpoint of curve = 0.074%

Volumetric System

A fit of 24 measurements gave:

F (std cc/min) = $0.4710 \times 10^{-5}\ P_f^2 + 0.07666\ P_f - 0.5865$

Standard deviation = 0.014

Percent deviation at midpoint of curve = 0.083%

Comparison of Two Systems

Percent difference in values calculated from the curves at the midpoint of the region where the two sets of data overlap: 0.12%

Note: Standard conditions referred to are 76 cm Hg at 25°C.

Table C-2

COMPARISON OF MEASURED AND
THEORETICAL VALUES FOR DIFFERENT GASES

	Gas	η/η_o	$\dot{w}_m/\dot{w}_o$	w_s/w_o
Steady State	N_2	1.000[a]		0.7091 ± 0.025
	A	0.9968 ± 0.0033		0.7218 ± 0.008
	Ne	1.0085 ± 0.0041		0.7300 ± 0.006
	He	1.0413 ± 0.0094		0.7209 ± 0.008
				0.7205
Pressure Decay	N_2	0.9873 ± 0.0013	0.99	0.7194 ± 0.0025
	A	0.9778 ± 0.0013	0.97	0.7787 ± 0.0308
	Ne	0.9798 ± 0.0030	0.95	0.7498 ± 0.0044
	He	0.9568 ± 0.0149	0.92	0.6993 ± 0.0020
				0.7368

[a]This was used as the reference point for comparison.

INTERNAL DISTRIBUTION

1. Barrier Manufacturing Division
   Strang, F.

2- 3. Engineering Division
   Patton, F. S.
   Rooks, W. E.

4-47. Gaseous Diffusion Development Division
   Brown, W. K. (4)
   Bundy, R. D.
   Burton, D. W.
   Collins, W. T.
   Fain, D. E. (25)
   Harris, E. B.
   Higgins, R. L.
   Kidd, G. J., Jr.
   King, C. J.
   Lund, L. M.
   Malling, G. F.
   McGill, R. M.
   Melroy, P. E.
   Pashley, J. H.
   Ritter, R. L.
   Streetman, K. D.
   Trammell, H. E.

48-51. Laboratory Division
   Barton, J. C.
   Garber, J. W.
   Smith, L. A.
   Ziehlke, K. T.

52-53. Planning and Analysis Division
   Lang, D. M.
   Von Halle, E.

54. Plant Library
   Ferguson, J. B.

55-56. Plant Records (RC)

57. Sommerfeld, K. W.

58. Wilcox, W. J., Jr.

59. Winkel, R. A.

60-61. Y-12 Plant
   Googin, J. M.
   Vanstrum, P. R.

EXTERNAL DISTRIBUTION

62-185. TIC-4500